Klaus Helmut Lang, BSc

Diffusion Monte Carlo applied to the two-dimensional fermion Hubbard Model

MASTER THESIS

For obtaining the academic degree
Diplom-Ingenieur

Master Programme of
Technical Physics

Graz University of Technology

Supervisor:
Univ.-Prof. Dipl.-Phys. Dr.rer.nat. Wolfgang von der Linden

Institute of Theoretical and Computational Physics

Graz, August 7, 2012

Deutsche Fassung:
Beschluss der Curricula-Kommission für Bachelor-, Master- und Diplomstudien vom 10.11.2008
Genehmigung des Senates am 1.12.2008

EIDESSTATTLICHE ERKLÄRUNG

Ich erkläre an Eides statt, dass ich die vorliegende Arbeit selbstständig verfasst, andere als die angegebenen Quellen/Hilfsmittel nicht benutzt, und die den benutzten Quellen wörtlich und inhaltlich entnommene Stellen als solche kenntlich gemacht habe.

Graz, am …… ……..
(Unterschrift)

Englische Fassung:

STATUTORY DECLARATION

I declare that I have authored this thesis independently, that I have not used other than the declared sources / resources, and that I have explicitly marked all material which has been quoted either literally or by content from the used sources.

…… ……..
date (signature)

Abstract

The Hubbard model, one of the simplest models in correlated quantum many-body physics, is used among other things to study magnetic properties of highly correlated systems. One also supposes that this model can be used to explain the phenomena of high-temperature superconductivity.
Despite its simplicity, an analytical solution is only possible for special cases (Bethe ansatz) and also straightforward numerical methods are restricted to small systems because of the exponential growths of the required computer capacities depending on the size of the system.

Diffusion Monte Carlo offers a different approach, whereby one is able to compute ground-state properties of the considered system with the help of stochastic processes. In this work we present that kind of Quantum Monte Carlo method and show how to use it to calculate expectation values of quantum mechanical observables. Therefore, one also needs a reasonable good approximation for the groundstate wavefunction.
In addition, three different methods to compute such an approximation applicable for the Hubbard Model are presented.

The so-called sign problem also creates difficulties during the calculation for fermionic systems. Its origin is discussed and a method to avoid this problem is also presented.

Kurzfassung

Das Hubbard Model, eines der einfachsten korrelierten Vielteilchenmodelle in der Quantenphysik, wurde in der Vergangenheit immer wieder herangezogen um unter anderen magnetische Eigenschaften von stark korrelierten Systemen zu untersuchen. Man vermutet auch, damit das Phänomen der Hochtemperatursupraleitung erklären zu können.
Trotz seiner einfachen Beschaffenheit ist eine analytische Lösung nur für ausgewählte Grenzfälle möglich (Bethe Ansatz). Ebenso können numerische Standardverfahren, aufgrund des mit der Systemgröße überexponentiell wachsenden Bedarfs an Computer Ressourcen, nur auf sehr kleine Systeme angewendet werden.

Diffusions Monte Carlo bietet eine andere Herangehensweise, wobei Grundzustandseigenschaften des betrachteten Systems mit Hilfe stochastischer Prozesse ermittelt werden können. Der Autor stellt diese Art von Quanten Monte Carlo vor und zeigt wie es verwendet werden kann um physikalische Observablen zu berechnen. Dafür wird auch eine hinreichend genaue Näherung der Grundzustandswellenfunktion benötigt, wobei in weiterer Folge drei Methoden für das Hubbard Modell vorgestellt werden.

Für fermionische Systeme stellt das sogenannte Sign Problem eine weitere Hürde in der Berechnung dar. Dessen Ursachen werden diskutiert und es wird eine Methode um dieses Problem zu umgehen präsentiert.

Danksagungen

Zunächst möchte ich meinem Betreuer Prof. Wolfgang von der Linden dafür danken, dass er es mir ermöglichte, eine Arbeit über dieses interessante Thema zu verfassen. Besonders hervorzuheben ist die hervorragende Betreuung von seiner Seite. In unzähligen Besprechungen nahm er sich die Zeit um mir Einblick in die Welt der Quanten Monte Carlo Simulationen zu geben und war mir durch Diskussionen über aktuelle Probleme stets eine Inspiration.

Des Weiteren möchte ich mich speziell bei Martin Nuss, Gerald Rescher und Richard Romirer (in alphabetischer Reihenfolge), die mir während der Arbeit bei Problemen computertechnischer Natur stets zur Seite standen, bedanken.

Besonderer Dank gilt selbstverständlich meinen Eltern, für die mein Bruder und ich unser gesamtes Leben lang immer an erster Stellen standen und die mir dieses Studium überhaupt erst ermöglicht haben.

Abschließend möchte ich mich bei denjenigen, die mich während des Studiums, aber auch abseits der Uni, begleitet haben, für die schöne Zeit bedanken.
Diejenigen, die ich meine, fühlen sich hoffentlich angesprochen! :)

Contents

1. The Hubbard Model

The Hubbard model, named after John Hubbard, is one of the simplest models in correlated quantum many-body physics. It was originally introduced in Ref. [1] and gives a description of strongly localized electrons on a rigid lattice, while taking account of the Pauli principle and the Coulomb interaction of the electrons. The Hamiltonian in second quantization only consists of two terms and takes the form

$$\hat{H} = -t \sum_{\substack{\langle i,j \rangle \\ \sigma}} c^{\dagger}_{i,\sigma}\, c_{j,\sigma} + U \sum_{i} n_{i,\uparrow}\, n_{i,\downarrow} \quad , \tag{1.1}$$

where $\langle i,j \rangle$ denotes to sum only over the nearest neighbours on the lattice.
The first term in Equation (1.1), the hopping term, is identical to the well-known Tight Binding Hamiltonian and represents the kinetic energy of the electrons. For the hopping parameter t only transitions between the nearest neighbour sites of the lattice are considered, as a result of the minor mobility of the electrons.
The second term describes the coulumb interaction of the electrons. In the Hubbard model it is assumed that the Coulomb potential is very short ranged because of screening, so that only electrons on the same lattice site are able to interact with each other. Therefore, the operator $\hat{D} = \sum_i n_{i,\uparrow}\, n_{i,\downarrow}$ simply counts the double occupations per basis state, as shown in Figure (1.2). Hence, each lattice site with two electrons on it costs the energy U.
Because of Pauli's principle, there are only four different possibilities to occupy a lattice site. It is either occupied by an electron with spin up or an electron with spin down or there are two electrons with different spins on it or the site is empty, as depicted in Figure (1.1). That means the coulumb interaction concerns only electrons with different spin on the same lattice site.

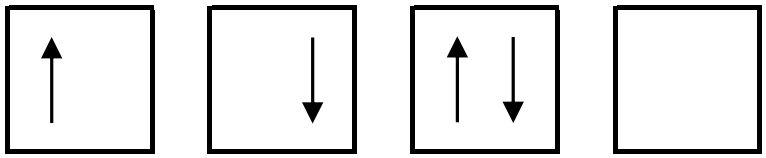

Figure 1.1.: To illustrate Pauli's principle, the four different possibilities to occupy a lattice site by electrons are shown. An arrow depicts an electron and its direction denotes the spin (either up or down).

Figure (1.2) displays an example for a manybody basis state χ of the Hubbard Hamiltonian in real space for a system size $L_X \times L_Y = 4 \times 4$. The number of electrons with spin up is equal to the electrons with spin down, therefore $N_\uparrow = N_\downarrow = 5$. In second quantization this basis state is

$$\begin{aligned} |\,\chi\,\rangle &= |\,\chi\,\rangle_\uparrow \otimes |\,\chi\,\rangle_\downarrow \\ &= \left(c^{\dagger}_{4,\uparrow}\, c^{\dagger}_{5,\uparrow}\, c^{\dagger}_{10,\uparrow}\, c^{\dagger}_{12,\uparrow}\, c^{\dagger}_{14,\uparrow}\right) \otimes \left(c^{\dagger}_{4,\downarrow}\, c^{\dagger}_{6,\downarrow}\, c^{\dagger}_{10,\downarrow}\, c^{\dagger}_{13,\downarrow}\, c^{\dagger}_{16,\downarrow}\right) |\,0\,\rangle \quad , \end{aligned}$$

where $|0\rangle$ denotes the vacuum state. Furthermore, the double occupied sites are marked in colour and hopping possibilites for the electron on site 6 are sketched. However, hopping to the right hand site, on site 10, is not possible, because of Pauli's principle.

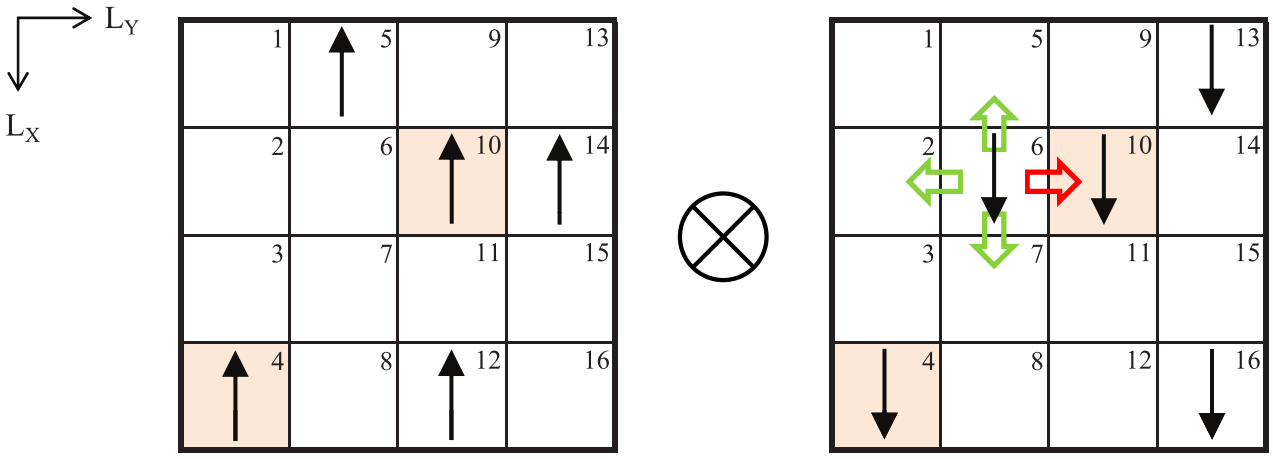

Figure 1.2.: A basis state of the Hubbard Hamiltonian in real space for a system size $L_X \times L_Y = 4 \times 4$. The double occupied sites are marked in colour and hopping possibilities for the electron on site 6 are sketched.

The different strategies to handle the hopping across the boundaries are described in Section 1.1 and in Section 1.2 we discuss the properties of the Hubbard Hamiltonian in reciprocal space. In Section 1.3, a calculation to obtain the exact groundstate wavefunction for a toy model is performed and in Section 1.4 we show that an exact diagonalisation of the Hubbard Hamiltonian is limited to small system sizes.

1.1. Boundary Conditions

A scenario that has to be discussed is what happens to an electron located on the edge of the system if it hops outwards. For example, the electron on site 5 in Figure (1.2) wants to move in the $-L_X$ direction.
There are three typical possibilities. Either the hopping across the boundaries is forbidden or one introduces *periodic boundary conditions* (pbc). That means if we consider the previous example, the new position for an electron hopping from site 5 in the $-L_X$ direction is site 8.

The third alternative, described among others in Ref. [2], is to use a periodic lattice and to modify the hopping by a Peierls phase

$$t_{i,j} \quad \Rightarrow \quad t_{i,j} \cdot \mathrm{e}^{\mathrm{i}\,\varphi\,(x_i - x_j)} \quad ,$$

which results in a gauge transformation (Equation (1.2)).

$$\tilde{c}_i = c_i \cdot \mathrm{e}^{-\mathrm{i}\,\varphi\,x_i} \qquad , \qquad \tilde{c}_i^\dagger = c_i^\dagger \cdot \mathrm{e}^{\mathrm{i}\,\varphi\,x_i} \tag{1.2}$$

(In the following the one dimensional case $L_X = N$ and $L_Y = 1$ is discussed. In two or more dimensions it is very similar, but for the Peierls phase also a direction has to be considered.)

This transformation causes that only the electrons hopping across the boundaries of the system get a phase factor (twisted boundary conditions)

$$\mathrm{e}^{-\mathrm{i}\,\phi} \quad \text{with} \quad \phi \,=\, N \cdot \varphi \quad ,$$

as shown below.

$$c^{\dagger}_{j+1}\, c_j \;= \tilde{c}^{\dagger}_{j+1}\, \tilde{c}_j \;\mathrm{e}^{-\mathrm{i}\,\varphi\, x_{j+1}}\, \mathrm{e}^{\mathrm{i}\,\varphi\, x_j} \;=\; \tilde{c}^{\dagger}_{j+1}\, \tilde{c}_j \;\mathrm{e}^{-\mathrm{i}\,\varphi}$$

But at the boundaries, and taking the periodicity of the lattice into account, the situation is different.

$$\begin{aligned} c^{\dagger}_{N+1}\, c_N \;&= \tilde{c}^{\dagger}_{N+1}\, \tilde{c}_N \;\mathrm{e}^{-\mathrm{i}\,\varphi\, x_{N+1}}\, \mathrm{e}^{\mathrm{i}\,\varphi\, x_N} \\ &= \tilde{c}^{\dagger}_{1}\, \tilde{c}_N \;\mathrm{e}^{-\mathrm{i}\,\varphi}\; \mathrm{e}^{\mathrm{i}\,\phi} \end{aligned}$$

Furthermore, Equation (1.2) does not affect the second term of the Hamiltonian $\hat{D} = \sum_i \, n_{i,\uparrow}\, n_{i,\downarrow}$, because

$$n_{i,\sigma} \;=\; c^{\dagger}_{i,\sigma}\, c_{i,\sigma} \;=\; \tilde{c}^{\dagger}_{i,\sigma}\, \tilde{c}_{i,\sigma}\; \mathrm{e}^{\mathrm{i}\,\varphi\,(x_i - x_i)} \;=\; \tilde{c}^{\dagger}_{i,\sigma}\, \tilde{c}_{i,\sigma} \;=\; \tilde{n}_{i,\sigma} \quad .$$

Periodic boundary conditions are a special case of this gauge transformation and can be obtained if we choose $\phi = 0$.

1.2. The Hubbard Hamiltonian in reciprocal space

In this Section, we start with the Hubbard Hamiltonian in real space

$$\hat{H} = \underbrace{-t \sum_{\substack{\langle i,j \rangle \\ \sigma}} c^{\dagger}_{i,\sigma}\, c_{j,\sigma}}_{\hat{H}_0} + \underbrace{U \sum_{i} n_{i,\uparrow}\, n_{i,\downarrow}}_{\hat{H}_1} \quad ,$$

and transform it into reciprocal space. Subsequent, the different terms of the Hamiltonian are discussed, similar to the previous Section.

The part of the Hamiltonian, which corresponds to the kinetic energy, is labeled as $\hat{H}_0$. The other one is labeled $\hat{H}_1$ and describes the Coulomb interaction between the electrons, which is a diagonal operator in real space. Again $\langle i,j \rangle$ denotes a sum over the nearest neighbours of the lattice.
The Fourier transformation of a creation operator takes the form

$$c^{\dagger}_{k,\sigma} \;=\; \frac{1}{\sqrt{N}} \sum_j \mathrm{e}^{\mathrm{i}\,k\,x_j}\, c^{\dagger}_{j,\sigma} \qquad \text{and} \qquad c^{\dagger}_{j,\sigma} \;=\; \frac{1}{\sqrt{N}} \sum_k \mathrm{e}^{-\mathrm{i}\,k\,x_j}\, c^{\dagger}_{k,\sigma} \quad \text{respectively,} \tag{1.3}$$

whereby j (k) denotes the index for the operator in real (momentum) space and N is the number of lattice sites. For an annihilation operator it is the complex conjugate of Equation (1.3). Therefore, using these definitions, one obtains the following result for $\hat{H}_0$.

$$\begin{aligned} \hat{H}_0 \;&= -\,t \sum_{\substack{\langle i,j \rangle \\ \sigma}} c^{\dagger}_{i,\sigma}\, c_{j,\sigma} \\ &= -\,t \sum_{\substack{\langle i,j \rangle \\ \sigma}} \sum_{k,\,k'} \frac{1}{N}\, \mathrm{e}^{-\mathrm{i}\,k\,x_i}\, c^{\dagger}_{k,\sigma}\, \mathrm{e}^{\mathrm{i}\,k'\,x_j}\, c_{k',\sigma} \\ &= -\,t \sum_{\substack{i,\,j=i+\eta \\ \sigma}} \sum_{k,\,k'} \frac{1}{N}\, \mathrm{e}^{-\mathrm{i}\,(k-k')\,x_i}\; \mathrm{e}^{\mathrm{i}\,k'\,x_\eta}\, c^{\dagger}_{k,\sigma}\, c_{k',\sigma} \end{aligned}$$

On a quadratic lattice the nearest neighbours are given by

$$\eta = \left\{ \begin{pmatrix} 1 \\ 0 \end{pmatrix}, \begin{pmatrix} -1 \\ 0 \end{pmatrix}, \begin{pmatrix} 0 \\ 1 \end{pmatrix}, \begin{pmatrix} 0 \\ -1 \end{pmatrix} \right\} \quad .$$

$$\begin{aligned} \hat{H}_0 &= \sum_{\substack{k,\,k' \\ \sigma}} \underbrace{\sum_i \frac{1}{N} \mathrm{e}^{-\mathrm{i}\,(k-k')\,x_i}}_{\delta_{k,k'}} \sum_\eta (-t)\, \mathrm{e}^{\mathrm{i}\,k'\,x_\eta}\, c^\dagger_{k,\sigma}\, c_{k',\sigma} \\ &= \sum_{\substack{k \\ \sigma}} c^\dagger_{k,\sigma}\, c_{k,\sigma}\, (-2t)\, \left(\cos(k_X) + \cos(k_Y)\right) \qquad (1.4) \\ &= \sum_{\substack{k \\ \sigma}} \epsilon_k\, c^\dagger_{k,\sigma}\, c_{k,\sigma} \qquad (1.5) \end{aligned}$$

The same calculation is done for the operator $\hat{H}_1$.

$$\begin{aligned} \hat{H}_1 &= U \sum_i n_{i,\uparrow}\, n_{i,\downarrow} \;=\; U \sum_i c^\dagger_{i,\uparrow} c_{i,\uparrow}\, c^\dagger_{i,\downarrow}\, c_{i,\downarrow} \\ &= U \sum_{k,l,m,n} \frac{1}{N^2} \underbrace{\sum_i \mathrm{e}^{-\mathrm{i}\,(k-l+m-n)\,x_i}}_{N\,\delta_{k+m,l+n}}\, c^\dagger_{k,\uparrow} c_{l,\uparrow}\, c^\dagger_{m,\downarrow}\, c_{n,\downarrow} \\ &= \frac{U}{N} \sum_{k,l,m} c^\dagger_{k,\uparrow} c_{l,\uparrow}\, c^\dagger_{m,\downarrow}\, c_{k+m-l,\downarrow} \end{aligned}$$

Next, we perform the index transformation $q = l - k$ respectively $l = k + q$ and obtain

$$\begin{aligned} \hat{H}_1 &= \frac{U}{N} \sum_q \underbrace{\sum_k c^\dagger_{k,\uparrow} c_{k+q,\uparrow}}_{\rho_q}\, \underbrace{\sum_m c^\dagger_{m,\downarrow} c_{m-q,\downarrow}}_{\rho_{-q}} \qquad (1.6) \\ &= \frac{U}{N} \sum_q \rho_q\, \rho_{-q} \quad . \qquad (1.7) \end{aligned}$$

The combination of Equation (1.5) and (1.7) yields the Hamiltonian in momentum space

$$\hat{H} = \underbrace{\sum_{\substack{k \\ \sigma}} \epsilon_k\, c^\dagger_{k,\sigma}\, c_{k,\sigma}}_{\hat{H}_0} + \underbrace{\frac{U}{N} \sum_q \rho_q\, \rho_{-q}}_{\hat{H}_1} \quad . \qquad (1.8)$$

In reciprocal space it is contrawise to real space, now $\hat{H}_0$ is a diagonal operator and $\hat{H}_1$ has off-diagonal elements.
Of course, Pauli's principle is also valid in reciprocal space, which means that a certain wavenumber can at most be occupied by one up and one down electron.

The term ϵ_k in Equation (1.5) respectively in (1.8) is the well-known dispersion relation of the Tight binding model. The wave vectors k_X and k_Y depend on the system size and can take the values

$$k_i = \frac{2\,\pi}{L_i}\,\nu \;, \qquad \nu \in \{0,\, 1,\, \cdots,\, L_i - 1\} \;, \quad i = X,\, Y \quad ,$$

assuming that the lattice constant is unique.
Figure (1.3) shows the dispersion relation for a one-dimensional system with periodic boundary conditions (red) for $U = 0$ and $t = 1$. The crosses chart the possible values of ϵ_k for a system with $N = 9$ sites. Close inspection reveals that the groundstate of $\hat{H}_0$ is degenerated if the number of electrons per spin direction is even (for the one-dimensional case).
If one introduces twisted boundary conditions, as described in Section 1.1, the operator $\hat{H}_0$ changes to

$$\begin{aligned}
\hat{H}_0 &= -t \sum_{\substack{\langle i,j \rangle \\ \sigma}} c^\dagger_{i,\sigma}\, c_{j,\sigma}\; \mathrm{e}^{\mathrm{i}\,\varphi\,(x_i - x_j)} \\
&= -t \sum_{\substack{\langle i,j \rangle \\ \sigma}} \sum_{k,\,k'} \frac{1}{N}\, \mathrm{e}^{-\mathrm{i}\,(k-k')\,(x_i - x_j)}\; \mathrm{e}^{\mathrm{i}\,\varphi\,(x_i - x_j)}\; c^\dagger_{k,\sigma}\, c_{k',\sigma} \\
&= -t \sum_{\substack{i,\eta \\ \sigma}} \sum_{k,\,k'} \frac{1}{N}\, \mathrm{e}^{-\mathrm{i}\,(k-k')\,x_i}\; \mathrm{e}^{\mathrm{i}\,(k'+\varphi)\,x_\eta}\; c^\dagger_{k,\sigma}\, c_{k',\sigma} \\
&= \sum_{\substack{k \\ \sigma}} \sum_{\eta} (-t)\, \mathrm{e}^{\mathrm{i}\,(k+\varphi)\,x_\eta}\, c^\dagger_{k,\sigma}\, c_{k,\sigma} \\
&= \sum_{\substack{k \\ \sigma}} c^\dagger_{k,\sigma}\, c_{k,\sigma}\, (-2t)\, \cos(k+\varphi) \quad .
\end{aligned}$$

Hence, it is possible to avoid this degeneration as depicted in Figure (1.3).

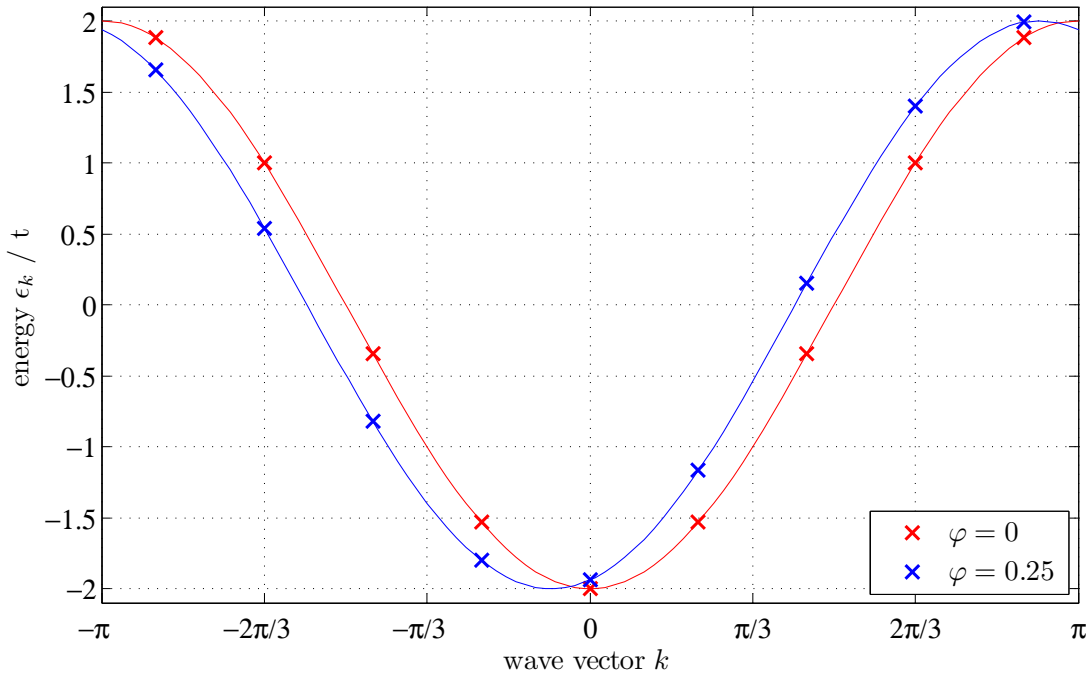

Figure 1.3.: Dispersion relation for a one-dimensional system ($U = 0$, $t = 1$) with periodic (red) and twisted boundary conditions (blue). The crosses sketch the possible values for ϵ_k for a system with $N = 9$ sites. The energies are given in units of t.

The operators ρ_q and ρ_{-q} (see Equation (1.8)) have the following impact on a manybody basis state. First, ρ_{-q} creates a momentum q in any spin direction and subsequently ρ_q annihilates a momentum q in the other spin direction. From this follows that $\hat{H}_1$ conserves momentum. (See Figure (1.4) for schematic illustration.)

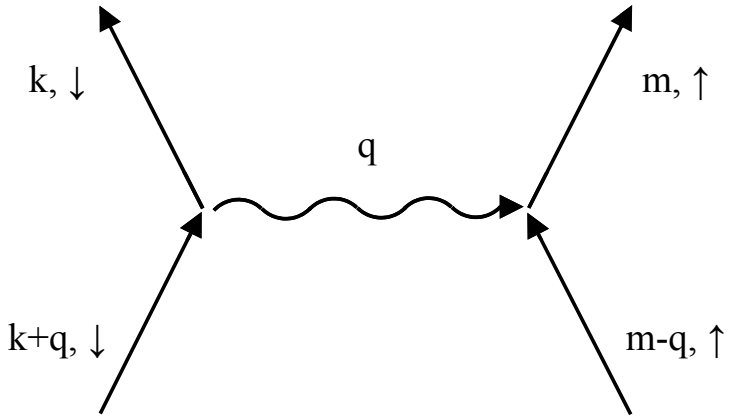

Figure 1.4.: Schematic illustration of a scattering process caused by the operator $\hat{H}_1$. The arrows denote the wavenumbers of the electrons before $(k+q,\, m-q)$ respectively after scattering $(k,\, m)$ and the waved arrow represents the exchanged momentum q, as described in Equation (1.6).

Figure (1.5) displays an example for a manybody basis state K in momentum space for a system size $L_X \times L_Y = 3 \times 3$ with $N_\uparrow = N_\downarrow = 5$. The consecutive number (black) is used to give a representation of this state in second quantization

$$\begin{aligned} |\, K \,\rangle &= |\, K \,\rangle_\uparrow \otimes |\, K \,\rangle_\downarrow \\ &= \left(c^\dagger_{2,\uparrow}\, c^\dagger_{4,\uparrow}\, c^\dagger_{5,\uparrow}\, c^\dagger_{6,\uparrow}\, c^\dagger_{8,\uparrow} \right) \otimes \left(c^\dagger_{2,\downarrow}\, c^\dagger_{4,\downarrow}\, c^\dagger_{5,\downarrow}\, c^\dagger_{6,\downarrow}\, c^\dagger_{8,\downarrow} \right) |\, 0 \,\rangle \quad , \end{aligned}$$

whereas the coloured numbers indicate the wavenumber of the sites.
The depicted state is a groundstate vector of $\hat{H}_0$ (in the following also denoted as *Fermi Sea* $|\, FS \,\rangle$), which has total momentum zero. As one can easily deduce, for this system configuration (system size and number of electrons) the groundstate of $\hat{H}_0$ is not degenerated and all shells are filled.
Applying the operator $\hat{H}_1$ to this basis state leads to particle hole excitations, but the momentum of the scattered states $\hat{H}_1 |\, K \,\rangle$ is still zero. One example of these scattered states is denoted in Figure (1.5) with the green arrows.

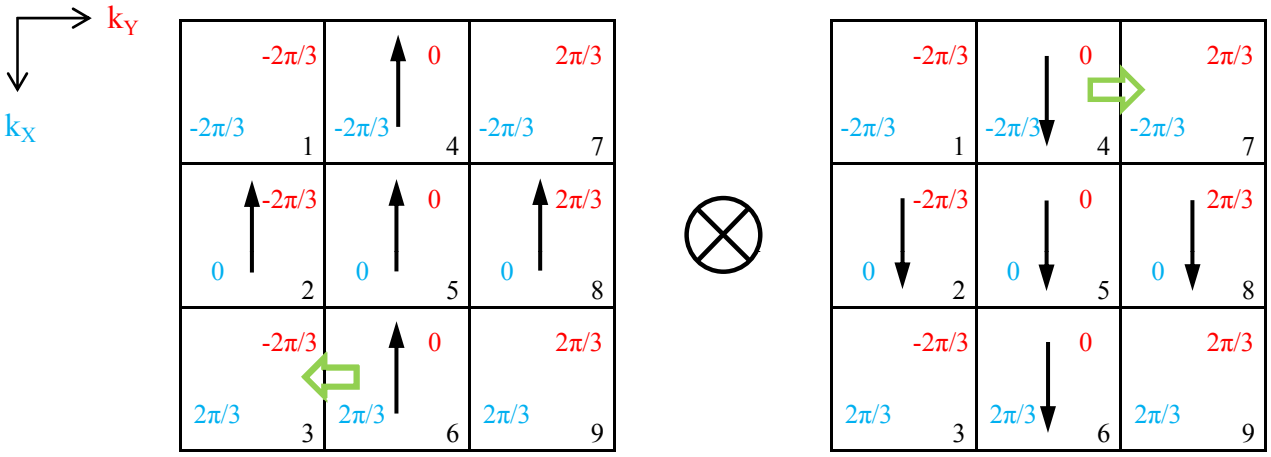

Figure 1.5.: A basis state of the Hubbard Hamiltonian in momentum space for a system size $L_X \times L_Y = 3 \times 3$. The coloured numbers indicate the wavenumber of the sites and the green arrows denote an example for a scattered state.

1.3. Analytical Solution of a Toy Model

In this Section, we perform an analytical calculation to obtain the groundstate energy and wavefunction of the Hubbard Hamiltonian

$$\hat{H} = -t \sum_{\substack{\langle i,j \rangle \\ \sigma}} c^{\dagger}_{i,\sigma} c_{j,\sigma} + U \sum_{i} n_{i,\uparrow} n_{i,\downarrow}$$

for a very small system. Considering a system with $N = 2$ sites and one electron per spin is the smallest system that makes sense. Furthermore, we forbid hopping across the boundaries.

This system has four different basis states, depicted in Equation (1.10), and is described by the Hamiltonian

$$H = \begin{pmatrix} U & -t & -t & 0 \\ -t & 0 & 0 & -t \\ -t & 0 & 0 & -t \\ 0 & -t & -t & U \end{pmatrix} . \tag{1.9}$$

$$
\begin{aligned}
|\,\Gamma_1\,\rangle &= c^\dagger_{1,\uparrow}\, c^\dagger_{1,\downarrow}\,|\,0\,\rangle \qquad \widehat{=} \\
|\,\Gamma_2\,\rangle &= c^\dagger_{1,\uparrow}\, c^\dagger_{2,\downarrow}\,|\,0\,\rangle \qquad \widehat{=} \\
|\,\Gamma_3\,\rangle &= c^\dagger_{2,\uparrow}\, c^\dagger_{1,\downarrow}\,|\,0\,\rangle \qquad \widehat{=} \\
|\,\Gamma_4\,\rangle &= c^\dagger_{2,\uparrow}\, c^\dagger_{2,\downarrow}\,|\,0\,\rangle \qquad \widehat{=}
\end{aligned}
$$

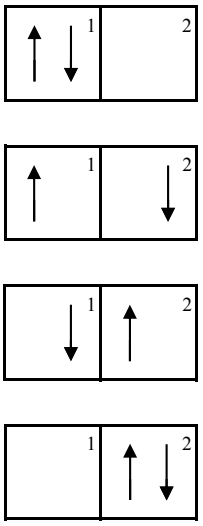

(1.10)

The eigenvalues of H, as it is generally known, are the roots of the secular equation, resulting from

$$\det\left(H - \lambda E\right) \,=\, 0 \quad ,$$

whereby E is the identity matrix. To calculate the determinant, we do an expansion in the first column and obtain

$$
\begin{vmatrix}
U-\lambda & -t & -t & 0 \\
-t & -\lambda & 0 & -t \\
-t & 0 & -\lambda & -t \\
0 & -t & -t & U-\lambda
\end{vmatrix} = 0
$$

$$
0 = (U-\lambda)\underbrace{\begin{vmatrix} -\lambda & 0 & -t \\ 0 & -\lambda & -t \\ -t & -t & U-\lambda \end{vmatrix}}_{①} + t\underbrace{\begin{vmatrix} -t & -t & 0 \\ 0 & -\lambda & -t \\ -t & -t & U-\lambda \end{vmatrix}}_{②} - t\underbrace{\begin{vmatrix} -t & -t & 0 \\ -\lambda & 0 & -t \\ -t & -t & U-\lambda \end{vmatrix}}_{③} \quad . \tag{1.11}
$$

The determinants in Equation (1.11) yield

$$
\begin{aligned}
① &= -\lambda\left((-\lambda)(U-\lambda) - t^2\right) + t^2\lambda \,=\, -\lambda^3 + \lambda^2 U + 2\lambda t^2 \\
② &= -t\left((-\lambda)(U-\lambda) - t^2\right) - t^3 \,=\, -\lambda^2 t + \lambda t U \\
③ &= t(t^2 - t^2) + (U-\lambda)(-\lambda t) \,=\, \lambda^2 t - \lambda t U \quad .
\end{aligned}
$$

Hence, the characteristic polynomial is given by

$$
\begin{aligned}
0 &= (U-\lambda)\left(-\lambda^3 + \lambda^2 U + 2\lambda t^2\right) + t\left(-\lambda^2 t + \lambda t U\right) - t\left(\lambda^2 t - \lambda t U\right) \\
0 &= \lambda^4 + \lambda^3(-2U) + \lambda^2(U - 4t^2) + \lambda(4t^2 U) \quad ,
\end{aligned}
$$

with analytically computable roots

$$\begin{aligned}
\lambda_1 &= 0 \quad , \\
\lambda_2 &= U \quad , \\
\lambda_3 &= \frac{1}{2}\left(U + \sqrt{16t^2 + U^2}\right) \quad \text{and} \\
\lambda_4 &= \frac{1}{2}\left(U - \sqrt{16t^2 + U^2}\right) \quad .
\end{aligned}$$

Since $U > 0$ and $t > 0$ the smallest eigenvalue of H is given by λ_4, which corresponds to the groundstate energy ϵ_0 of the system.

Next, we calculate the coefficients c_ν of the groundstate wavefunction

$$|\,\Phi_0\,\rangle \;=\; \sum_{\nu=1}^{4} c_\nu\,|\,\Gamma_\nu\,\rangle \quad ,$$

which lead to the following system of linear equations,

$$\begin{pmatrix} U-\epsilon_0 & -t & -t & 0 \\ -t & -\epsilon_0 & 0 & -t \\ -t & 0 & -\epsilon_0 & -t \\ 0 & -t & -t & U-\epsilon_0 \end{pmatrix} \cdot \begin{pmatrix} c_1 \\ c_2 \\ c_3 \\ c_4 \end{pmatrix} \;=\; 0 \tag{1.12}$$

respectively, using the abbreviation $S = \sqrt{16t^2 + U^2}$ to

$$0 = (U+S)\,\frac{1}{2}\,c_1 - t\,c_2 - t\,c_3 \tag{1.13}$$

$$0 = -\,t\,c_1 + (S-U)\,\frac{1}{2}\,c_2 - t\,c_4 \tag{1.14}$$

$$0 = -\,t\,c_1 + (S-U)\,\frac{1}{2}\,c_3 - t\,c_4 \tag{1.15}$$

$$0 = -\,t\,c_2 - t\,c_3 + (U+S)\,\frac{1}{2}\,c_4 \tag{1.16}$$

$$\tag{1.17}$$

Substracting Equation (1.13) from (1.16) respectively (1.14) from (1.15) yields

$$c_1 \;=\; c_4 \quad \text{and} \quad c_2 \;=\; c_3 \quad .$$

By comparing Equation (1.13) and (1.14) we obtain

$$\begin{aligned}
(U+S)\,\frac{1}{2}\,c_1 - 2t\,c_2 &= -\,2t\,c_1 + (S-U)\,\frac{1}{2}\,c_2 \\
c_2 &= \frac{4t+U+S}{4t-U+S}\,c_1 \\
c_2 &= \frac{4t+U+S}{4t-U+S}\,\frac{4t}{U+S}\,\frac{U+S}{4t}\,c_1 \\
c_2 &= \frac{16t^2+4tU+4tS}{4tU-U^2+US+4tS-US+S^2}\,\frac{U+S}{4t}\,c_1 \\
c_2 &= \frac{16t^2+4tU+4tS}{4tU-U^2+4tS+16t^2+U^2}\,\frac{U+S}{4t}\,c_1 \\
c_2 &= \frac{U+S}{4t}\,c_1 \quad .
\end{aligned}$$

Thus, the set of linear equations is solved and the groundstate wavefunction (not normalised) results in

$$|\,\Phi_0\,\rangle \;=\; |\,\Gamma_1\,\rangle + \frac{U+\sqrt{16t^2+U^2}}{4t}\,|\,\Gamma_2\,\rangle + \frac{U+\sqrt{16t^2+U^2}}{4t}\,|\,\Gamma_3\,\rangle + |\,\Gamma_4\,\rangle \quad , \tag{1.18}$$

as also shown in Ref [3]. As one can see, the groundstate is a linear combination of the four basis states, but those without double occupations ($|\,\Gamma_2\,\rangle$ and $|\,\Gamma_3\,\rangle$) are energetically favorable and therefore weighted more strongly.

1.4. The size of the Hilbert Space

In the previous Section, we did an analytical calculation to obtain the exact groundstate wavefunction for a very small system of the Hubbard Hamiltonian. Of course, this procedure is not feasible if one wants to treat larger system sizes.
In this Section, we want to demonstrate that this is also a difficult task for numerical methods, due to the size of the Hilbert space N_H.

Let us consider a system with $N_\uparrow$ electrons with spin up and $N_\downarrow$ electrons with spin down on N lattice sites. Thus, the number of basis states is determined by Equation (1.19), which increases exponentially with the system size.

$$N_H \;=\; \binom{N}{N_\uparrow} \cdot \binom{N}{N_\downarrow} \tag{1.19}$$

That means, if one uses, for example, the Lanczos algorithm to calculate the ground state of the Hamiltonian, one has to store three vectors of length N_B, datatype `double` [4]. To store a variable of type `double` on a 32 bit system, one typically needs 8 bytes.
Table 1.1 lists the size of the Hilbert space N_H and the memory requirements to store three lanczos vectors of that size, for different systems of the Hubbard model. One realises that the storage capacity of today's computers limits an exact diagonalisation to small systems.
This is why one searches for other methods, such as Diffusion Monte Carlo, to calculate groundstate properties of the Hubbard model, which do not require such a huge main memory.

Table 1.1.: Comparison of the required memory to store three lancos vectors for different system sizes of the Hubbard model.

sites N	$N_\uparrow$	$N_\downarrow$	Hilbert Space N_H	required memory	
4	2	2	36	864	B
8	4	4	4900	117.6	kB
10	5	5	63504	1.5	MB
16	5	5	19.0794e+06	457.9	MB
16	8	8	165.6369e+06	4.0	GB
18	9	9	2.3639e+09	56.7	GB
20	10	10	34.1348e+09	819.2	GB
26	13	13	108.1725e+12	2.6	PB*
36	18	18	82.3581e+18	2.0	ZB**

* petabyte (PB) = 10^{15} byte
** zettabyte (ZB) = 10^{21} byte

2. Diffusion Monte Carlo

To describe the time evolution of an arbitrary state $|\,\psi\,\rangle = \sum_\nu c_\nu\,|\,\chi_\nu\,\rangle$ in a quantum mechanical system, represented by the Hamiltonian $\hat{H}$, one usually starts with the time - dependent Schrödinger equation (2.1). (In this context the $|\,\chi_\nu\,\rangle$ denote basis states of the Hamiltonian.)

$$\mathrm{i}\hbar\frac{\partial}{\partial t}\,|\,\psi\,\rangle \;=\; \hat{H}\,|\,\psi\,\rangle \tag{2.1}$$

If the Hamiltonian does not depend on time, the time evolution operator is simple

$$\hat{U}(t,\,t_0) = \mathrm{e}^{-\frac{\mathrm{i}}{\hbar}(t-t_0)\hat{H}}$$

and we obtain

$$|\,\psi(t)\,\rangle \;=\; \mathrm{e}^{-\frac{\mathrm{i}}{\hbar}(t-t_0)\hat{H}}\,|\,\psi(t_0)\,\rangle \quad .$$

Next, we perform the transformation $\tau = \mathrm{i}\cdot t$, called Wicks rotation of time and adopt time units in which Planck's constant is unity. Furthermore, we introduced an energy shift S.

$$|\,\psi_{(\tau)}\,\rangle \;=\; \mathrm{e}^{-\tau(\hat{H}-S)}\,|\,\psi_{(0)}\,\rangle \tag{2.2}$$

It can be shown [5], that in the long time limit, ψ_τ converges to the groundstate wavefunction Φ_0 of the Hamiltonian, if

- $\psi_{(0)}$ has a non - vanishing overlap with the groundstate Φ_0,
- the groundstate energy ϵ_0 is not degenerated[1] and
- the energy shift S is the exact, at this time unknown, groundstate energy of the system.

$$\begin{aligned}|\,\psi_{(\tau)}\,\rangle \;&=\mathrm{e}^{-\tau(\hat{H}-S)}\,|\,\psi_{(0)}\,\rangle \;=\; \mathrm{e}^{-\tau(\hat{H}-S)}\underbrace{\sum_i |\,\Phi_i\,\rangle\langle\,\Phi_i\,|}_{\hat{\mathbb{1}}}\,|\,\psi_{(0)}\,\rangle \;=\; \mathrm{e}^{-\tau(\hat{H}-S)}\sum_i \underbrace{\langle\,\Phi_i\,|\,\psi_{\tau=0}\,\rangle}_{d_i}\,|\,\Phi_i\,\rangle \\ &= \sum_i \mathrm{e}^{-\tau(\hat{H}-S)}\,d_i\,|\,\Phi_i\,\rangle \;=\; \sum_i \mathrm{e}^{-\tau(\epsilon_i-S)}\,d_i\,|\,\Phi_i\,\rangle\end{aligned}$$

In the previous lines, we first inserted a complete set of eigenvectors of the Hamiltonian and subsequently replaced $\hat{H}$ by its eigenvalues ϵ_i.

$$\begin{aligned}&= \mathrm{e}^{-\tau(\epsilon_0-S)}\,d_0\,|\,\Phi_0\,\rangle + \sum_{i=1}\mathrm{e}^{-\tau(\epsilon_i-S)}\,d_i\,|\,\Phi_i\,\rangle \\ &= d_0\,\mathrm{e}^{-\tau(\epsilon_0-S)}\left(|\,\Phi_0\,\rangle + \sum_{i=1}\mathrm{e}^{-\tau(\epsilon_i-S)+\tau(\epsilon_0-S)}\,\frac{d_i}{d_0}\,|\,\Phi_i\,\rangle\right) \\ &= d_0\,\mathrm{e}^{-\tau(\epsilon_0-S)}\left(|\,\Phi_0\,\rangle + \sum_{i=1}\mathrm{e}^{\underbrace{-\tau\left(\epsilon_i-\epsilon_0\right)}_{>0}}\,\frac{d_i}{d_0}\,|\,\Phi_i\,\rangle\right)\end{aligned}$$

[1] If it is degenerated, $\psi_{(\tau)}$ converges to an arbitrary linear combination of degenerated groundstate wavefunctions.

$$\lim_{\tau\to\infty} |\,\psi_\tau\,\rangle \;=\; \lim_{\tau\to\infty} d_0\, \mathrm{e}^{-\tau(\epsilon_0 - S)} \left(|\,\Phi_0\,\rangle + \sum_{i=1} \mathrm{e}^{-\tau(\epsilon_i-\epsilon_0)}\, \frac{d_i}{d_0}\, |\,\Phi_i\,\rangle \right) \;=\; |\,\Phi_0\,\rangle \tag{2.3}$$

The main task of Diffusion Monte Carlo (DMC) is to perform the long time limit in Equation (2.3) in a stochastic way. In order to realise this aim, one introduces an artificial object, called walker. Each walker occupies a basis state χ_ν of the Hamiltonian and is able to propagate through the Hilbert space randomly.
While its movement through configuration space, every walker can spawn progeny and is also able to die. The destiny of each walker depends on the one hand on its state χ_ν and furthermore on the Hamiltonian $\hat{H}$. On the other hand, the energy shift S controls the walker population. That means, if the groundstate energy is less than the energy shift, the mean number of walkers increases and vice versa [6]. This fact follows directly from Equation (2.3).

$$\begin{aligned} S < \epsilon_0 \qquad &\rightarrow \qquad \lim_{\tau\to\infty} |\,\psi_{(\tau)}\,\rangle \;=\; \lim_{\tau\to\infty} d_0\, \mathrm{e}^{-\tau(\epsilon_0 - S)}\, |\,\Phi_0\,\rangle \;=\; 0 \\ S > \epsilon_0 \qquad &\rightarrow \qquad \lim_{\tau\to\infty} |\,\psi_{(\tau)}\,\rangle \;=\; \lim_{\tau\to\infty} d_0\, \mathrm{e}^{-\tau(\epsilon_0 - S)}\, |\,\Phi_0\,\rangle \;=\; \infty \end{aligned}$$

The exact rules, how this population dynamics are realised, differ from algorithm to algorithm. (cf. Section 2.2 and 2.3)
If the groundstate wavefunction Φ_0 of the Hamiltonian is strictly positive, that means

$$\langle\, \chi_\nu \,|\, \Phi_0 \,\rangle \;=\; c_\nu \;, \qquad c_\nu \geq 0 \quad \forall \nu \;, \qquad \sum_\nu c_\nu = 1 \;, \tag{2.4}$$

one can interpret Φ_0 as a probability density function (pdf). Under these circumstances and if the current walker population propageted sufficiently long in imaginary time (thermalisation time of the MC algorithm), that all excited eigenstates of the Hamiltonian decayed to zero, the walkers are distributed proportionally to the groundstate wavefunction Φ_0. In other words, basis states χ_ν of the groundstate with a large coefficient c_ν are occupied more often by walkers than those with a small coefficient.
All walkers of the simulation (afterwards named walker configuration or a generation of walkers) at particular time τ give a represenation of a wavefunction

$$|\,\psi_{(\tau)}\,\rangle \;=\; \sum_\nu n_\nu(\tau)\, |\,\chi_\nu\,\rangle \;, \qquad n_\nu(\tau) \in \mathbb{N}_0 \quad ,$$

whereby $n_\nu(\tau)$ is the number of walkers in state $|\,\chi_\nu\,\rangle$. The expectation value of such wavefunctions is proportional to the groundstate of the Hamiltonian $\hat{H}$.

$$|\,\Phi_0\,\rangle \;\propto\; \langle\, |\,\psi_{(\tau)}\,\rangle \,\rangle \;=\; \left\langle \sum_\nu n_\nu(\tau)\, |\,\chi_\nu\,\rangle \right\rangle \;=\; \sum_\nu \langle n_\nu(\tau)\rangle\, |\,\chi_\nu\,\rangle \;\propto\; \sum_\nu c_\nu\, |\,\chi_\nu\,\rangle \tag{2.5}$$

In Equation (2.5) we used the fact that the expectation value of a multinomial distributed random number is proportional to its probability of occurrence.

In the next Section, we describe how to calculate the expectation value of an observable using DMC. In Section 2.2 respectively 2.3, two different DMC algorithms are presented and in Section 2.4 the meaning of the guiding respectively the trial function is discussed.

2.1. The expectation value of a quantum mechanical operator

The expectation value of a quantum mechanical operator $\hat{O}$, given an arbitrary wavefunction $|\Psi\rangle$, is usually

$$\left\langle \hat{O} \right\rangle = \frac{\langle \Psi | \hat{O} | \Psi \rangle}{\langle \Psi | \Psi \rangle} \quad .$$

If the wavefunction is generated using DMC, this exercise is a little bit more complicated. Let us start, given a single walker configuration at a specific imaginary time τ, represented by the wavefunction $\psi_{(\tau)}$, then the expectation value $\hat{O}_{(\tau)}$ is calculated in exactly the same manner as mentioned above.

$$\hat{O}_{(\tau)} = \frac{\langle \psi_{(\tau)} | \hat{O} | \psi_{(\tau)} \rangle}{\langle \psi_{(\tau)} | \psi_{(\tau)} \rangle} = \frac{\sum_{\nu,\nu'} n_\nu(\tau)\, n_{\nu'}(\tau) \langle \chi_\nu | \hat{O} | \chi_{\nu'} \rangle}{\sum_{\nu,\nu'} n_\nu(\tau)\, n_{\nu'}(\tau) \langle \chi_\nu | \chi_{\nu'} \rangle} = \frac{\sum_{\nu,\nu'} n_\nu(\tau)\, n_{\nu'}(\tau) \langle \chi_\nu | \hat{O} | \chi_{\nu'} \rangle}{\sum_\nu n_\nu(\tau)^2}$$

However, to obtain a more appropriate estimation for the expectation value of an observable $\hat{O}$ in the groundstate wavefunction, we need several (in the best case an endless number), as uncorrelated as possible, different walker configurations $\psi_{(\tau)}$. In addition, it is very important to average the numerator and the denominator separately before they are divided by each other.

$$\overline{\hat{O}_{(\tau)}} = \frac{\overline{\langle \psi_{(\tau)} | \hat{O} | \psi_{(\tau)} \rangle}}{\overline{\langle \psi_{(\tau)} | \psi_{(\tau)} \rangle}} = \frac{\sum_\tau \left(\sum_{\nu,\nu'} n_\nu(\tau)\, n_{\nu'}(\tau) \langle \chi_\nu | \hat{O} | \chi_{\nu'} \rangle \right)}{\sum_\tau \left(\sum_\nu n_\nu(\tau)^2 \right)} \tag{2.6}$$

Next, we discuss the ideal case, described in the previous lines, by means of the numerator of Equation (2.6). That means, we are able to replace the arithmetic mean $\sum_\tau(\ \dots\ )$ by the expectation value $\langle\ \dots\ \rangle$.

$$\begin{aligned} \left\langle \langle \psi_{(\tau)} | \hat{O} | \psi_{(\tau)} \rangle \right\rangle = \left\langle \sum_{\nu,\nu'} n_\nu(\tau)\, n_{\nu'}(\tau) \langle \chi_\nu | \hat{O} | \chi_{\nu'} \rangle \right\rangle = \sum_{\nu,\nu'} \langle n_\nu(\tau)\, n_{\nu'}(\tau) \rangle \langle \chi_\nu | \hat{O} | \chi_{\nu'} \rangle \neq \\ \neq \sum_{\nu,\nu'} \langle n_\nu(\tau) \rangle \langle n_{\nu'}(\tau) \rangle \langle \chi_\nu | \hat{O} | \chi_{\nu'} \rangle \propto \sum_{\nu,\nu'} c_\nu\, c_{\nu'} \langle \chi_\nu | \hat{O} | \chi_{\nu'} \rangle = \langle \Phi_0 | \hat{O} | \Phi_0 \rangle \end{aligned} \tag{2.7}$$

To repeat the quintessence of Equation (2.7), even if there is an endless number of walker configurations, there is a systematic error in our calculation because

$$\sum_{\nu,\nu'} \langle n_\nu\, n_{\nu'} \rangle \neq \sum_{\nu,\nu'} \langle n_\nu \rangle \langle n_{\nu'} \rangle \quad .$$

It is possible to prevent this error if one calulates the so called *mixed estimator* [5]. This involves replacing one of the $\psi_{(\tau)}$'s with a trial wavefunction $|\Psi_T\rangle = \sum_\nu a_\nu |\chi_\nu\rangle$, when calculating the expectation value of an operator.

$$\hat{O}_{(\tau)} = \frac{\langle \Psi_T | \hat{O} | \psi_{(\tau)} \rangle}{\langle \Psi_T | \psi_{(\tau)} \rangle} \tag{2.8}$$

Typically, this trial state Ψ_T is either a walker configuration, which already gives a quite good approach for Φ_0, or some kind of analytical approximation for the groundstate of the system. But keep in mind that Ψ_T is not a random variable anymore.

Therefore, if we consider the special case that $\hat{O} = \hat{H}$, we obtain the true groundstate energy of the system, otherwise the result would be variational.

$$\begin{aligned}\left\langle \hat{H} \right\rangle &= \frac{\left\langle \langle \Psi_T \,|\, \hat{H} \,|\, \psi_{(\tau)} \rangle \right\rangle}{\left\langle \langle \Psi_T \,|\, \psi_{(\tau)} \rangle \right\rangle} = \frac{\left\langle \sum_{\nu,\nu'} a_\nu \, n_{\nu'}(\tau) \, \langle \chi_\nu \,|\, \hat{H} \,|\, \chi_{\nu'} \rangle \right\rangle}{\left\langle \sum_{\nu,\nu'} a_\nu \, n_{\nu'}(\tau) \, \langle \chi_\nu \,|\, \chi_{\nu'} \rangle \right\rangle} \\ &= \frac{\sum_{\nu,\nu'} a_\nu \, \langle n_{\nu'}(\tau) \rangle \, \langle \chi_\nu \,|\, \hat{H} \,|\, \chi_{\nu'} \rangle}{\sum_{\nu,\nu'} a_\nu \, \langle n_{\nu'}(\tau) \rangle \, \langle \chi_\nu \,|\, \chi_{\nu'} \rangle} = \frac{\sum_{\nu,\nu'} a_\nu \, c_{\nu'} \, \langle \chi_\nu \,|\, \hat{H} \,|\, \chi_{\nu'} \rangle}{\sum_{\nu,\nu'} a_\nu \, c_{\nu'} \, \langle \chi_\nu \,|\, \chi_{\nu'} \rangle} \\ &= \frac{\langle \Psi_T \,|\, \hat{H} \,|\, \Phi_0 \rangle}{\langle \Psi_T \,|\, \Phi_0 \rangle} = \epsilon_0 \frac{\langle \Psi_T \,|\, \Phi_0 \rangle}{\langle \Psi_T \,|\, \Phi_0 \rangle} = \epsilon_0\end{aligned} \tag{2.9}$$

Furthermore, it can be demonstrated that the expectation value of an estimator

$$E^* = \frac{\overline{\langle \Psi_T \,|\, \hat{H} \,|\, \psi_{(\tau)} \rangle}}{\overline{\langle \Psi_T \,|\, \psi_{(\tau)} \rangle}} \tag{2.10}$$

is biased of order $1/N$, whereby N denotes the number of walker configurations [7].

$$\langle E^* \rangle = \epsilon_0 + \mathcal{O}(1/N) \tag{2.11}$$

But there are analytical and numerical methods to remove this bias, see Appendix A for further details.

2.2. Algorithm a la Ceperley / Alavi

In Equation (2.3), we showed that an arbitrary wavefunction converges in the long time limit, under certain conditions, to the true groundstate of the Hamiltonian. In this Section, we present a DMC algorithm to perform this long time limit to obtain walker configurations according to the groundstate wavefunction.

If one accepts small time step errors, the imaginary time propagator $\mathrm{e}^{-\tau(\hat{H}-S)}$ can be linearised, in the following way, as also demonstrated in [8, p. 3].

$$\mathrm{e}^{-\tau(\hat{H}-S)} \overset{n\cdot\Delta\tau=\tau}{=} \left(\mathrm{e}^{-\Delta\tau(\hat{H}-S)}\right)^n = \left(\hat{\mathbb{1}} - \Delta\tau(\hat{H}-S) + \mathcal{O}(\Delta\tau^2)\right)^n \approx \left(\hat{\mathbb{1}} - \Delta\tau(\hat{H}-S)\right)^n \tag{2.12}$$

It is easy to see that in the limit of $\Delta\tau \to 0$ and $n \to \infty$ the approach in Equation (2.12) becomes exact again.
In Ref. [5] and [9] the imaginary time propagation of the walkers is divided into discrete time steps $\Delta\tau$, whereby the walker configuration after n time steps is generated from the preceding walker configuration, by applying the Green function G.

$$|\, \psi_{(n)} \rangle = G \,|\, \psi_{(n-1)} \rangle = \left(\hat{\mathbb{1}} - \Delta\tau(\hat{H}-S)\right) |\, \psi_{(n-1)} \rangle \tag{2.13}$$

The Green function G in (2.13) (introduced to remain consistent with nomenclature of A. Alavi and D.M. Ceperley) causes a change of populations on each basis state proportional to $\Delta\tau$. Hence, $\Delta\tau$ is a very important parameter of the simulation, which has to be calibrated in the right way.
If the time step $\Delta\tau$ is chosen appropriately, as discussed in Ref. [5], the repeated application of G to an initial set of walkers $\psi_{(0)}$ achieves that in the long time limit the walkers are distributed according to the groundstate wavefunction Φ_0 of the Hamiltonian.

In case the time step is too large, the excited eigenstates of the Hamiltonian do not decay to zero with time [9]. On the other hand, a small $\Delta\tau$ leads to minor modifications of the walker population per time step, that means $\psi_{(n)}$ and $\psi_{(n+1)}$ do not differ greatly from each other. To compensate this, one requires either a longer simulation or an additional ingredient to the algorithm, called *contiuous time* [10].

The first walker generation of the simulation $\psi_{(0)}$ is commonly generated proportionally to a trial state Ψ_T [6], whereby Ψ_T is a reasonable good guess for the groundstate wavefunction of the system.
For the special case of the Hubbard Hamiltonian, there is an additional possibility to distribute the walkers. If one only considers the diagonal elements of $\hat{H}$, it is pretty easy to extract those basis states χ_ν, which are energetically favorable. That means in real space, states without double occupations and in reciprocal space, states with a specific wavevector k. Typically, one selects basis states with zero momentum.
But, if the groundstate wavefunction does not have momentum zero and the initial walker configuration has, one never reaches the groundstate within the DMC run. This is obvious, because the Hubbard Hamiltonian in k-space conserves momentum, as described in Section 1.2.

$$\langle\, \Phi_0(k \neq 0) \,|\, G^n \,|\, \psi_{(0)}(k = 0) \,\rangle \;=\; \langle\, \Phi_0(k \neq 0) \,|\, \psi_{(n)}(k = 0) \,\rangle \;=\; 0$$

2.2.1. The fermion sign

In Ref. [5], DMC is used to treat a Bose system. As a consequence, the propagator G and the groundstate wavefunction Φ_0 are both non-negative. That means, a walker configuration $\psi_{(\tau)}$ can be thought of a probability density.
For systems with interacting fermions, this condition does not hold [6]. For this reason, the artificial object walker gets an extra attribute, the sign. Hence, each walker carries a positive or a negative sign, while its propagation through the Hilbert space [9] and therefore one earns the possibilty to represent the antisymmetries of a femionic wavefunction using a walker configuration $\psi_{(\tau)}$.

$$|\, \psi_{(\tau)} \,\rangle \;=\; \sum_\nu \underline{n_\nu}(\tau) \,|\, \chi_\nu \,\rangle \;=\; \sum_\nu s_\nu \, n_\nu(\tau) \,|\, \chi_\nu \,\rangle \;, \qquad s_\nu \in \{1, -1\} \;, \quad n_\nu(\tau) \in \mathbb{N}_0 \tag{2.14}$$

2.2.2. Population dynamics

The authors of Ref. [9] developed a population dynamics algorithm consisting of three basic processes. By applying these rules to each walker at any time step, the propagation of the walkers in configuration space is controlled.

i) *The diagonal death / cloning process*:
For each walker one has to compute

$$p_1 \;=\; \Delta\tau(H_{\nu,\nu} - S) \quad . \tag{2.15}$$

If $p_1 > 0$, the walker dies with the probability p_1. Thereby, the move of this walker through configuration space is terminated and it is not part of the next generation.
If $p_1 < 0$, the walker is cloned with the probability $|\, p_1 \,|$.

ii) *The spawning process*:
With probability

$$p_2 \;=\; \Delta\tau |\, H_{\nu,\nu'} \,| \quad , \tag{2.16}$$

the walker spawns progeny on the basis state $\chi_{\nu'}$. The newly created walker has the same sign as its parent, if $H_{\nu,\nu'} < 0$, and the opposite one, otherwise.
It is noteworthy that every walker has only once the possibility per time step to spawn progeny.

With probability $p_3 = 1 - p_1 - p_2$ a walker remains in its state and is part of the next generation without any changes.

iii) *The annihilation step*:
Both steps, i) and ii), can be applied to a walker independently to all other ones until the global annihilation step follows. That means, if two walkers with opposite sign occupy the same basis state, these two walkers are removed from the simulation and the population is reduced by two, schematically depicted in Figure (2.1). This process is a major ingredient of the algorithm and helps to reduce the minus sign problem (see Chapter 4).

The above listed rules result in an algorithm with an underlying imaginary time propagator defined in Equation (2.13), as verified in the following master equation [11].

$$\begin{aligned}
\underline{n_\nu^{(\tau)}} &= s_\nu \, n_\nu^{(\tau)} \\
\Delta\hat{H} &= \begin{cases} H_{\nu,\nu'} - S & \text{if } \nu = \nu' \\ H_{\nu,\nu'} & \text{if } \nu \neq \nu' \end{cases}
\end{aligned}$$

$\underline{n_\nu^{(\tau)}}$ means, that at time τ basis state χ_ν is occupied by n walkers with sign s, $\Delta\hat{H}$ is merely an abbreviation. Using step i) and ii), one is able to describe the change of the walker population during a time step.

$$\begin{aligned}
\underline{n_\nu^{(\tau+1)}} &= \underline{n_\nu^{(\tau)}} - 1 \cdot p_1 \, \underline{n_\nu^{(\tau)}} + 1 \cdot \sum_{\nu' \neq \nu} p_2 \, \underline{n_{\nu'}^{(\tau)}} \\
\underline{n_\nu^{(\tau+1)}} &= \underline{n_\nu^{(\tau)}} - 1 \cdot \Delta\tau \Delta H_{\nu,\nu} \, \underline{n_\nu^{(\tau)}} + 1 \cdot \sum_{\nu' \neq \nu} \Delta\tau |\, \Delta H_{\nu,\nu'} \,| \, \underline{n_{\nu'}^{(\tau)}} \\
\underline{n_\nu^{(\tau+1)}} &= \underline{n_\nu^{(\tau)}} - 1 \cdot \Delta\tau \Delta H_{\nu,\nu} \, \underline{n_\nu^{(\tau)}} - 1 \cdot \sum_{\nu' \neq \nu} \Delta\tau \, \Delta H_{\nu,\nu'} \, \underline{n_{\nu'}^{(\tau)}} \\
\underline{n_\nu^{(\tau+1)}} &= \underline{n_\nu^{(\tau)}} - \sum_{\nu'} \Delta\tau \Delta H_{\nu,\nu'} \, \underline{n_{\nu'}^{(\tau)}} \\
\underline{n_\nu^{(\tau+1)}} &= \sum_{\nu'} \left(\delta_{\nu,\nu'} - \Delta\tau \Delta H_{\nu,\nu'} \right) \underline{n_{\nu'}^{(\tau)}} \\
|\, \psi_{(\tau+1)} \,\rangle &= \left(\hat{\mathbb{1}} - \Delta\tau \Delta\hat{H} \right) |\, \psi_{(\tau)} \,\rangle = G \,|\, \psi_{(\tau)} \,\rangle
\end{aligned}$$

During this derivation, the relation

$$|\, \Delta H_{\nu,\nu'} \,| \, \underline{n_\nu^{(\tau)}} = s_H \Delta H_{\nu,\nu'} \, s_\nu \, n_\nu^{(\tau)} = \begin{cases} (-1) \, \Delta H_{\nu,\nu'} \, (+1) \, s_\nu \, n_\nu^{(\tau)} & \text{if } H_{\nu,\nu'} < 0 \\ (+1) \, \Delta H_{\nu,\nu'} \, (-1) \, s_\nu \, n_\nu^{(\tau)} & \text{if } H_{\nu,\nu'} > 0 \end{cases},$$

which follows directly from ii), was used. In this context, s_H denotes the sign of the off-diagonal elements of the Hamiltonian.

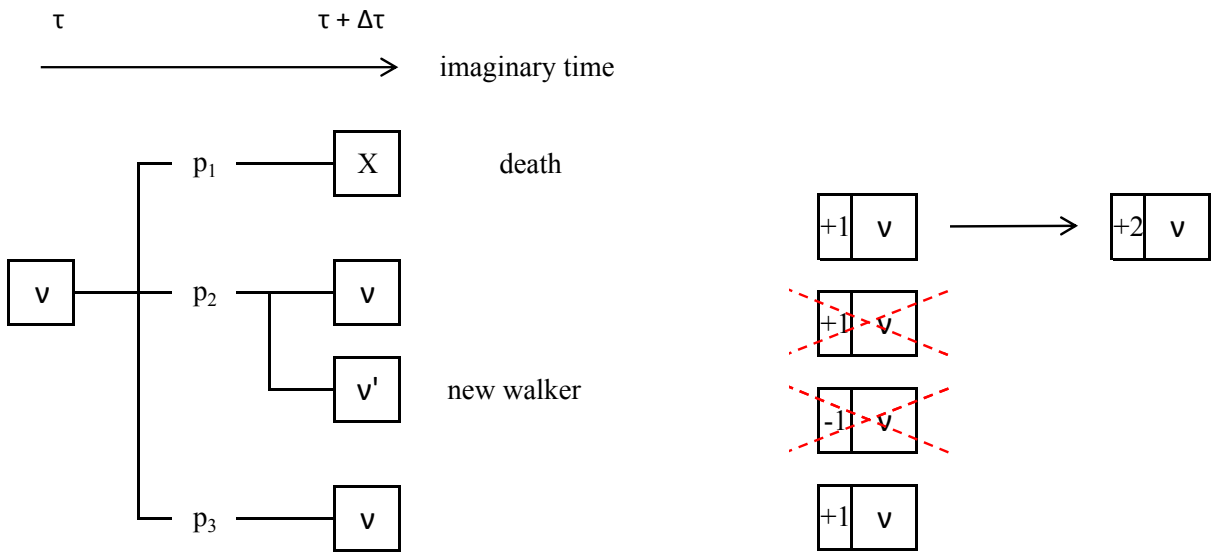

Figure 2.1.: Schematic illustration of the fundamental processes of the algorithm described in Section 2.2.2.
The opportunities of each walker occupying state χ_ν at time τ (death or spawning) are shown on the left hand side. On the right hand side an example for annihilation is pictured, assuming four walkers are in state χ_ν, three of them with sign $+1$ and one walker with sign -1.

2.2.3. Application to the Hubbard Hamiltonian in reciprocal space

This Section describes an effective implementation of the spawning process (Section 2.2.2) for the Hubbard Hamiltonian in reciprocal space, Equation (2.17).

$$\hat{H} = \sum_{\substack{k \\ \sigma}} \epsilon_k \, c^\dagger_{k,\sigma} \, c_{k,\sigma} + \frac{U}{N} \sum_q \rho_q \, \rho_{-q} \tag{2.17}$$

In Equation (2.17), ϵ_k is the die dispersion relationship of the kinetic energy and U/N is the absolute value of the off-diagonal elements, whereby N denotes the number of sites of the system. See Section 1.2 for details.
Suppose a walker occupies a basis state χ_ν, then the probability to spawn a new walker on state $\chi_{\nu'}$ within the next time step is

$$p_2 = \Delta\tau | \, H_{\nu,\nu'} \, | \quad .$$

If one wants to implement this process brute force, one usually generates a uniformly distributed random number $r \in U(0,1)$ and checks if r is in the intervall $[0, p_2]$ or not. This procedure must be repeated for every basis state to which this walker can spawn onto. In k-space, $\hat{H}$ has a lot of nonzero off-diagonal elements, which make this technique very ineffective.
Therefore, one divides the spawning event into three steps, using the fact that the maximum number of off-diagonal elements is

$$N_\sigma \cdot (N - N_\sigma) \cdot N_{\overline{\sigma}} \quad ,$$

whereby N_σ denotes the number of electrons with spin σ.

- Step 1: Compute
$$\tilde{p_2} \;=\; \Delta\tau \,\frac{U}{N}\, N_\sigma \,(N - N_\sigma)\, N_{\overline{\sigma}} \quad ,$$
which gives the maximal probability, that a spawning event occurs to this walker in general and check if a random number $r \in U(0,1)$ is in the intervall $[0, \tilde{p_2}]$.

- Step 2: Choose an electron with spin σ randomly and let it scatter into a free hole, also chosen randomly. The probability for this process is
$$p_S(\sigma) \;=\; \frac{1}{N_\sigma}\,\frac{1}{(N - N_\sigma)} \quad .$$

- Step 3: Choose an electron with spin $\overline{\sigma}$ randomly and check if the total scattering process is possible, under the constraint, that momentum is conserved.
$$p_S(\overline{\sigma}) \;=\; \begin{cases} 1/N_{\overline{\sigma}} & \text{if possible} \\ 0 & \text{otherwise} \end{cases}$$

These three steps can be realized independently and together they result in the orginal spawning probability p_2.

$$\tilde{p_2} \cdot p_S(\sigma) \cdot p_S(\overline{\sigma}) \;=\; \Delta\tau \,\frac{U}{N}\, N_\sigma \,(N - N_\sigma)\, N_{\overline{\sigma}} \cdot \frac{1}{N_\sigma}\,\frac{1}{(N - N_\sigma)} \cdot \frac{1}{N_{\overline{\sigma}}} \;=\; \Delta\tau |\, H_{\nu,\nu'} \,| \;=\; p_2$$

2.3. Algorithm a la Schmidt

The authors of Ref. [12] developed an algorithm to sample the imaginary time propagator

$$G(\tau) \;=\; \mathrm{e}^{-\tau(\hat{H} - S)}$$

without any time step error. In contrast to, for example Ref. [5], they do not linearise G but they did a transformation, which results in an integral equation. Then probability theory is used to get rules to control the propagation of each walker through the configuration space. In this Section this DMC algorithm is described.

Suppose there is a known Green function $G^0(\tau)$ for a Hamiltonian $\hat{H}^0$, which satisfies Equation (2.18). Then it is possible to form a relationship to the full imaginary time Green function $G(\tau)$.

$$\left(\hat{H}^0 - S\right) G^0(\tau) \;=\; -\,\frac{\partial G^0(\tau)}{\partial \tau} \tag{2.18}$$

If one considers the Hubbard Hamiltonian in reciprocal space, for example, this known $\hat{H}^0$ would be the contribution of the kinetic energy to $\hat{H}$.
In order to deduce the abovementioned connection between $G^0(\tau)$ and $G(\tau)$ one uses the beneath listed relations.

$$G^0(0) \;= G(0) \;=\; \hat{\mathbb{1}} \tag{2.19}$$

$$G\hat{H}G^0 - G\hat{H}^0G^0 \;= G\left(\hat{H} - \hat{H}^0 + \hat{H}^0\right) G^0 - G\hat{H}^0G^0 \;=\; G\left(\hat{H} - \hat{H}^0\right) G^0 \tag{2.20}$$

$$\begin{aligned} \mathrm{e}^{-\tau(\hat{H} - S)} \;=\; G(\tau) \;&= G^0(\tau) - \int_0^\tau d\tau' \,\frac{\partial}{\partial \tau'}\left(G(\tau - \tau')\, G^0(\tau')\right) \\ &= G^0(\tau) - \left(G(0)\, G^0(\tau) - G(\tau)\, G^0(0)\right) \\ &= G^0(\tau) - G^0(\tau) + G(\tau) \end{aligned} \tag{2.21}$$

The derivation to get the exact Green function in Ref. [12] starts with Equation (2.21) and uses (2.18), as shown below.

$$\begin{aligned} G(\tau) &= G^0(\tau) - \int_0^\tau d\tau' \, \frac{\partial}{\partial \tau'} \left(G(\tau - \tau') \, G^0(\tau') \right) \\ &= G^0(\tau) - \int_0^\tau d\tau' \, \left(G(\tau - \tau') \, \left(\hat{H} - S \right) G^0(\tau') - G(\tau - \tau') \, \left(\hat{H}^0 - S \right) G^0(\tau') \right) \\ &= G^0(\tau) + \int_0^\tau d\tau' \, \left(G(\tau - \tau') \, \left(\hat{H}^0 - \hat{H} \right) G^0(\tau') \right) \end{aligned} \tag{2.22}$$

Again a walker population at time $\tau + \Delta\tau$ is generated if one applies the imaginary time propagator G, defined in Equation (2.22), to a walker population at time τ. But, by construction, there is no constraint to the size of the time step, in contrast to the algorithm presented in Ref. [9].

$$| \, \psi_{(\tau + \Delta\tau)} \, \rangle \; = \; G(\Delta\tau) \, | \, \psi_{(\tau)} \, \rangle$$

That also means it is possible to choose $\Delta\tau$ in such a manner that the difference between a new walker generation and the preceding one is large enough to keep correlations small.
After each time step there is also a global annihilation process, as described in Section 2.2.2, and subsequently one typically uses the walker configuration to calculate some kind of observable.

At this point the authors of Ref. [12] introduce *importance sampling*. The idea behind it is to define a new random walk, using an approach for the groundstate wavefunction Ψ_G, with the aim that the walkers spend more time in the important regions [13]. Thereby, the propagators and the densities of the algorithm change in the following way.

$$\tilde{G}(\tau) \; = \; \frac{\Psi_G \, G(\tau)}{\Psi_G} \; , \quad \tilde{G}^0(\tau) \; = \; \frac{\Psi_G \, G^0(\tau)}{\Psi_G} \; , \quad \tilde{\hat{H}}(\tau) \; = \; \frac{\Psi_G \, \hat{H}(\tau)}{\Psi_G} \; , \quad \tilde{\psi}_{(\tau)} \; = \; \Psi_G \, \psi_{(\tau)}$$

In our calculations we do not use a guiding function, that means $\Psi_G = 1$, see Section 2.4 for details. Therefore, the tilde is omitted in the following.

In the next step G (Equation (2.22)) is converted to earn a population dynamics algorithm, which gives the probability to find a walker in state χ_i at time τ if it has occupied state χ_j at time 0. However, to interpret the imaginary time propagator as a probability density one has to add additional terms, see Equation (2.23) and Ref. [12, Eq. (25)].

$$\begin{aligned} G_{i,j}(\tau) \; = \; & \left[\frac{G^0_{i,j}(\tau)}{\sum_n G^0_{n,j}(\tau)} \right]_2 \left[\sum_n G^0_{n,j}(\tau) \right]_1 + \int_0^\tau \sum_{k,l} \left[G_{i,k}(\tau - \tau') \right]_7 \left[\frac{\sum_{m,n} \left[\hat{H}^0_{m,n} - \hat{H}_{m,n} \right] G^0_{m,n}(\tau')}{\sum_{m,n} \left[\hat{H}^0_{m,n} - S\delta_{m,n} \right] G^0_{n,j}(\tau')} \right]_6 \\ & \times \left[\frac{\hat{H}^0_{k,l} - \hat{H}_{k,l}}{\sum_m \left[\hat{H}^0_{m,l} - \hat{H}_{m,l} \right]} \right]_5 \left[\frac{\sum_m \left[\hat{H}^0_{m,l} - \hat{H}_{m,l} \right] G^0_{l,j}(\tau')}{\sum_{m,n} \left[\hat{H}^0_{m,n} - \hat{H}_{m,n} \right] G^0_{m,n}(\tau')} \right]_4 \left[- \frac{\partial}{\partial \tau'} \sum_n G^0_{n,j}(\tau') \, d\tau' \right]_3 \end{aligned} \tag{2.23}$$

Those terms in Equation (2.23), which are marked with the same colour, cancel each other and one obtains

$$G_{i,j}(\tau) \; = \; G^0_{i,j}(\tau) + \int_0^\tau \sum_{k,l} G_{i,k}(\tau - \tau') \, \left(\hat{H}^0_{k,l} - \hat{H}_{k,l} \right) G^0_{l,j}(\tau') \, d\tau' \quad ,$$

what is identical to Equation (2.22). To cancel term 3, Equation (2.18) was used.

If one considers the Hubbard Hamiltonian in real or reciprocal space, the simplest choice for the known Green function G^0 is to take $\hat{H}^0$ to be the diagonal part of $\hat{H}$. Thereby, (2.18) becomes

$$G^0_{i,j}(\tau) \;=\; \mathrm{e}^{-(\hat{H}_{j,j}-S)\,\tau}\,\delta_{i,j} \quad ,$$

which is decaying exponential if S is chosen appropriately. This is necessary in order to interpret $G^0(\tau)$ as a normalized probability distribution. Since G^0 is diagonal, term 4 in Equation (2.23) reduces to $\delta_{l,j}$ and term 2 cancels out. Using these simplifications Equation (2.23) results in (2.24), Ref. [12, Eq. (30)].

$$\begin{aligned} G_{i,j}(\tau) \;=\; \delta_{i,j}\left[\mathrm{e}^{-(\hat{H}_{j,j}-S)\,\tau}\right]_1 + \int_0^\tau d\tau' \sum_k \left[G_{i,k}(\tau-\tau')\right]_7 \left[\frac{\hat{H}_{j,j}-\sum_m \hat{H}_{m,j}}{\hat{H}_{j,j}-S}\right]_6 \\ \times \left[\frac{-\hat{H}_{k,j}\,(1-\delta_{k,j})}{\sum_m \left(-\hat{H}_{m,j}\right)(1-\delta_{m,j})}\right]_5 \left[\left(\hat{H}_{j,j}-S\right)\mathrm{e}^{-(\hat{H}_{j,j}-S)\,\tau'}\right]_3 \end{aligned} \tag{2.24}$$

Suppose a walker in state χ_j and the time left to propagate at the beginning of the time step is τ, then the algorithm to sample a new state χ_i, resulting from Equation (2.24), is the following:

i) Generate a time τ' according to the probability distribution in term 3. The probability that $\tau' > \tau$ is

$$1 - \int_0^\tau d\tau' \left(\hat{H}_{j,j}-S\right)\mathrm{e}^{-(\hat{H}_{j,j}-S)\,\tau'} \;=\; \mathrm{e}^{-(\hat{H}_{j,j}-S)\,\tau} \quad ,$$

what is exactly term 1.
That means, if $\tau' > \tau$, the walker has finished its propagation for this time step and remains in state χ_j.

ii) If $\tau' < \tau$, the walker switches into a state $\chi_k \neq \chi_j$ with a probability proportional to the numerator of term 5.

iii) The walker in basis state χ_k gains a weight

$$w \;=\; \frac{\hat{H}_{j,j}-\sum_m \hat{H}_{m,j}}{\hat{H}_{j,j}-S}$$

according to term 6. This weight and a random number $r \in U(0,1)$ determine the destiny of the walker. One calculates

$$n_k = \mathrm{int}\,(w+r) \quad ,$$

where int(x) denotes the integer part of x and n_k is the new number or walkers in basis state χ_k. If, for example $n_k = 1$, one walker persists in this state, as depicted in Figure (2.2).
This choice to control the walker population ensures that on average every walker gets the weight w.

iv) Only term 7 of Equation (2.24) is left, which is the full Green function for a walker to propagate from state χ_k into state χ_i in time $\tau - \tau'$.
That means, subtract τ' from the remaining time and repeat step i) to iii) until the walker has finished its time step or died during propagation.

For a better understanding step i) to iii) are schematically depicted in Figure (2.2).

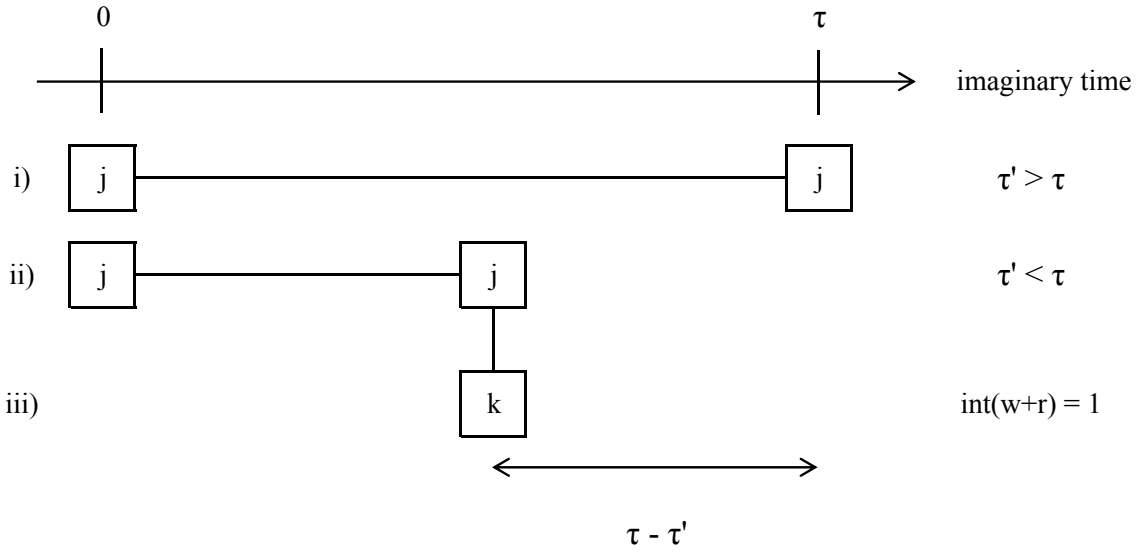

Figure 2.2.: Schematic illustration of the algorithm resulting from Equation (2.24).
If $\tau' > \tau$, the walker has finished its time step, if not, the walker hops into state k.
To be part of the next generation, it has to propagate the remaining time $\tau - \tau'$.

2.4. Importance sampling

In literature (for example Ref. [13], [5], [12]) one often reads, that it is possible to improve the behaviour of the random walk if there is a reasonable good approximation for the groundstate wavefunction of the system available. The fundamental idea behind it is to use this function to guide the walkers of the DMC simulation into important regions of the Hilbert space. Thus, these regions are sampled more often by the walkers, which should result in a reduction of the variance of the calculated observables.

In DMC one has two different functions, the guiding function Ψ_G and the trial function Ψ_T, but often these are the same functions. This is why the nomenclature in literature is not clear.

2.4.1. The guiding function

As abovementioned Ψ_G is used to bias the random walk, which leads to a modification of the imaginary time propagator [14].

$$\tilde{G}_{n,m} = \frac{\Psi_n^G \, G_{n,m}}{\Psi_m^G} \tag{2.25}$$

The repeated application of $\tilde{G}$ to a biased initial walker configuration $\tilde{\psi}^{(0)} = \Psi^G \psi^{(0)}$, leads to

$$\begin{aligned}
\tilde{\psi}_n^{(1)} &= \sum_m \tilde{G}_{n,m}\, \tilde{\psi}_m^{(0)} = \sum_m \frac{\Psi_n^G\, G_{n,m}}{\Psi_m^G}\, \Psi_m^G\, \psi_m^{(0)} = \Psi_n^G \sum_m G_{n,m}\, \psi_m^{(0)} = \Psi_n^G\, \psi_n^{(1)} \\
\tilde{\psi}_n^{(2)} &= \sum_m \tilde{G}_{n,m}\, \tilde{\psi}_m^{(1)} = \Psi_n^G\, \psi_n^{(2)} \\
&\cdots \\
\tilde{\psi}_n^{(N)} &= \sum_m \tilde{G}_{n,m}\, \tilde{\psi}_m^{(N-1)} = \Psi_n^G\, \psi_n^{(N)} \quad ,
\end{aligned}$$

or in matrix notation

$$\tilde{\psi}^{(N)} = \tilde{G}\, \tilde{\psi}^{(N-1)} = \Psi^G\, \psi^{(N)} = \Psi^G\, G^N\, \psi^{(0)} \quad .$$

In each time step the walker population is first of all divided and subsequently multiplied by the guiding function. This results in the orginal algorithm, without *importance sampling* with the exception, that the final walker population is multiplied by the guiding function. That means, using a guiding function costs extra computational effort, without any improvement to the variance of the calculated observables, as also noticed during our calculations.

But there is different effect of the guiding function, which is expedient numerically. The fluctuations of the walker population during the simulation are smaller. This becomes apparent in Equation (2.24) term 6, which determines the multiplication of the walkers. If one considers *ideal importance sampling*, which means $\Psi_G = \Phi_0$, the weight factor yields

$$\frac{\hat{H}_{j,j} - \sum_m \tilde{\hat{H}}_{m,j}}{\hat{H}_{j,j} - S} = \frac{\hat{H}_{j,j} - \sum_m \frac{\Psi_m^G \hat{H}_{m,j}}{\Psi_j^G}}{\hat{H}_{j,j} - S} \overset{\Psi^G = \Phi_0}{=} \frac{\hat{H}_{j,j} - \epsilon_0}{\hat{H}_{j,j} - S} = w \cong 1 \quad .$$

If the weight factor $w = 1$, the walker population is constant.

2.4.2. The trial function

The trial function is typically used to calculate an expectation value of an observable, as described in Section 2.1.
In Ref. [14], D. Ceperley did a calculation to estimate the variance of the energy computed by DMC, assuming that $\Psi_G = \Psi_T$. It turns out, that the variance reduction comes from the trial function in the energy estimator

$$\begin{aligned}
E^* &= \frac{1}{N} \sum_{\tau=1}^{N} \left(\frac{1}{Z} \langle\, \psi^{(\tau)} \,|\, \hat{H} \,|\, \Psi^T \,\rangle \right) \\
&= \frac{1}{N} \sum_{\tau=1}^{N} \left(\frac{1}{Z} \langle\, \tilde{\psi}^{(\tau)} \,/\, \Psi^T \,|\, \hat{H} \,|\, \Psi^T \,\rangle \right) \\
&= \frac{1}{N} \sum_{\tau=1}^{N} \left(\frac{1}{Z} \sum_n \left(\Psi_n^T\right)^{-1} \left(\hat{H} \,|\, \Psi^T \,\rangle \right)_n \tilde{\psi}_n^{(\tau)} \right) \\
&= \frac{1}{N} \sum_{\tau=1}^{N} \left(\frac{1}{Z} \sum_n E_n^L\, \tilde{\psi}_n^{(\tau)} \right) \\
&= \frac{1}{N} \sum_{\tau=1}^{N} E^L(\tau)
\end{aligned}$$

that is based on the local energy E^L. The expectation value of this estimator is asymptotically unbiased and independent of the trial function as proven in Equation (2.9).
Without loss of generality, one can assume that the ground state energy ϵ_0 is zero, which simplifies the calculation. The variance of this estimator is thus given by

$$\begin{aligned} V &= \frac{1}{N^2} \sum_{i,j} \left\langle E^L(i)\, E^L(j) \right\rangle \\ &= \underbrace{\frac{1}{N^2} \sum_{i} \left\langle \left(E^L(i)\right)^2 \right\rangle}_{\sigma_E^2/N} + \underbrace{\frac{2}{N^2} \sum_{i>j} \left\langle E^L(i)\, E^L(j) \right\rangle}_{V_2} \\ &= \frac{\sigma_E^2}{N} + V_2 \quad , \end{aligned} \tag{2.26}$$

whereby N denotes the number of the sampled walker configurations after the thermalization phase of the DMC simulation.
Furthermore, we assume that the trial function is close to the ground state wavefuntion Φ^0 of the Hamiltonian.

$$|\, \Psi^T \,\rangle = |\, \Phi^0 \,\rangle + |\, \Delta\Psi^T \,\rangle \tag{2.27}$$

$$\hat{H}\, |\, \Psi^T \,\rangle = \epsilon_0\, |\, \Phi^0 \,\rangle + \hat{H}\, |\, \Delta\Psi^T \,\rangle = \hat{H}\, |\, \Delta\Psi^T \,\rangle \tag{2.28}$$

The first term in Equation (2.26) can be transformed with the help of (2.27) and (2.28) that it only depends on $\Delta\Psi$.

$$\begin{aligned} \sigma_E^2 &= \left\langle \left(E^L(i)\right)^2 \right\rangle \\ &= \frac{1}{Z} \sum_n \left(E^L\right)_n^2 \left\langle \tilde{\psi}_n^{(i)} \right\rangle \\ &= \frac{1}{Z} \sum_n \left(\Psi_n^T\right)^{-2} \left(\hat{H}\, |\, \Psi^T \,\rangle\right)_n^2 \Psi_n^T\, \Phi_n^0 \\ &= \frac{1}{Z} \sum_n \left(\Psi_n^T\right)^{-1} \left(\hat{H}\, |\, \Psi^T \,\rangle\right)_n^2 \left(\Psi_n^T - \Delta\Psi_n\right) \\ &= \frac{1}{Z} \sum_n \left(\hat{H}\, |\, \Delta\Psi^T \,\rangle\right)_n^2 \left(1 - \frac{\Delta\Psi_n}{\Psi_n^T}\right) \end{aligned} \tag{2.29}$$

If the ground state wavefunction Φ^0 is normalized, the normalization constant Z is

$$Z = \sum_n \Phi_n^0\, \Psi_n^T = \sum_n \Phi_n^0 \left(\Phi_n^0 + \Delta\Psi_n\right) = 1 + \langle\, \Phi^0 \,|\, \Delta\Psi^T \,\rangle \quad .$$

To compute the second term of Equation (2.26), we first insert the definition of the local energy.

$$\begin{aligned} V_2 &= \frac{2}{N^2} \sum_{i>j} \left\langle E^L(i)\, E^L(j) \right\rangle \\ &= \frac{2}{N^2} \sum_{i>j} \left\langle \left(\frac{1}{Z} \sum_m E_m^L\, \tilde{\psi}_m^{(i)}\right) \left(\frac{1}{Z} \sum_n E_n^L\, \tilde{\psi}_n^{(j)}\right) \right\rangle \\ &= \frac{2}{N^2} \sum_{i>j} \sum_{m,n} E_m^L\, p(m \in i \,|\, n \in j)\, E_n^L\, p(n \in j) \end{aligned} \tag{2.30}$$

The term $p(m \in i \,|\, n \in j)$ in Equation (2.30) gives the probability to find a walker in state m in generation i under the condition that there was one in state n in a preceding generation j. In the derivation for V_2, David Ceperley considers those walkers only in generation i which are descendants from generation j. All other correlations ("cousin correlation") are neglected, what gives a lower bound to the actual variance, as described in Ref. [14]. In addition, one assumes that the number of generations in the equilibrated random walk is sufficiently large, that all descendants of a given walker in state n in generation j are eventually sampled.
Using these approximations, the conditional probability in Equation (2.30) reduces to

$$p(m \in i \,|\, n \in j) \;=\sum_{\tau=1}^{\infty} \tilde{G}^{(\tau)}_{m,n} \;=\; \sum_{\tau=1}^{\infty} \Psi^T_m \, G^{(\tau)}_{m,n} \, \left(\Psi^T_n\right)^{-1} \quad ,$$

resulting in

$$V_2 \;= \frac{2}{N\,Z} \sum_{m,\,n} E^L_m \left(\sum_{\tau=1}^{\infty} \Psi^T_m \, G^{(\tau)}_{m,n} \, \left(\Psi^T_n\right)^{-1} \right) E^L_n \, \Psi^T_n \, \Phi^0_n \quad . \tag{2.31}$$

Whereby, $\tau = 1$ means to sum over the descendants of generation j after one time step, $\tau = 2$ to sum over the descendants after two time steps and so on.
The expression in Equation (2.31) can be further simplified, which leads to

$$\begin{aligned}
V_2 \;&= \frac{2}{N\,Z} \sum_{m,\,n} \left(\Psi^T_m\right)^{-1} \, \Big(\hat{H} \,|\, \Psi^T \,\rangle \Big)_m \sum_{\tau=1}^{\infty} \Psi^T_m \, G^{(\tau)}_{m,n} \, E^L_n \, \Phi^0_n \\
&= \frac{2}{N\,Z} \sum_{m,\,n} \langle\, \Psi^T \,|\, \hat{H} \,|\, m \,\rangle \sum_{\tau=1}^{\infty} G^{(\tau)}_{m,n} \, E^L_n \, \Phi^0_n \\
&= \frac{2}{N\,Z} \sum_{m,\,n} \langle\, \Psi^T \,|\, \hat{H} \,|\, m \,\rangle \sum_{\tau=1}^{\infty} \langle\, m \,| \left(\frac{1}{\hat{\mathbb{1}} + \tau(\hat{H} - S)} \right)^{\tau} |\, n \,\rangle \, E^L_n \, \Phi^0_n \\
&= \frac{2}{N\,Z} \sum_{n} \langle\, \Psi^T \,|\, \hat{H} \,| \sum_{\tau=1}^{\infty} \left(\frac{1}{\hat{\mathbb{1}} + \tau(\hat{H} - S)} \right)^{\tau} |\, n \,\rangle \, E^L_n \, \Phi^0_n \quad .
\end{aligned}$$

In the next step, a complete set of eigenvectors of $\hat{H}$ is introduced. However, the ground state drops out, because we set the ground state energy to be zero.

$$V_2 \;= \frac{2}{N\,Z} \sum_{\alpha>0} \sum_{n} \langle\, \Psi^T \,|\, \hat{H} \,|\, \alpha \,\rangle \sum_{\tau=1}^{\infty} \left(\frac{1}{\hat{\mathbb{1}} + \tau(\epsilon_\alpha - S)} \right)^{\tau} \langle\, \alpha \,|\, n \,\rangle \, E^L_n \, \Phi^0_n$$

Using the simple relation

$$\sum_{t=1}^{\infty} \left(\frac{1}{1+x} \right)^t \overset{y=1/(1+x)}{=} -1 + \sum_{t=0}^{\infty} y^t \;=\; \frac{y}{1-y} \;=\; \frac{1}{x}$$

yields

$$V_2 \;= \frac{2}{N\,Z} \sum_{\alpha>0} \sum_{n} \langle\, \Psi^T \,|\, \alpha \,\rangle \, \frac{\epsilon_\alpha}{\tau(\epsilon_\alpha - S)} \, \langle\, \alpha \,|\, n \,\rangle \, E^L_n \, \Phi^0_n \quad .$$

Since $S \approx \epsilon_0 = 0$ we obtain

$$V_2 = \frac{2}{N\,Z\,\tau} \sum_{\alpha>0} \sum_{n} \langle\, \Psi^T \,|\, \alpha \,\rangle \langle\, \alpha \,|\, n \,\rangle\, E_n^L\, \Phi_n^0 \quad .$$

To complete the sum over α we add and subtract a term, which results in

$$V_2 = \frac{2}{N\,Z\,\tau} \sum_{\alpha} \sum_{n} \langle\, \Psi^T \,|\, \alpha \,\rangle \langle\, \alpha \,|\, n \,\rangle\, E_n^L\, \Phi_n^0 - \frac{2}{N\,Z\,\tau} \sum_{n} \langle\, \Psi^T \,|\, \Phi^0 \,\rangle \langle\, \Phi^0 \,|\, n \,\rangle\, E_n^L\, \Phi_n^0 \quad . \tag{2.32}$$

The first term in Equation (2.32) vanishes because

$$\begin{aligned}
\sum_{\alpha} \sum_{n} \langle\, \Psi^T \,|\, \alpha \,\rangle \langle\, \alpha \,|\, n \,\rangle\, E_n^L\, \Phi_n^0 &= \sum_{n} \langle\, \Psi^T \,|\, n \,\rangle\, E_n^L\, \Phi_n^0 \\
&= \sum_{n} \langle\, \Psi^T \,|\, n \,\rangle\, \left(\Psi_n^T\right)^{-1} \left(\hat{H}\,|\,\Psi^T\,\rangle\right)_n \Phi_n^0 \\
&= \sum_{n} \Psi_n^T\, \left(\Psi_n^T\right)^{-1} \left(\hat{H}\,|\,\Psi^T\,\rangle\right)_n \Phi_n^0 \\
&= \underbrace{\langle\, \Phi^0 \,|\, \hat{H}}_{\epsilon_0}\, |\, \Psi^T \,\rangle \;=\; \epsilon_0 \,\langle\, \Phi^0 \,|\, \Psi^T \,\rangle \;=\; 0 \quad .
\end{aligned}$$

Hence, we get the following result for the expression V_2.

$$V_2 \;=\; -\frac{2}{N\,Z\,\tau} \sum_{n} \underbrace{\langle\, \Psi^T \,|\, \Phi^0 \,\rangle}_{Z} \langle\, \Phi^0 \,|\, n \,\rangle\, E_n^L\, \Phi_n^0 \;=\; -\frac{2}{N\,\tau} \sum_{n} E_n^L\, \left(\Phi_n^0\right)^2 \tag{2.33}$$

Therefore, the total variance a la Ceperley is given by

$$V_2 \;=\; \frac{\sigma_e^2}{N} - \frac{2}{N\,\tau} \sum_{n} E_n^L\, \left(\Phi_n^0\right)^2 \quad . \tag{2.34}$$

3. Approximations for the groundstate wavefunction

In this Chapter, three different methods to calculate an approximation for the groundstate wavefunction of the Hubbard Hamiltonian are discussed. In the following, these wavefunctions can be used within a DMC simulation to generate an initial walker configuration, to calculate the mixed estimator (see Section 2.1) or as a trial function in the Fixed Node Approximation. The Gutzwiller Wavefunction respectively the RVB Wavefunction are described in Section 3.1 respectively 3.2, which can be applied to the fermion Hubbard model. In Section 3.3, an approach for the groundstate based on probability theory is presented.

3.1. The Gutzwiller Wavefunction

In Ref. [15], Martin C. Gutzwiller described a general wavefunction for electrons in narrow s bands. In this Section, we apply this *Gutzwilller Wavefunction* (GWF) to the Hubbard Hamiltonian to obtain an analytical approximation for the groundstate. Subsequently some results are presented.

To compute the GWF, one starts with the groundstate in momentum space ($|\, FS\,\rangle$) for $U = 0$, accomplishes a Fourier transformation to real space and finally the basis states are weighted depending on their double occupations.

$$|\, \Psi_{GWF}\,\rangle \;=\; \sum_{\Gamma} g^{\hat{D}}\,|\, \Gamma\,\rangle\,\langle\, \Gamma\,|\, FS\,\rangle \;=\; \sum_{\Gamma_\uparrow,\Gamma_\downarrow} g^{\hat{D}}\,|\, \Gamma_\uparrow\,\rangle \otimes |\, \Gamma_\downarrow\,\rangle\,\langle\, \Gamma_\uparrow\,|\, FS_\uparrow\,\rangle\,\langle\, \Gamma_\downarrow\,|\, FS_\downarrow\,\rangle \tag{3.1}$$

In Equation (3.1), $|\, \Gamma_\sigma\,\rangle$ denotes a manybody basis state in real space

$$|\, \Gamma_\sigma\,\rangle \;=\; \prod_{i\in N}^{N_\sigma} c^\dagger_{i,\sigma}\,|\, 0\,\rangle$$

for N_σ electrons per spin direction σ on N lattice sites (e.g. Figure (1.2)), respectively $|\, FS_\sigma\,\rangle$ is the ground state in reciprocal space in the appendant spin direction. The operator $\hat{D}$ simply counts the double occupations, as described in Chapter 1.
The parameter g is defined to minimise

$$E_{GWF}(g) \;=\; \frac{\langle\, \Psi_{GWF}(g)\,|\, \hat{H}\,|\, \Psi_{GWF}(g)\,\rangle}{\langle\, \Psi_{GWF}(g)\,|\, \Psi_{GWF}(g)\,\rangle} \quad , \tag{3.2}$$

whereupon $E_{GWF}(g)$ has a global minimum in the intervall $g \in (0,\, 1]$, as noticed during our calculations. For the special case $U = 0$, the Gutzwiller wavefunction is consistent with the groundstate wavefuntion of the system if we choose $g = 1$. But this is not surprising because we already started with this function in momentum-space.
With increasing U the difference between E_{GWF} and the groundstate energy ϵ_0 increases too and the optimal value of g is shifted to smaller values, as depicted in Tabular 3.2 and 3.3.

The meaning of the terms $\langle\, \Gamma_\sigma \,|\, FS_\sigma \,\rangle$ becomes clear if one performs the Fourier transformation of $|\, FS_\sigma \,\rangle$ by hand. Let us consider a system with $N = 3$ sites and a basis state in momentum space for a spin direction given by

$$|\, K \,\rangle \;=\; c^\dagger_{k_1}\, c^\dagger_{k_2}\, |\, 0 \,\rangle \quad .$$

Using Equation (1.3) we yield

$$\begin{aligned}
|\, K \,\rangle \;&= \frac{1}{N} \left(\mathrm{e}^{\mathrm{i}\, k_1\, x_1}\, c^\dagger_{x_1} + \mathrm{e}^{\mathrm{i}\, k_1\, x_2}\, c^\dagger_{x_2} + \mathrm{e}^{\mathrm{i}\, k_1\, x_3}\, c^\dagger_{x_3}\right) \left(\mathrm{e}^{\mathrm{i}\, k_2\, x_1}\, c^\dagger_{x_1} + \mathrm{e}^{\mathrm{i}\, k_2\, x_2}\, c^\dagger_{x_2} + \mathrm{e}^{\mathrm{i}\, k_2\, x_3}\, c^\dagger_{x_3}\right) \\
&= \frac{1}{N} \Big(\left(\mathrm{e}^{\mathrm{i}\, k_1\, x_1}\, \mathrm{e}^{\mathrm{i}\, k_2\, x_2} - \mathrm{e}^{\mathrm{i}\, k_1\, x_2}\, \mathrm{e}^{\mathrm{i}\, k_2\, x_1}\right) c^\dagger_{x_1}\, c^\dagger_{x_2} \\
&\qquad + \left(\mathrm{e}^{\mathrm{i}\, k_1\, x_1}\, \mathrm{e}^{\mathrm{i}\, k_2\, x_3} - \mathrm{e}^{\mathrm{i}\, k_1\, x_3}\, \mathrm{e}^{\mathrm{i}\, k_2\, x_1}\right) c^\dagger_{x_1}\, c^\dagger_{x_3} \\
&\qquad + \left(\mathrm{e}^{\mathrm{i}\, k_1\, x_2}\, \mathrm{e}^{\mathrm{i}\, k_2\, x_3} - \mathrm{e}^{\mathrm{i}\, k_1\, x_3}\, \mathrm{e}^{\mathrm{i}\, k_2\, x_2}\right) c^\dagger_{x_2}\, c^\dagger_{x_3} \Big) \\
&\quad \frac{1}{N} \left(\begin{vmatrix} \mathrm{e}^{\mathrm{i}\, k_1\, x_1} & \mathrm{e}^{\mathrm{i}\, k_1\, x_2} \\ \mathrm{e}^{\mathrm{i}\, k_2\, x_1} & \mathrm{e}^{\mathrm{i}\, k_2\, x_2} \end{vmatrix} c^\dagger_{x_1}\, c^\dagger_{x_2} + \begin{vmatrix} \mathrm{e}^{\mathrm{i}\, k_1\, x_1} & \mathrm{e}^{\mathrm{i}\, k_1\, x_3} \\ \mathrm{e}^{\mathrm{i}\, k_2\, x_1} & \mathrm{e}^{\mathrm{i}\, k_2\, x_3} \end{vmatrix} c^\dagger_{x_1}\, c^\dagger_{x_3} + \begin{vmatrix} \mathrm{e}^{\mathrm{i}\, k_1\, x_2} & \mathrm{e}^{\mathrm{i}\, k_1\, x_3} \\ \mathrm{e}^{\mathrm{i}\, k_2\, x_2} & \mathrm{e}^{\mathrm{i}\, k_2\, x_3} \end{vmatrix} c^\dagger_{x_2}\, c^\dagger_{x_3} \right) \\
&= \frac{1}{N} \sum_{\Gamma} \left(\sum_{\mathbb{P}} \prod_i (-1)^{\mathbb{P}}\, \mathrm{e}^{\mathrm{i}\, k_i\, x_{\Gamma_i}} \right) |\, \Gamma \,\rangle \quad ,
\end{aligned}$$

whereby $\sum_{\mathbb{P}}$ sums over all permutation of the $c^\dagger$'s and the factor $(-1)^{\mathbb{P}}$ considers the sign occuring to sort the creation operators in ascending order. Hence, we obtain the general form for the Gutzwiller wavefunction

$$|\, \Psi_{GWF} \,\rangle \;=\; \sum_{\Gamma_\uparrow, \Gamma_\downarrow} g^{\hat{D}}\, \det\left(\frac{\exp(\mathrm{i}\, K_\uparrow\, \Gamma_\uparrow)}{\sqrt{N}}\right) \det\left(\frac{\exp(\mathrm{i}\, K_\downarrow\, \Gamma_\downarrow)}{\sqrt{N}}\right) |\, \Gamma_\uparrow \,\rangle \otimes |\, \Gamma_\downarrow \,\rangle \quad . \tag{3.3}$$

As one can see in Equation (3.3), one is able to calculate the determinants for each spin direction independently of each other. Therefore, the number of determinants to compute and to store is only

$$\binom{N}{N_\uparrow} + \binom{N}{N_\downarrow} \qquad \text{instead of} \qquad \binom{N}{N_\uparrow} \cdot \binom{N}{N_\downarrow} \quad ,$$

what is very expedient, concerning memory requirements and calculating time.

Furthermore, the coefficients of the GWF are usually complex numbers, that means

$$|\, \Psi_{GWF} \,\rangle \;=\; \sum_\nu c_\nu\, |\, \Gamma_\nu \,\rangle \;, \qquad c_\nu \in \mathbb{C} \quad .$$

Since we want to use the GWF, as a guiding function or as a trial function in the Fixed Node Approximation, it would be useful if the c_ν's are real numbers. This is why we did the minimisation in Equation (3.2) always twice, once using only the real, and once using only the imaginary part of the c_ν's. The wavefunction, which corresponds to the lower energy, was used for further calculations.
Despite of neglecting a lot of information in the wavefunction, it turns out that the obtained energy E_{GWF} is mostly the same as for complex coefficients, sometimes better and seldom worse.

If the groundstate of $\hat{H}_0$ (the term of the Hamiltonian corresponding to the kinetic energy) is degenerated, every linear combination of groundstate vectors is a groundstate vector as well.

That means, there is an enormous number of possibilities to construct $|FS\rangle$ respectively to compute the GWF.
During our calculations, it turned out that if the different spin directions have combined momentum zero (an example is depicted in Figure (3.1)), one obtains a suitable function to calculate the GWF. However, this choice for example is limited to systems with $N_\uparrow = N_\downarrow$ and does not mean that there are no better functions available.
For systems, which are not degenerated in $\hat{H}_0$ (Figure (1.5)), the fermi sea is accurately defined resulting in a significantly better approximation for the groundstate energy ϵ_0 in comparison to degenerated systems (see Figure (3.3) and (3.4)).
But maybe there are also possibilities to improve this wavefunction, for example, if one takes particle hole excitations into account.

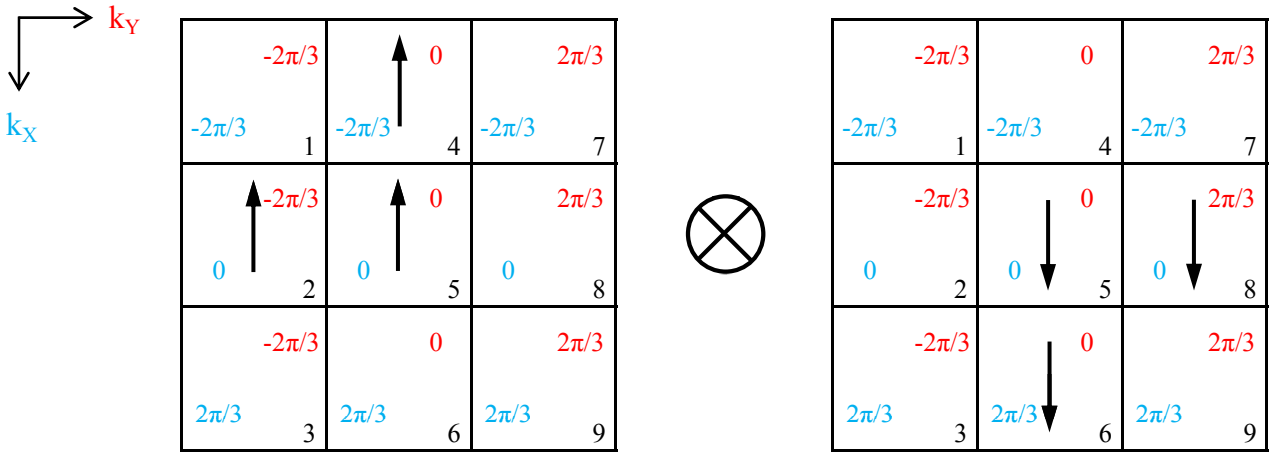

Figure 3.1.: A basis state of the Hubbard Hamiltonian in momentum space for a system size $L_X \times L_Y = 3 \times 3$ and $N_\uparrow = N_\downarrow = 3$. The coloured numbers indicate the wavenumber of the sites.
As one can recognize, this state is a groundstate of $\hat{H}_0$ and has momentum zero.

3.1.1. Results of the Gutzwiller Wavefunction

In this Section, the true groundstate energy ϵ_0 for different systems is compared to the corresponding energy E_{GWF}, obtained using the GWF.

Figure (3.2) shows the energy E_{GWF} as a function of the variational parameter g for a system with $L_X \times L_Y = 3 \times 3$ sites and $N_\uparrow = N_\downarrow = 5$ electrons.

Figure (3.3) shows the exact groundstate energy ϵ_0 and the approximation E_{GWF} using the GWF as a function of U/t for a system with $L_X \times L_Y = 3 \times 3$ sites and $N_\uparrow = N_\downarrow = 5$ electrons. The approximation is exact for $U = 0$ and becomes inexact with increasing U. The values belonging to Figure (3.3) are listed in Table 3.2.
Figure (3.4) is the same as Figure (3.3), but for a system with only $N_\uparrow = N_\downarrow = 3$ electrons. The corresponding values are listed in Table 3.3.

To sum up, some results for different systems are listed in Table 3.1 for $U/t = 4$.

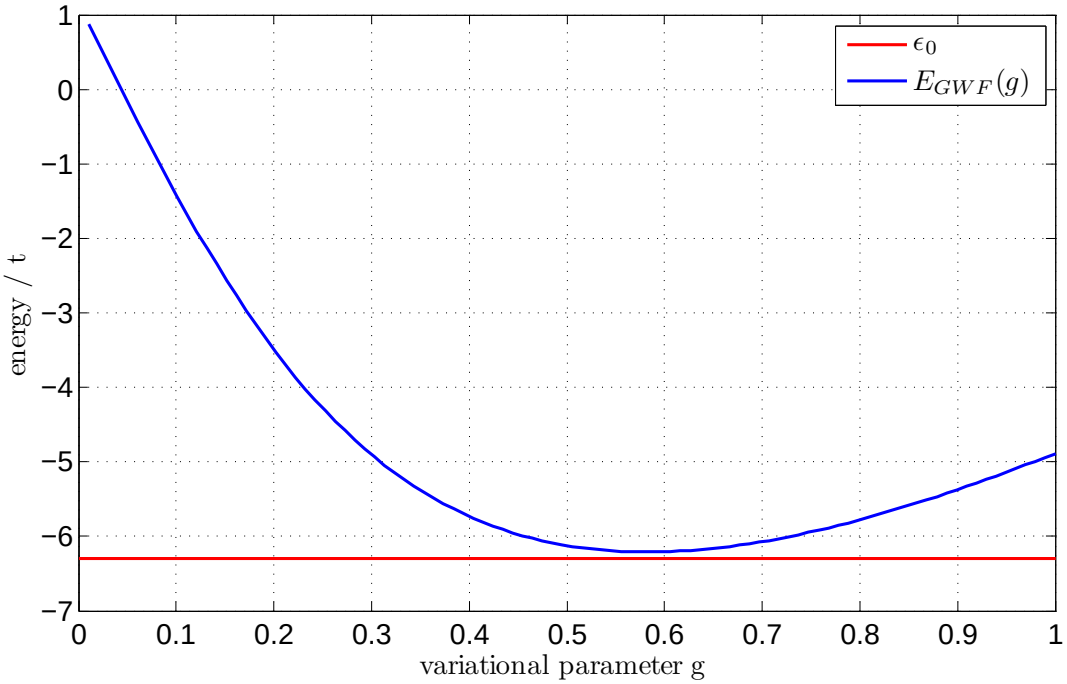

Figure 3.2.: The energy E_{GWF} as a function of the variational parameter g in comparison to the groundstate energy ϵ_0 for a system with $L_X \times L_Y = 3 \times 3$, $N_\uparrow = N_\downarrow = 5$ and $U/t = 4$. The energies are given in units of t.

Table 3.1.: Comparison of the energies obtained for different systems by means of the GWF (E_{GWF}) and exact diagonalisation (ϵ_0) for a value of $U/t = 4$.
The $\Im$ or $\Re$ denote, if the real or the imaginary part of the GWF was used to calculate the energy. The energies are given in units of t.

L_X	L_Y	$N_\uparrow$	$N_\downarrow$	$\Im$ or $\Re$	E_{GWF}	ϵ_0
2	4	4	4	$\Re$	-9.8885	-10.2530
3	3	4	4	$\Im$	-8.7167	-9.3648
3	4	2	2	$\Im$	-11.2836	-11.3464
3	4	3	3	$\Re$	-13.9043	-13.9962
3	4	4	4	$\Im$	-14.2193	-14.3635
3	4	6	6	$\Re$	-9.9818	-10.3090
4	4	5	5	$\Re$	-19.3874	-19.5808*
4	4	8	8	$\Re$	-11.3711	-13.6224*

* adopted from Ref. [16]

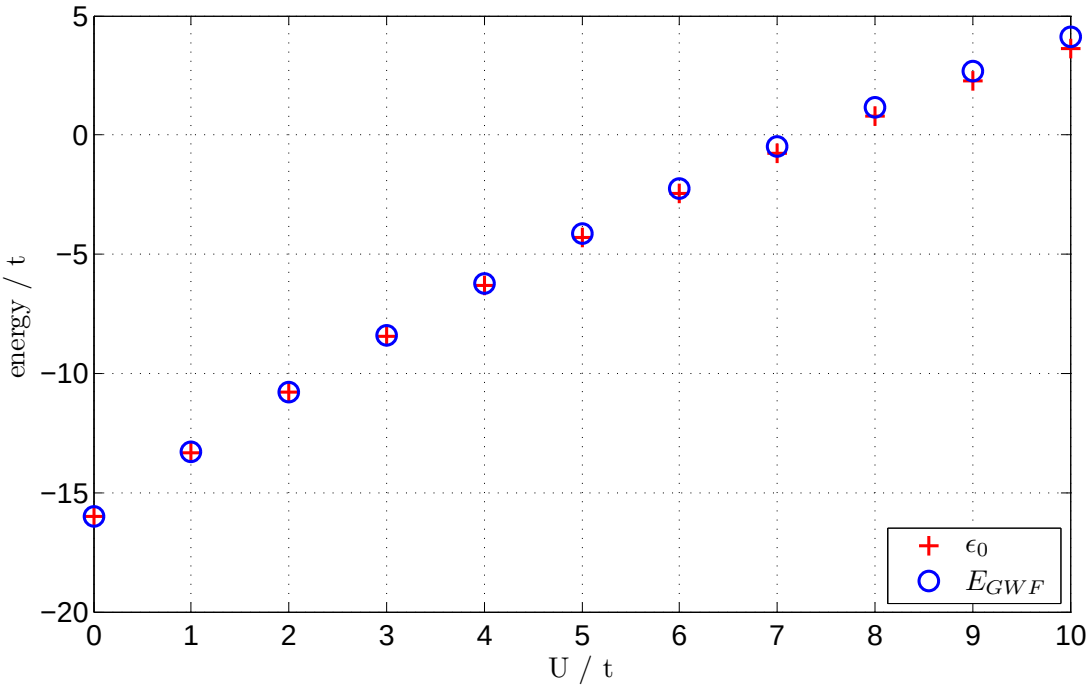

Figure 3.3.: Comparison of the exact groundstate energy ϵ_0 and the approximation E_{GWF} as a function of U/t for a system with $L_X \times L_Y = 3 \times 3$ and $N_\uparrow = N_\downarrow = 5$.
To calculate E_{GWF} the real part of the GWF was used. The energies are given in units of t.

Table 3.2.: Corresponding values of Figure (3.3). g_{opt} denotes the value, which minimises Equation (3.2). The energies are given in units of t.

U/t	E_{GWF}	ϵ_0	g_{opt}
0	-16.0000	-16.0000	1.0000
1	-13.3080	-13.3127	0.8742
2	-10.7829	-10.8014	0.7647
3	-8.4187	-8.4616	0.6683
4	-6.2104	-6.2911	0.5826
5	-4.1537	-4.2880	0.5059
6	-2.2439	-2.4467	0.4372
7	-0.4745	-0.7541	0.3765
8	1.1648	0.8094	0.3241
9	2.6889	2.2667	0.2800
10	4.1156	3.6394	0.2437

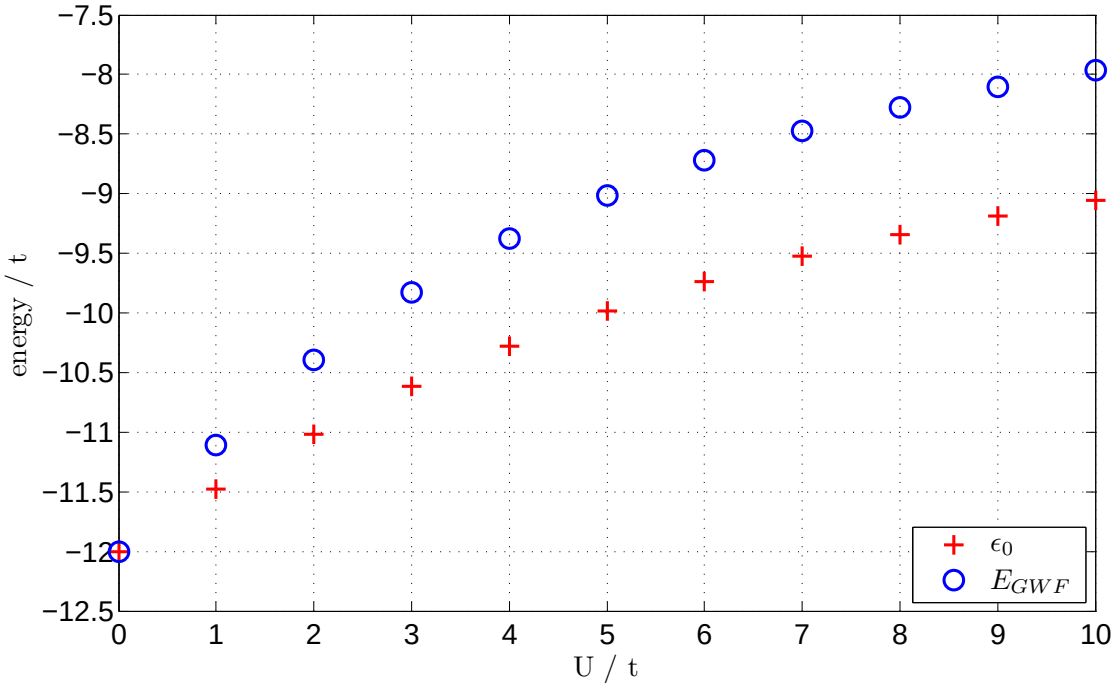

Figure 3.4.: Comparison of the exact groundstate energy ϵ_0 and the approximation E_{GWF} as a function of U/t for a system with $L_X \times L_Y = 3 \times 3$ and $N_\uparrow = N_\downarrow = 3$.
To calculate E_{GWF} the real part of the GWF was used. The energies are given in units of t.

Table 3.3.: Corresponding values of Figure (3.4). g_{opt} denotes the value, which minimises Equation (3.2). The energies are given in units of t.

U/t	E_{GWF}	ϵ_0	g_{opt}
0	-12.0000	-12.0000	1.0000
1	-11.1057	-11.4763	0.8489
2	-10.3947	-11.0162	0.7248
3	-9.8288	-10.6175	0.6230
4	-9.3765	-10.2754	0.5396
5	-9.0125	-9.9836	0.4714
6	-8.7171	-9.7352	0.4156
7	-8.4750	-9.5236	0.3697
8	-8.2744	-9.3426	0.3318
9	-8.1065	-9.1871	0.3001
10	-7.9645	-9.0527	0.2735

3.2. The RVB Wavefunction

In Ref. [17], P. W. Anderson suggested that on a two dimensional square lattice the spins are in a resonation-valence-bond (RVB) state of spin pairs with total spin zero. Iske and Caspers used this spin pairs (singlets) to approximate the groundstate of the antiferromagnetic Heisenberg model [18]. The authors of Ref. [3] adopted this concept and proposed to use the RVB approximation for the groundstate wavefunction of the Hubbard model.
This Section describes in detail, how to compute an approach for the groundstate of the Hubbard Hamiltonian using RVB, whereupon we restrict ourselves to the half filled case $N_\uparrow = N_\downarrow = N/2$.

The idea of the RVB approximation is to cover the whole lattice with spin pairs (also called bonds, dimers or singlets) between two nearest neighbour sites. Such a bond between site i and j is defined by

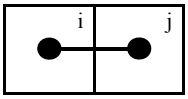

$$\widehat{=} \qquad |\,\psi(i,j)\,\rangle = \left[\left(c^\dagger_{i,\uparrow}\,c^\dagger_{j,\downarrow} + c^\dagger_{j,\uparrow}\,c^\dagger_{i,\downarrow}\right) x + c^\dagger_{i,\uparrow}\,c^\dagger_{i,\downarrow} + c^\dagger_{j,\uparrow}\,c^\dagger_{j,\downarrow}\right] |\,0\,\rangle \quad \text{with}$$

$$x = \frac{U + \sqrt{16t^2 + U^2}}{4t} \quad , \tag{3.4}$$

what is exactly the groundstate of a system with $N = 2$ sites and $N_\uparrow = N_\downarrow = 1$ electron (see Equation (1.18)). If one considers periodic boundary conditions, these bonds are also allowed to reach across the boundaries (see Figure (3.8)).
A lattice, that is completely covered by bonds, is called dimer covering as depicted in Figure (3.5). Thereby, it is very important that each lattice site is only occupied by one dimer.

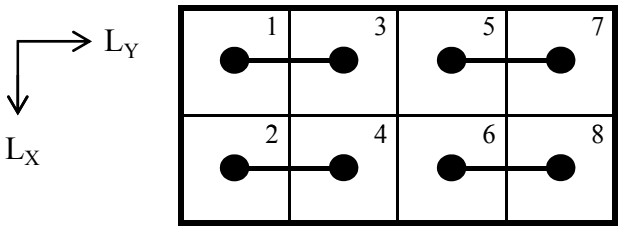

Figure 3.5.: An example for a dimer covering for a system size $L_X \times L_Y = 2 \times 4$.

The wavefunction corresponding to a given dimer covering D is the product of the wavefunctions of its bonds

$$\psi_D = \prod_{\substack{(i,j)\in D \\ i<j}} \psi(i,j) \quad , \tag{3.5}$$

whereby D sums over all bonds concerning to the covering. For the example in Figure (3.5)

$$D = \{(1,3),(2,4),(5,7),(6,8)\} \quad .$$

Thus, each dimer covering occupies at most $4^{N/2}$ basis states of the Hamiltonian, where $N/2$ is the number of bonds per covering. The different weights of the basis states depending on their

double occupations are taken into account by the factor x in Equation (3.4). The rule $i < j$ in the product of Equation (3.5) is needed to obtain the correct sign of the basis states.

The RVB wavefunction Ψ_{RVB} is given by a linear combination of all possible dimer coverings N_D of the considered system [3]. Subsequently, a Gutzwiller factor is added to improve the result.

$$|\,\Psi_{RVB}\,\rangle \;=\; g^{\hat{D}} \left(\sum_{n=1}^{N_D} c_n \, \psi_{D_n} \right) |\,0\,\rangle \tag{3.6}$$

The coefficients $\vec{c}$ and g in Equation (3.6) are variational parameters and are determined by

$$\min_{\vec{c},\,g} \; E_{RVB} \;=\; \min_{\vec{c},\,g} \; \frac{\langle\,\Psi_{RVB}\,|\,\hat{H}\,|\,\Psi_{RVB}\,\rangle}{\langle\,\Psi_{RVB}\,|\,\Psi_{RVB}\,\rangle} \quad . \tag{3.7}$$

The operator $\hat{D}$, again, simply counts the double occupations of the basis states.
This minimisation is a task in $N_D + 1$ dimensions, for what the following procedure has proved to be successful during our calculations.

i) Optimise the coefficients $\vec{c}$ independently of the Gutzwiller factor $g^{\hat{D}}$. This leads to the generalized eigenvalue problem

$$H\,\vec{c} \;=\; E\,S\,\vec{c} \qquad \text{where} \qquad H_{i,j} \;=\; \langle\,\psi_{D_i}\,|\,\hat{H}\,|\,\psi_{D_j}\,\rangle \qquad \text{and} \qquad S_{i,j} \;=\; \langle\,\psi_{D_i}\,|\,\psi_{D_j}\,\rangle \quad .$$

ii) Use the result for the $\vec{c}$ form i), but leave them constant and perform a minimisation in one dimension for the parameter g. For example, use Brents method, as described in Ref. [19].

iii) Use the results from i) and ii) as initial values for the simplex algorithm, also described in Ref. [19], to compute E_{RVB}.

Thereby, it is not assured to find the global minimum, but one obtains a feasible result for E_{RVB}. An improvement of this procedure is achievable if one first divides the dimer coverings into classes, whereby coverings within a class are related by the symmetry of the bonds [18].
A further possibility to improve this approximation is to allow also bonds between the next nearest neighbours. Thus, more basis states of the Hubbard Hamiltonian are occupied and one obtains a more appropriate approach for the groundstate wavefunction.
It is mentionable that the coefficients $\vec{c}$ and g are real. That means the RVB wavefuntion is also real and one can use it as a trial function in the Fixed Node Approximation (see Chapter 5) without any changes.

Table 3.4.: The number of possible dimer coverings for different system sizes considering the nearest neighbour bonds respectively also the next nearest neighbour bonds.

L_X	L_Y	nearest neighbours	next nearest neighbours
2	2	2	-
2	4	9	33
4	4	272	17552

3.2.1. Results for the system $L_X \times L_Y = 2 \times 2$

In this Section, we show how to calculate the coefficients of a dimer covering for the system $L_X \times L_Y = 2 \times 2$ by hand. Then, the obtained approximation for the groundstate energy E_{RVB} is compared to the true groundstate energy ϵ_0 and to the result from the Gutzwiller Wavefunction E_{GWF}.

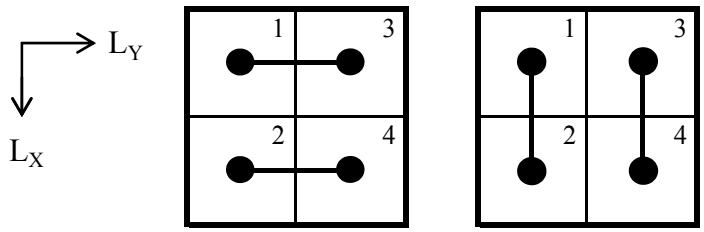

Figure 3.6.: The two possible dimer coverings for the system $L_X \times L_Y = 2 \times 2$.

Figure (3.6) shows the two possible dimer coverings for the considered system, whereby the left-sided covering (horizontal bonds) corresponds to the following wavefunction.

$$
\begin{aligned}
\psi_{D_1} &= \psi(1,3)\,\psi(2,4) \\
&= \left(x\left(c^\dagger_{1,\uparrow}c^\dagger_{3,\downarrow} + c^\dagger_{3,\uparrow}c^\dagger_{1,\downarrow}\right) + c^\dagger_{1,\uparrow}c^\dagger_{1,\downarrow} + c^\dagger_{3,\uparrow}c^\dagger_{3,\downarrow}\right)\left(x\left(c^\dagger_{2,\uparrow}c^\dagger_{4,\downarrow} + c^\dagger_{4,\uparrow}c^\dagger_{2,\downarrow}\right) + c^\dagger_{2,\uparrow}c^\dagger_{2,\downarrow} + c^\dagger_{4,\uparrow}c^\dagger_{4,\downarrow}\right) \\
&= x^2\left(c^\dagger_{1,\uparrow}c^\dagger_{3,\downarrow}c^\dagger_{2,\uparrow}c^\dagger_{4,\downarrow} + c^\dagger_{1,\uparrow}c^\dagger_{3,\downarrow}c^\dagger_{4,\uparrow}c^\dagger_{2,\downarrow} + c^\dagger_{3,\uparrow}c^\dagger_{1,\downarrow}c^\dagger_{2,\uparrow}c^\dagger_{4,\downarrow} + c^\dagger_{3,\uparrow}c^\dagger_{1,\downarrow}c^\dagger_{4,\uparrow}c^\dagger_{2,\downarrow}\right) \\
&+ x\left(c^\dagger_{1,\uparrow}c^\dagger_{3,\downarrow}c^\dagger_{2,\uparrow}c^\dagger_{2,\downarrow} + c^\dagger_{1,\uparrow}c^\dagger_{3,\downarrow}c^\dagger_{4,\uparrow}c^\dagger_{4,\downarrow} + c^\dagger_{3,\uparrow}c^\dagger_{1,\downarrow}c^\dagger_{2,\uparrow}c^\dagger_{2,\downarrow} + c^\dagger_{3,\uparrow}c^\dagger_{1,\downarrow}c^\dagger_{4,\uparrow}c^\dagger_{4,\downarrow}\right. \\
&\qquad \left. + c^\dagger_{1,\uparrow}c^\dagger_{1,\downarrow}c^\dagger_{2,\uparrow}c^\dagger_{4,\downarrow} + c^\dagger_{1,\uparrow}c^\dagger_{1,\downarrow}c^\dagger_{4,\uparrow}c^\dagger_{2,\downarrow} + c^\dagger_{3,\uparrow}c^\dagger_{3,\downarrow}c^\dagger_{2,\uparrow}c^\dagger_{4,\downarrow} + c^\dagger_{3,\uparrow}c^\dagger_{3,\downarrow}c^\dagger_{4,\uparrow}c^\dagger_{2,\downarrow}\right) \\
&+ \left(c^\dagger_{1,\uparrow}c^\dagger_{1,\downarrow}c^\dagger_{2,\uparrow}c^\dagger_{2,\downarrow} + c^\dagger_{1,\uparrow}c^\dagger_{1,\downarrow}c^\dagger_{4,\uparrow}c^\dagger_{4,\downarrow} + c^\dagger_{3,\uparrow}c^\dagger_{3,\downarrow}c^\dagger_{2,\uparrow}c^\dagger_{2,\downarrow} + c^\dagger_{3,\uparrow}c^\dagger_{3,\downarrow}c^\dagger_{4,\uparrow}c^\dagger_{4,\downarrow}\right)
\end{aligned}
$$

Shifting all $c^\dagger_\uparrow$'s to the left hand side and all $c^\dagger_\downarrow$'s to the right hand side and a subsequent sorting by ascending order yields the sign of the basis states.

$$
\begin{aligned}
&= x^2\left(-c^\dagger_{1,\uparrow}c^\dagger_{2,\uparrow}c^\dagger_{3,\downarrow}c^\dagger_{4,\downarrow} + c^\dagger_{1,\uparrow}c^\dagger_{4,\uparrow}c^\dagger_{2,\downarrow}c^\dagger_{3,\downarrow} + c^\dagger_{2,\uparrow}c^\dagger_{3,\uparrow}c^\dagger_{1,\downarrow}c^\dagger_{4,\downarrow} - c^\dagger_{3,\uparrow}c^\dagger_{4,\uparrow}c^\dagger_{1,\downarrow}c^\dagger_{2,\downarrow}\right) \\
&+ x\left(c^\dagger_{1,\uparrow}c^\dagger_{2,\uparrow}c^\dagger_{2,\downarrow}c^\dagger_{3,\downarrow} - c^\dagger_{1,\uparrow}c^\dagger_{4,\uparrow}c^\dagger_{3,\downarrow}c^\dagger_{4,\downarrow} + c^\dagger_{2,\uparrow}c^\dagger_{3,\uparrow}c^\dagger_{1,\downarrow}c^\dagger_{2,\downarrow} - c^\dagger_{3,\uparrow}c^\dagger_{4,\uparrow}c^\dagger_{1,\downarrow}c^\dagger_{4,\downarrow}\right. \\
&\qquad \left. - c^\dagger_{1,\uparrow}c^\dagger_{2,\uparrow}c^\dagger_{1,\downarrow}c^\dagger_{4,\downarrow} - c^\dagger_{1,\uparrow}c^\dagger_{4,\uparrow}c^\dagger_{1,\downarrow}c^\dagger_{2,\downarrow} + c^\dagger_{2,\uparrow}c^\dagger_{3,\uparrow}c^\dagger_{3,\downarrow}c^\dagger_{4,\downarrow} + c^\dagger_{3,\uparrow}c^\dagger_{4,\uparrow}c^\dagger_{2,\downarrow}c^\dagger_{3,\downarrow}\right) \\
&- \left(c^\dagger_{1,\uparrow}c^\dagger_{2,\uparrow}c^\dagger_{1,\downarrow}c^\dagger_{2,\downarrow} + c^\dagger_{1,\uparrow}c^\dagger_{4,\uparrow}c^\dagger_{1,\downarrow}c^\dagger_{4,\downarrow} + c^\dagger_{2,\uparrow}c^\dagger_{3,\uparrow}c^\dagger_{2,\downarrow}c^\dagger_{3,\downarrow} + c^\dagger_{3,\uparrow}c^\dagger_{4,\uparrow}c^\dagger_{3,\downarrow}c^\dagger_{4,\downarrow}\right)
\end{aligned}
$$

The same calculation has to be done for the right-sided dimer covering (vertical bonds) of Figure (3.6).

$$
\begin{aligned}
\psi_{D_2} &= \psi(1,2)\,\psi(3,4) \\
&= -x^2 \left(c^\dagger_{1,\uparrow} c^\dagger_{3,\uparrow} c^\dagger_{2,\downarrow} c^\dagger_{4,\downarrow} + c^\dagger_{2,\uparrow} c^\dagger_{3,\uparrow} c^\dagger_{1,\downarrow} c^\dagger_{4,\downarrow} + c^\dagger_{1,\uparrow} c^\dagger_{4,\uparrow} c^\dagger_{2,\downarrow} c^\dagger_{3,\downarrow} + c^\dagger_{2,\uparrow} c^\dagger_{4,\uparrow} c^\dagger_{1,\downarrow} c^\dagger_{3,\downarrow} \right) \\
&\quad - x \Big(c^\dagger_{1,\uparrow} c^\dagger_{3,\uparrow} c^\dagger_{1,\downarrow} c^\dagger_{4,\downarrow} + c^\dagger_{2,\uparrow} c^\dagger_{3,\uparrow} c^\dagger_{2,\downarrow} c^\dagger_{4,\downarrow} + c^\dagger_{1,\uparrow} c^\dagger_{4,\uparrow} c^\dagger_{2,\downarrow} c^\dagger_{3,\downarrow} + c^\dagger_{2,\uparrow} c^\dagger_{4,\uparrow} c^\dagger_{2,\downarrow} c^\dagger_{3,\downarrow} \\
&\qquad + c^\dagger_{1,\uparrow} c^\dagger_{3,\uparrow} c^\dagger_{2,\downarrow} c^\dagger_{3,\downarrow} + c^\dagger_{2,\uparrow} c^\dagger_{3,\uparrow} c^\dagger_{1,\downarrow} c^\dagger_{3,\downarrow} + c^\dagger_{1,\uparrow} c^\dagger_{4,\uparrow} c^\dagger_{2,\downarrow} c^\dagger_{4,\downarrow} + c^\dagger_{2,\uparrow} c^\dagger_{4,\uparrow} c^\dagger_{1,\downarrow} c^\dagger_{4,\downarrow} \Big) \\
&\quad - \left(c^\dagger_{1,\uparrow} c^\dagger_{3,\uparrow} c^\dagger_{1,\downarrow} c^\dagger_{3,\downarrow} + c^\dagger_{2,\uparrow} c^\dagger_{3,\uparrow} c^\dagger_{2,\downarrow} c^\dagger_{3,\downarrow} + c^\dagger_{1,\uparrow} c^\dagger_{4,\uparrow} c^\dagger_{1,\downarrow} c^\dagger_{4,\downarrow} + c^\dagger_{2,\uparrow} c^\dagger_{4,\uparrow} c^\dagger_{2,\downarrow} c^\dagger_{4,\downarrow} \right)
\end{aligned}
$$

Using the wavefunctions ψ_{D_1} and ψ_{D_2} for the dimer coverings and applying the steps i) to iii) of the procedure to calculate E_{RVB}, described in the previous Section, leads to a result that is in a very good agreement with the exact groundstate energy ϵ_0 of the system.

Figure (3.7) respectively Table 3.5 compare the obtained approximation for the groundstate energy using the Gutzwiller Wavefunction and the RVB wavefunction to ϵ_0 for different values of the parameters U/t.

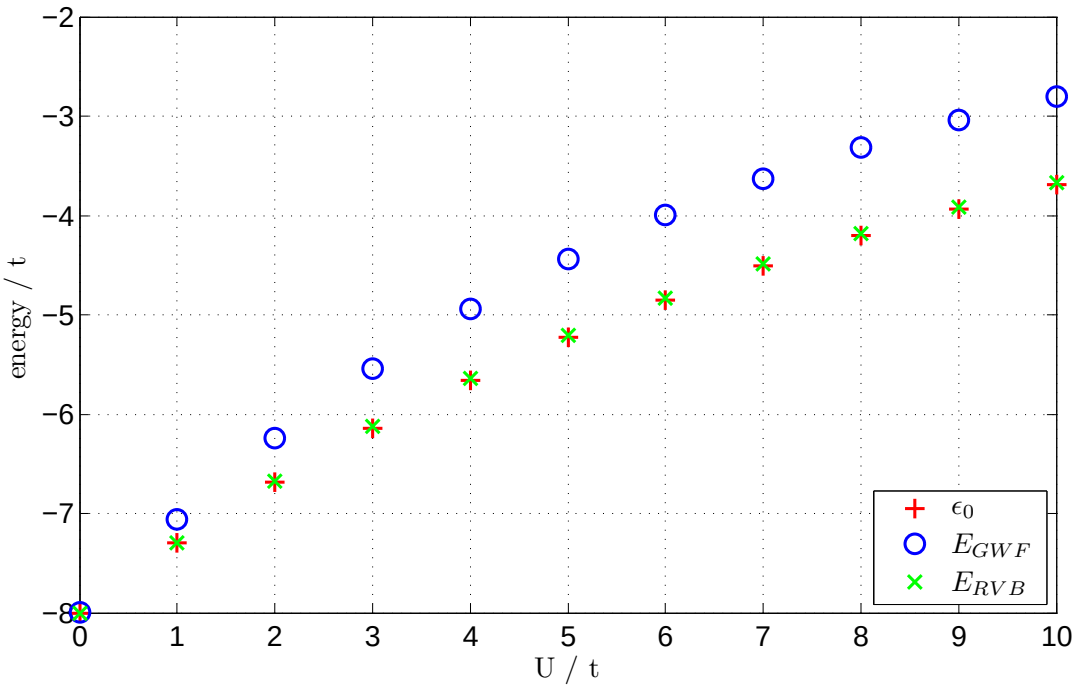

Figure 3.7.: Comparison of the exact groundstate energy ϵ_0 and the approximations E_{GWF} and E_{RVB} as a function of U/t for a system with $L_X \times L_Y = 2 \times 2$ and $N_\uparrow = N_\downarrow = 2$. The energies are given in units of t.

Table 3.5.: Corresponding values of Figure (3.7). The energies are given in units of t.

U/t	E_{GWF}	E_{RVB}	ϵ_0
0	-8.0000	-8.0000	-8.0000
1	-7.0623	-7.2957	-7.2980
2	-6.2462	-6.6747	-6.6817
3	-5.5440	-6.1264	-6.1381
4	-4.9443	-5.6412	-5.6569
5	-4.4340	-5.2113	-5.2294
6	-4.0000	-4.8294	-4.8489
7	-3.6301	-4.4895	-4.5092
8	-3.3137	-4.1861	-4.2055
9	-3.0416	-3.9147	-3.9332
10	-2.8062	-3.6712	-3.6886

3.2.2. Results for the system $L_X \times L_Y = 2 \times 4$

In this Section, again, the obtained result of the RVB approximation E_{RVB} is compared to the groundstate energy ϵ_0.
But, in contrast to Section 3.2.1, it was useful for the minimisation procedure to divide the possible dimer coverings for this system, shown in Figure (3.5) and (3.8), into classes first. The classification of the coverings was done according to the number of veritical bonds. That means, class one is depicted in Figure (3.5), class two in the first row of Figure (3.8) and class three in the second row of Figure (3.8).
The wavefunction, corresponding to a class, is a linear combination of the wavefunction of its dimer coverings, whereby each dimer covering has got the same weight and a sign as depicted in Figure (3.8). (The sign was found within a trial and error process.)

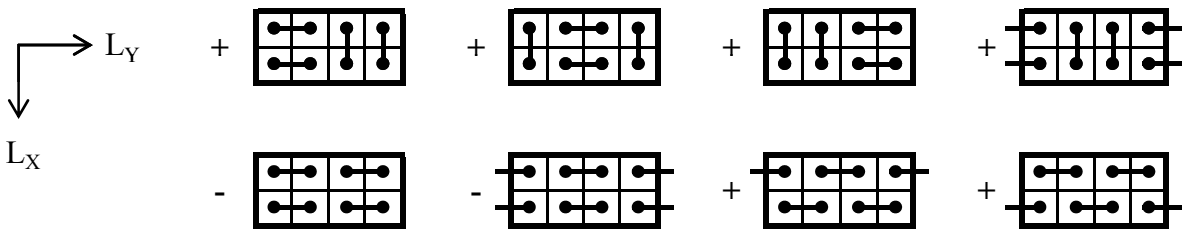

Figure 3.8.: Eight of the nine possible dimer coverings for the system $L_X \times L_Y = 2 \times 4$, whereby those pictured in the same row, belong to the same class. The + or − show the sign of the corresponding covering within a class.

Therefore, the minimisation procedure of Equation (3.7) is a task in 4 dimensions. Furthermore, it has shown to be advantageous if one neglects step i) of the minimisation procedure and to use the same weight factors for all classes instead of that.

The results of the calculations are depicted in Figure (3.9) and Table 3.6. As one can see, the RVB approximation gives a lower energy than the Gutzwiller Wavefunction and thus has to be preferred for this system.
However, the agreement with the groundstate energy is not as good as for the system $L_X \times L_Y = 2 \times 2$.

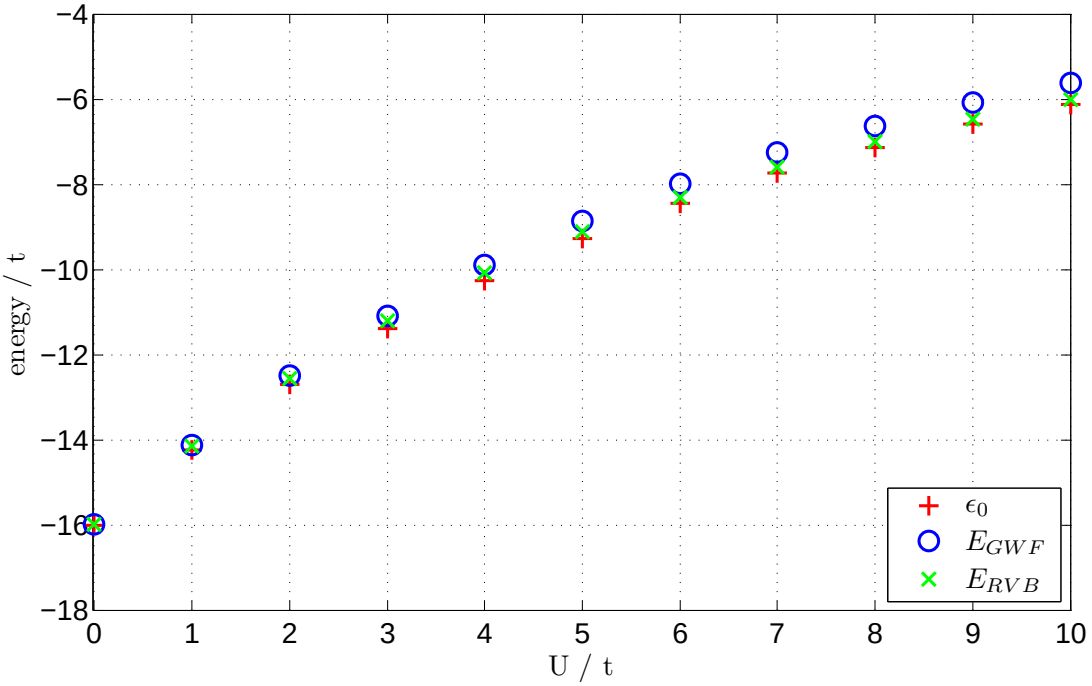

Figure 3.9.: Comparison of the exact groundstate energy ϵ_0 and the approximations E_{GWF} and E_{RVB} as a function of U/t for a system with $L_X \times L_Y = 2 \times 4$ and $N_\uparrow = N_\downarrow = 4$. The energies are given in units of t.

Table 3.6.: Corresponding values of Figure (3.9). The energies are given in units of t.

U/t	E_{GWF}	E_{RVB}	ϵ_0
0.00	-16.0000	-16.0000	-16.0000
1.00	-14.1245	-14.1420	-14.2395
2.00	-12.4924	-12.5569	-12.7053
3.00	-11.0880	-11.2157	-11.3839
4.00	-9.8885	-10.0822	-10.2530
5.00	-8.8680	-9.1210	-9.2861
6.00	-8.0000	-8.3015	-8.4574
7.00	-7.2603	-7.5984	-7.7441
8.00	-6.6274	-6.9912	-7.1267
9.00	-6.0832	-6.4634	-6.5894
10.00	-5.6125	-6.0018	-6.1190

3.2.3. Results for the system $L_X \times L_Y = 4 \times 4$

For this system we used the minimisation procedure as described in Section 3.2. The result of the RVB approximation using parameters $U/t = 4$ after the first two steps is

$$\begin{aligned} i) \quad & E_{RVB} = -9.5155 \quad \text{and} \\ ii) \quad & E_{RVB} = -10.6617 \quad , \end{aligned}$$

what is not in a good agreement with the groundstate energy ϵ_0 (see Table 3.1). This is why step iii) was not performed for this system.
Maybe by the use of the RVB wavefunction, an insufficient number of basis states of the Hamiltonian are occupied, what is at most

$$272 \cdot 4^8$$

merely 10.8 % of the size of the Hilbert space.
Furthermore, one would be able to improve the result by taking also the next nearest neighbour bonds into account, but this leads to an unworthy long computing time.

3.3. A variational approach based on the maximum entropy principle

In Ref. [20] Canosa, Plastino and Rossignoli describe, that a quantum state in a complete orthonormal basis can be treated as probability density, if it is positive definite. Thus, one can define a quantal entropy and use the maximum entropy principle to give an approach for the groundstate wavefunction. This procedure is applied to the one-dimensional fermion Hubbard model in Ref. [21].
In this Section, we will give a short overview of the derivation in Ref. [20] and use this principle to compute an approximation of the groundstate wavefuntion of the two-dimensonal hardcore-boson Hubbard model. That means, occupation numbers like fermions, but commutator relations like bosons.

Let us assume an arbitrary wavefunction

$$|\,\psi\,\rangle = \sum_\nu c_\nu\,|\,\chi_\nu\,\rangle\;, \qquad c_\nu \in \mathbb{R}\;, \qquad c_\nu \geq 0 \quad \forall \nu\;, \tag{3.8}$$

represented in a complete orthonormal basis $|\,\chi\,\rangle$ with

$$\rho = \langle\,\psi\,|\,\psi\,\rangle = \sum_\nu |c_\nu|^2 \quad ,$$

then one is able to define a quantal entropy S associated with the probability distribution ρ.

$$S = -\sum_\nu \rho(\nu)\,\ln\rho(\nu) = -\sum_\nu 2\,c_\nu^2\,\ln(c_\nu) \tag{3.9}$$

Furthermore, let us suppose that the available information of the treated system, assumed to be in the groundstate, is given by a set of n linear independent expectation values of observables

$$O_i = \langle\,\psi\,|\,\hat{O}_i\,|\,\psi\,\rangle = \sum_{\nu,\nu'} c_\nu\,c_{\nu'}\,\langle\,\chi_\nu\,|\,\hat{O}_i\,|\,\chi_{\nu'}\,\rangle\;, \qquad i = 1, \cdots, n \quad . \tag{3.10}$$

We use the *maximum* (*quantum*) *entropy* (MQE) principle to compute the coefficients c_ν of Equation (3.8). That means to choose that wavefunction, which extremalizes Equation (3.9) considering the constraints in Equation (3.10). For every constraint O_i, a Lagrange multiplier λ_i is introduced and for simplification we restrict ourselves to diagonal operators.
Therefore, the Lagrange equation is given by

$$\mathscr{L} \;=\; S - \sum_i \lambda_i \, O_i \;=\; -\sum_\nu 2\, c_\nu^2 \, \ln\left(c_\nu\right) - \sum_i \lambda_i \left(\sum_\nu c_\nu^2 \, \langle\, \chi_\nu \,|\, \hat{O}_i \,|\, \chi_\nu \,\rangle \right) \quad . \tag{3.11}$$

The calculation of the extremum yields

$$\begin{aligned} \frac{\partial \mathscr{L}}{\partial c_\nu} \;\stackrel{!}{=}\; 0 \;&=\; -4c_\nu \ln c_\nu - 2c_\nu - \sum_i \lambda_i \, 2c_\nu \, \langle\, \chi_\nu \,|\, \hat{O}_i \,|\, \chi_\nu \,\rangle \\ &=\; -2 \ln c_\nu - 1 - \sum_i \lambda_i \, \langle\, \chi_\nu \,|\, \hat{O}_i \,|\, \chi_\nu \,\rangle \\ \Rightarrow \quad c_\nu \;&=\; \frac{1}{Z} \, \exp\left(- \sum_i \lambda_i \, \langle\, \chi_\nu \,|\, \hat{O}_i \,|\, \chi_\nu \,\rangle \right) \quad , \end{aligned} \tag{3.12}$$

whereby Z is simply a normalization constant. The Lagrange multipliers $\vec{\lambda}$ in Equation (3.12) become a set of variational parameters and are determined by minimising the expectation value of the Hamiltonian $\hat{H}$.

$$\min_{\vec{\lambda}} \; E_{MQE} \;=\; \min_{\vec{\lambda}} \; \frac{\langle\, \psi(\vec{\lambda}) \,|\, \hat{H} \,|\, \psi(\vec{\lambda}) \,\rangle}{\langle\, \psi(\vec{\lambda} \,|\, \psi(\vec{\lambda}) \,\rangle} \tag{3.13}$$

For the concrete example, the two-dimensonal hardcore-boson Hubbard model, we used three operators to calculate the approximation for the groundstate energy.

- The local correlation operator

$$\hat{D} \;=\; \sum_i n_{i,\uparrow} \, n_{i,\downarrow} \quad , \tag{3.14}$$

  which simply counts the double occupations of the basis state,

- the spin-spin correlation operator

$$\hat{C}_{SS} \;=\; \sum_{\langle i,j \rangle} \hat{S}_i \, \hat{S}_j \quad \text{and} \tag{3.15}$$

- the density-density correlation operator

$$\hat{C}_{NN} \;=\; \sum_{\langle i,j \rangle} \hat{N}_i \, \hat{N}_j \quad . \tag{3.16}$$

In this context $\langle i,j \rangle$ denotes to sum only over the nearest neighbours, while $\hat{S}_i = n_{i,\uparrow} - n_{i,\downarrow}$ and $\hat{N}_i = n_{i,\uparrow} + n_{i,\downarrow}$, as also described in Ref. [21]. These operators describe the main correlations of the system and are diagonal in real space.

In Figure (3.10), the exact groundstate energy ϵ_0 is compared to the approach E_{MQE}, based on Equation (3.12) till (3.16), as a function of U/t for a system with $L_X \times L_Y = 3 \times 3$ and $N_\uparrow = N_\downarrow = 3$ hardcore-bosons. As one can see, they are in a very good agreement.
The corresponding values of Figure (3.10) are depicted in Table 3.7.

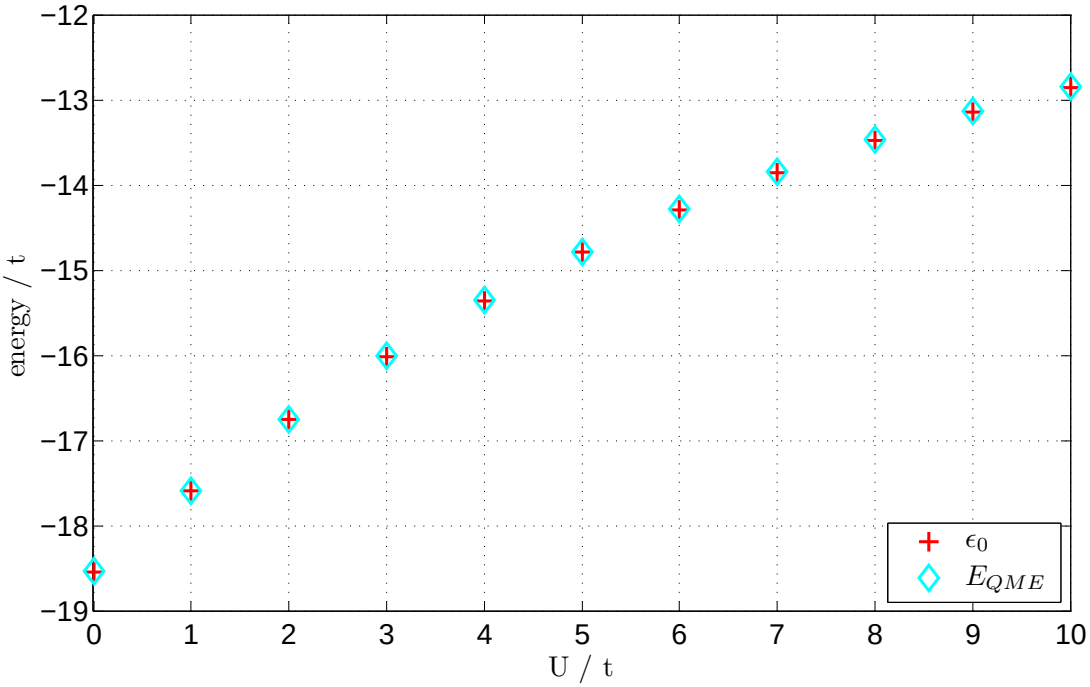

Figure 3.10.: Comparison of the exact groundstate energy ϵ_0 and the approximation E_{MQE}, based on maximum quantum entropy, as function of U/t for a system with $L_X \times L_Y = 3 \times 3$ and $N_\uparrow = N_\downarrow = 3$ hardcore-bosons. To calculate E_{MQE} the operators $\hat{D}$, $\hat{C}_{SS}$ and $\hat{C}_{NN}$ were taken into account. The energies are given in units of t.

Table 3.7.: Corresponding values of Figure (3.10). The energies are given in units of t.

U/t	E_{MQE}	ϵ_0
0	-18.5375	-18.5424
1	-17.5921	-17.5972
2	-16.7514	-16.7572
3	-16.0085	-16.0152
4	-15.3554	-15.3631
5	-14.7834	-14.7924
6	-14.2839	-14.2942
7	-13.8481	-13.8596
8	-13.4677	-13.4805
9	-13.1351	-13.1491
10	-12.8436	-12.8587

4. The Sign Problem

In this Chapter we discuss a topic, named in the literature of Diffusion Monte Carlo respectively Greens Function Monte Carlo, the sign problem and its impacts. In the following Section, an additional ingredient of the DMC algorithm is presented, originally introduced by A. Alavi and his co-workers in Ref. [22], which helps to reduce the sign problem.

One is able to describe the sign problem in a few sentences [23]. Suppose there is a walker in basis state χ_ν with sign s at time τ and it is propagating through the Hilbert space. While its movement, the walker can pick up a sign if the Hamiltonian of the system has off-diagonal elements with different signs. Let us assume, this walker, or one of its descendants, returns to this basis state at time $\tau' > \tau$, but with a sign $-s$. Thus, the problem arises, that the average value of the coefficient of this basis state has a large variance, which results in large fluctuations of the calculated observables.
The annihilation step, described in Section 2.2.2, works against this problem. Thereby, one assumes that after a time step the majority of the walkers on a basis state has the correct sign and those walkers with the wrong sign are annihilated. This part of the algorithm should ensure that the coefficients of the basis states earn the correct sign on the average.
However, if the size of the Hilbert space N_H is much bigger than the number of walkers N_W, used within a DMC simulation, annihilation events become seldom.

Figure (4.1) shows the results of some DMC calculations as a function of the mean number of walkers N_W, used within the simulation, divided by the size of the Hilber space N_H. Both, the obtained energy E_{DMC} (calculated using Equation (2.9)) and the mean value of the energy shift $\langle S \rangle$ should actually be in agreement with the true groundstate energy ϵ_0.
But, as you can realise, the obtained results depend on the ratio N_W/N_H. That means, if the Hamiltonian has off-diagonal elements with different signs, there is a critical value N_C of required walkers (in the example, depicted in Figure (4.1), it's about 80 % of the size of the Hilbert space) to achieve convergence. To repeat quintessence, not before $N_W/N_H > N_C$ are E_{DMC} and $\langle S \rangle$ in an agreement with the groundstate energy ϵ_0 and N_C scales with the size of the Hilbert space, as observed during our calculations.
This is, of course, a terrible result, because the required memory to store the walkers within a DMC simulation is in the range as for the lanczos algorithm. Keep in mind that without the sign problem theoretically a handful of walkers suffice to obtain an exact result for the groundstate energy.

For further information regarding the sign problem and its impact to DMC simulations, see Ref. [24].

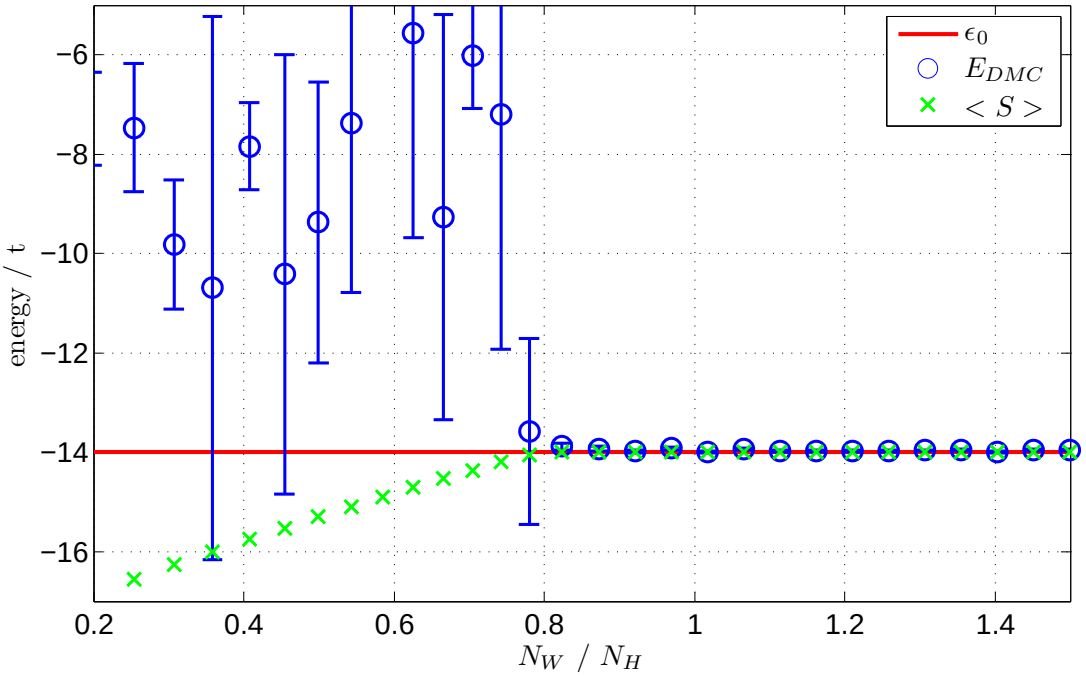

Figure 4.1.: Comparison of the exact groundstate energy $\epsilon_0 = -13.9962$ to the energy obtained from the DMC simulation E_{DMC} and to the corresponding mean value of the energy shift $\langle S \rangle$ as a function of the mean number of walkers N_W divided by the size of the Hilbert space N_H.
The parameters of the considered system are $L_X \times L_Y = 4 \times 3$, $N_\uparrow = N_\downarrow = 3$ and $U/t = 4$. The energies are given in units of t.
The errorbars for E_{DMC} are plotted for a confidence interval of $\pm\sigma$ and were computed using Equation (A.4). For $\langle S \rangle$ no errorbars are plotted, because they are smaller than the markers.

Table 4.1.: Corresponding values of Figure (4.1).
Comparison of the exact groundstate energy $\epsilon_0 = -13.9962$ to the energy obtained from the DMC simulation $E_{DMC} \pm \sigma_{DMC}$ and to the corresponding mean value of the energy shift $\langle S \rangle$ as a function of the mean number of walkers N_W divided by the size of the Hilbert space N_H.
The parameters of the considered system are $L_X \times L_Y = 4 \times 3$, $N_\uparrow = N_\downarrow = 3$ and $U/t = 4$. The energies are given in units of t.

N_W/N_H	$\langle S \rangle$	E_{DMC}	σ_{DMC}
0.14	-17.19	-7.15	2.40
0.20	-16.86	-7.29	0.93
0.25	-16.56	-7.47	1.29
0.31	-16.27	-9.82	1.31
0.36	-16.00	-10.69	5.47
0.41	-15.76	-7.84	0.87
0.45	-15.52	-10.41	4.43
0.50	-15.31	-9.37	2.83
0.54	-15.10	-7.37	3.40
0.58	-14.90	-799.62	165.57
0.63	-14.71	-5.55	4.13
0.67	-14.53	-9.27	4.09
0.70	-14.36	-6.02	1.06
0.74	-14.20	-7.20	4.73
0.78	-14.05	-13.59	1.87
0.82	-13.99	-13.88	0.07
0.87	-13.99	-13.93	0.04
0.92	-14.00	-13.98	0.04
0.97	-13.99	-13.92	0.03
1.02	-13.99	-14.00	0.03
1.07	-14.00	-13.94	0.02
1.11	-14.00	-13.98	0.02
1.16	-14.00	-13.97	0.02
1.21	-14.00	-13.97	0.02
1.26	-14.00	-13.97	0.02
1.31	-14.00	-13.97	0.02
1.35	-13.99	-13.96	0.02
1.40	-13.99	-13.99	0.02
1.45	-13.99	-13.95	0.02
1.50	-13.99	-13.95	0.02

4.1. Initiator Diffusion Monte Carlo

In this Section, we describe a strategy, presented in Ref. [22], to reduce the required number of walkers to achieve convergence of a DMC simulation. This strategy contains some kind of survival criterion to newly spawned walkers and results in additional rules, which can easily be adopted in the DMC algorithm.

i) If a basis state is occupied by n_a or more walkers, those walkers become *initiators*. Only initiators are allowed to spawn progeny onto unoccupied basis states.
This ability gets lost if the number of walkers in this state is less than n_a.

ii) The progeny of walkers, which are no initators, survive only if they are spawned onto an occupied basis state.

iii) The exception of i) and ii) is the special case, whereby two non-initators spawn new walkers with the same sign onto a previously unoccupied basis state.

Using these rules, one wants to ensure that an unoccupied state is only populated by a new walker if its parent walkers have a well established sign. Thus, one assumes that newly spawned walkers are also sign coherent.
Using this initiator algorithm is associated with a systematic error. Since obviously in the limit of $n_a \to 0$ and $N_W \to \infty$ this algorithm reduces to the original one and the error removes also within these limits.
For further details of the initator approximation see also Ref. [25].

5. The Fixed Node Approximation

As described in Chapter 4, the Diffusion Monte Carlo method can only be applied to fermionic systems with huge efforts to the required memory, because of the sign problem. In this Chapter, we present an approximation, originally introduced by Ceperley and Alder in Ref. [26], to avoid the sign problem by replacing the full Hamiltonian by an effective Hamiltonian and show in Section 5.1, that this approximation gives an upper bound for the true groundstate energy of the system.
In Section 5.2, we do a calculation for a toy model to demonstrate how the *Fixed Node Approximation* (FNA) works and subsequently present some results for different system sizes in Section 5.3. Section 5.4 describes that under certain conditions, the FNA can be used as input for another calculation, called *Nodal Release*, to obtain the ground state energy of the full Hamiltonian.

Suppose there is quite a good approach Ψ_T for the groundstate wavefunction ϕ_0 of the Hamiltonian available. (In the case of the Hubbard model with periodic boundary conditions this wavefunction can be real.)
The idea of the FNA is to avoid the sign problem by dividing the configuration space into nodal regions, depending on the nodes of a trial wavefunction Ψ_T, which results in an effective Hamiltonian $\hat{H}_{eff}$. A nodal region is a set of basis states connected by the Hamiltonian in which the trial function has the same sign. This effective Hamiltonian is designed that a walker remains in its nodal region and therefore can never collect an unwanted sign during its propagation.
An unwanted sign only occurs if off-diagonal matrix elements of $\hat{H}$ exist with

$$\hat{H}_{n,m}\,\Psi_n^T\,\Psi_m^T > 0 \quad . \tag{5.1}$$

To avoid the hopping of the walkers across the nodal regions, those elements are set to zero in the effective Hamiltonian.

$$\langle \chi_n \,|\, \hat{H}_{eff} \,|\, \chi_m \rangle = \begin{cases} \langle \chi_n \,|\, \hat{H} \,|\, \chi_m \rangle & \text{if} \quad \hat{H}_{n,m}\,\Psi_n^T\,\Psi_m^T < 0 \\ 0 & \text{otherwise} \end{cases} \tag{5.2}$$

The diagonal elements of the effective Hamiltonian are given by

$$\langle \chi_n \,|\, \hat{H}_{eff} \,|\, \chi_n \rangle = \langle \chi_n \,|\, \hat{H} \,|\, \chi_n \rangle + \langle \chi_n \,|\, \hat{V}_{sf} \,|\, \chi_n \rangle \quad . \tag{5.3}$$

The last term in Equation (5.3) is called the sign-flip potential. It is defined by

$$\langle \chi_n \,|\, \hat{V}_{sf} \,|\, \chi_n \rangle = \sum_m^{sf} \langle \chi_n \,|\, \hat{H} \,|\, \chi_m \rangle \frac{\Psi_m^T}{\Psi_n^T} \quad , \tag{5.4}$$

whereby the summation is over all matrix elements for which Equation (5.1) holds. In the effective Hamiltonian, the hopping across the nodes is replaced by a positive diagonal potential. This is essential, because without $\hat{V}_{sf}$ the value of the wavefunction at the nodes would be too high and its energy too low, as found in Ref. [27].

5.1. Proof for an upper bound

In Ref. [28], D. M. Ceperley and his co-workers did a calculation to proof that the FNA gives an upper bound for the groundstate energy of $\hat{H}$. They started by introducing a truncated Hamiltonian $\hat{H}_{tr}$ and a sign-flip Hamiltonian $\hat{H}_{sf}$.

$$\hat{H} = \hat{H}_{tr} + \hat{H}_{sf} \tag{5.5}$$

$$\hat{H}_{eff} = \hat{H}_{tr} + \hat{V}_{sf} \tag{5.6}$$

The matrix elements of $\hat{H}_{tr}$ are defined by

$$\langle \chi_n \,|\, \hat{H}_{tr} \,|\, \chi_n \rangle = \langle \chi_n \,|\, \hat{H} \,|\, \chi_n \rangle \qquad \text{and} \qquad \langle \chi_n \,|\, \hat{H}_{tr} \,|\, \chi_m \rangle = \langle \chi_n \,|\, \hat{H}_{eff} \,|\, \chi_m \rangle \quad ,$$

and $\hat{H}_{sf}$ only contains the off-diagonal elements of $\hat{H}$, which are set to be zero in $\hat{H}_{eff}$. Furthermore, an arbitrary normed wavefunction ψ is used to calculate the energy difference between $\hat{H}_{eff}$ and $\hat{H}$.

$$\begin{aligned}
\Delta E &= \langle \psi \,|\, \left(\hat{H}^{eff} - \hat{H} \right) \,|\, \psi \rangle \\
\Delta E &= \langle \psi \,|\, \left(\hat{V}^{sf} - \hat{H}^{sf} \right) \,|\, \psi \rangle \\
\Delta E &= \sum_n \psi_n^* \, \hat{V}^{sf}_{n,n} \, \psi_n - \sum_n \psi_n \left(\hat{H}^{sf} \,|\, \psi \rangle \right)_n \\
\Delta E &= \sum_n \psi_n^* \left[\hat{V}^{sf}_{n,n} \, \psi_n - \sum_m \hat{H}^{sf}_{n,m} \, \psi_m \right]
\end{aligned}$$

Next, we replace the operators $\hat{V}^{sf}$ and $\hat{H}^{sf}$ with terms of the original Hamiltonian $\hat{H}$.

$$\Delta E = \sum_n \psi_n^* \left[\sum_m^{sf} \hat{H}_{n,m} \frac{\Psi_m^T}{\Psi_n^T} \, \psi_n - \sum_m^{sf} \hat{H}_{n,m} \, \psi_m \right] \tag{5.7}$$

In the double summation in the previous line each combination of $(n,\, m)$ occurs twice. That means, we are able to rewrite Equation (5.7) as a summation over pairs.

$$\Delta E = \sum_{(n,m)}^{sf} \hat{H}_{n,m} \left[|\psi_n|^2 \frac{\Psi_m^T}{\Psi_n^T} + |\psi_m|^2 \frac{\Psi_n^T}{\Psi_m^T} - \psi_n^* \, \psi_m - \psi_m^* \, \psi_n \right] \tag{5.8}$$

Since the sum considers only terms for which condition (5.1) holds, the first two terms of Equation (5.8) in combination with $\hat{H}_{n,m}$ are strictly positive. For the second two terms we have to mind the sign $s_{n,m}$ of the matrix elements $\hat{H}_{n,m}$.

$$\begin{aligned}
\Delta E &= \sum_{(n,m)}^{sf} |\hat{H}_{n,m}| \left[|\psi_n|^2 \left| \frac{\Psi_m^T}{\Psi_n^T} \right| + |\psi_m|^2 \left| \frac{\Psi_n^T}{\Psi_m^T} \right| - s_{n,m} \, \psi_n^* \, \psi_m - s_{m,n} \psi_m^* \, \psi_n \right] \\
\Delta E &= \sum_{(n,m)}^{sf} |\hat{H}_{n,m}| \left[\psi_n \sqrt{\left| \frac{\Psi_m^T}{\Psi_n^T} \right|} - s_{n,m} \, \psi_m \sqrt{\left| \frac{\Psi_n^T}{\Psi_m^T} \right|} \right]^2 \geq 0
\end{aligned} \tag{5.9}$$

It is mentionable that one does not have to worry about the case $\Psi_n^T = 0$, because such a configuration does not occur in the summation.

As one can see in Equation (5.9), ΔE is positive for an arbitrary wavefunction ψ. That means, the groundstate energy of the effective Hamiltonian E_{FNA} is an upper bound for the true groundstate energy ϵ_0.
If we consider the special case of $\Psi_T = \psi$, one can easily verify with the help of Equation (5.8), that $\Delta E = 0$ and therefore

$$\epsilon_0 \leq E_{FNA} \leq \frac{\langle \Psi_T \,|\, \hat{H}_{eff} \,|\, \Psi_T \rangle}{\langle \Psi_T \,|\, \Psi_T \rangle} = \frac{\langle \Psi_T \,|\, \hat{H} \,|\, \Psi_T \rangle}{\langle \Psi_T \,|\, \Psi_T \rangle} \quad , \tag{5.10}$$

where the second inequality follows from the usual variational principle. Naturally, the better the trial wavefunction corresponds to the groundstate wavefunction of the Hamiltonian, the better the result of the FNA.
To repeat the quintessence, the groundstate energy E_{FNA} of the effective Hamiltonian can be computed with the DMC method without a sign problem, gives an upper bound for ϵ_0 and improves the energy, obtained from the trial wavefunction.

5.2. Example for the Fixed Node Procedure

In this Section, we use a toy model to illustrate how the effective Hamiltonian in the FNA is created and demonstrate that Equation (5.10) holds.

For simplicity we choose the Hubbard Hamiltonian for spinless fermions

$$\hat{H} = -t \sum_{\langle i,j \rangle} c_i^\dagger \, c_j$$

and consider a one-dimensional system with four sites, periodic boundary conditions and two particles in it. This system has six different basis states, depicted in Equation (5.12), and is described by the Hamiltonian

$$H = \begin{pmatrix} 0 & -t & 0 & 0 & +t & 0 \\ -t & 0 & -t & -t & 0 & +t \\ 0 & -t & 0 & 0 & -t & 0 \\ 0 & -t & 0 & 0 & -t & 0 \\ +t & 0 & -t & -t & 0 & -t \\ 0 & +t & 0 & 0 & -t & 0 \end{pmatrix} \quad , \tag{5.11}$$

with the groundstate energy $\epsilon_0 = -2\,t$.

$$
\begin{aligned}
|\,\Gamma_1\,\rangle &= c_1^\dagger\, c_2^\dagger\,|\,0\,\rangle \quad \widehat{=} \\
|\,\Gamma_2\,\rangle &= c_1^\dagger\, c_3^\dagger\,|\,0\,\rangle \quad \widehat{=} \\
|\,\Gamma_3\,\rangle &= c_2^\dagger\, c_3^\dagger\,|\,0\,\rangle \quad \widehat{=} \\
|\,\Gamma_4\,\rangle &= c_1^\dagger\, c_4^\dagger\,|\,0\,\rangle \quad \widehat{=} \\
|\,\Gamma_5\,\rangle &= c_2^\dagger\, c_4^\dagger\,|\,0\,\rangle \quad \widehat{=} \\
|\,\Gamma_6\,\rangle &= c_3^\dagger\, c_4^\dagger\,|\,0\,\rangle \quad \widehat{=}
\end{aligned}
$$

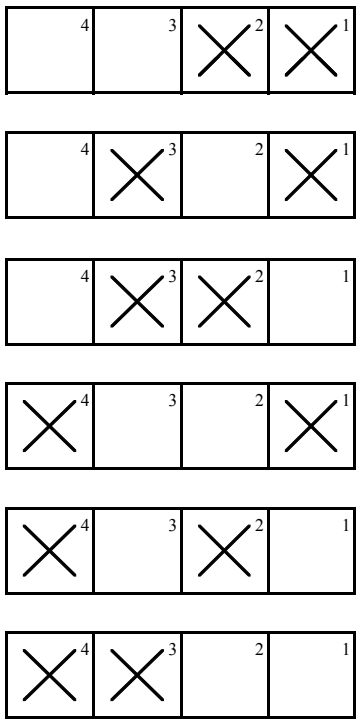

(5.12)

We consider a very simple trial wavefunction, given by

$$|\,\Psi_T\,\rangle = \frac{1}{\sqrt{6}}\left(|\,\Gamma_1\,\rangle + |\,\Gamma_2\,\rangle + |\,\Gamma_3\,\rangle + |\,\Gamma_4\,\rangle + |\,\Gamma_5\,\rangle + |\,\Gamma_6\,\rangle\right) \quad ,$$

to calculate the effective Hamiltonian $\hat{H}_{eff}$ of the FNA. Using Equation (5.2), (5.3) and (5.4) we obtain

$$H_{eff} = \begin{pmatrix} +t & -t & 0 & 0 & 0 & 0 \\ -t & +t & -t & -t & 0 & 0 \\ 0 & -t & 0 & 0 & -t & 0 \\ 0 & -t & 0 & 0 & -t & 0 \\ 0 & 0 & -t & -t & +t & -t \\ 0 & 0 & 0 & 0 & -t & +t \end{pmatrix} \quad , \tag{5.13}$$

whereby the adaptations are highlighted in color. That means, for example, hopping from basis state $|\,\Gamma_1\,\rangle$ to $|\,\Gamma_5\,\rangle$ is not possible anymore, because of the sign-flip in the original Hamiltonian. The groundstate energy of the effective Hamiltonian is given by $E_{FNA} = -1.709\,t$.
Finally, we calculate

$$\frac{\langle\,\Psi_T\,|\,\hat{H}_{eff}\,|\,\Psi_T\,\rangle}{\langle\,\Psi_T\,|\,\Psi_T\,\rangle} = \frac{\langle\,\Psi_T\,|\,\hat{H}\,|\,\Psi_T\,\rangle}{\langle\,\Psi_T\,|\,\Psi_T\,\rangle} = -\frac{4}{3}\,t \quad ,$$

to verify Equation (5.10).

This concept can be generalized straightforwardly to more complicated systems. In our special case we applied the FNA to the fermion Hubbard model and used the Gutzwiller Wavefunction respectively the RVB Wavefunction (described in Section 3.1 and 3.2) as trial functions.
Also for the FNA, the initial walker configuration is distributed according to the trial wavefunction. However, if a nodal region is not occupied by at least one walker at the beginning, the whole region isn't sampled during the whole DMC simulation. This is why the effective Hamiltonian forbids the hopping across nodal boundaries.

5.3. Results of the FNA

In this Section, the true groundstate energy ϵ_0 for different systems is compared to the results obtained using the FNA. In addition, the energy of the corresponding trial wavefunction is also depicted.
The results are listed in Table 5.1, whereby instead of a DMC simulation, exact diagonalisation was used in the calculations.

For the system $L_X \times L_Y = 3 \times 3$ with $N_\uparrow = N_\downarrow = 3$ electrons, which is degenerated in k-space for $U = 0$, two different Gutzwiller trial wavefunctions were used. They differ in the groundstate wavefunctions, which were used for the Fourier transformation.
For the result, marked with $*^1$, the wavefunction in reciprocal space is chosen, so that each spin direction has momentum zero. That one, marked with $*^2$, is chosen according to Figure (3.1).

Table 5.1.: Comparison of the obtained results for the FNA to the exact groundstate energy ϵ_0 for different systems for a value of $U/t = 4$. To calculate E_{FNA}, different trial functions were used, their energies E_T are also listed.
The $\Im$ or $\Re$ denote, if the real or the imaginary part of the GWF was used to calculate the energy. The energies are given in units of t.

L_X	L_Y	$N_\uparrow$	$N_\downarrow$	Type			E_T	E_{FNA}	ϵ_0
2	2	2	2	GWF	$\Re$		-4.9443	-4.9443	-5.6569
2	2	2	2	RVB			-5.6412	-5.6569	-5.6569
2	4	4	4	GWF	$\Re$		-9.8885	-9.8885	-10.2530
2	4	4	4	RVB			-10.0822	-10.1268	-10.2530
3	3	3	3	GWF	$\Re$	$*^1$	-9.1884	-9.9575	-10.2754
3	3	3	3	GWF	$\Re$	$*^2$	-9.3765	-10.1441	-10.2754
3	3	5	5	GWF	$\Re$		-6.2104	-6.2519	-6.2911

* see text for information

5.4. Nodal Release

In this Section we present an improvement to the FNA, the *Nodal Relaxation* method, described by Ceperley and Alder in Ref. [29].
The basic idea behind is the following: One uses a walker configuration in the FNA as input for the Nodal Relaxation method, but now the walkers are again allowed to cross the nodes of the trial function. That means, one replaces the effective Hamiltonian of the FNA by the original one of the system.
Those walker generations, which belong to the same time step after the nodal release, are used to calculate the mixed estimator. The nodal release process must occur quickly, because after some time steps this estimator starts fluctuating because of the sign problem. However, if the

nodes of the trial function are in good agreement with those of the groundstate wavefunction, one obtains the exact groundstate energy of the system.

For our calculations, we decided to use two DMC simulations simultaneously. The first one computes the FNA in constant walker mode. That means, the energy shift is regulated after each time step to keep the walker population constant. Once in a while, we used a walker configuration from this simulation as input for the Nodal Release method.
The Nodal Relaxation method was computed in constant shift mode, which causes an increase of the walker population. This calculation was performed for a few time steps till the number of walker reaches a specified limit. This limit was introduced to keep the walker population always in a region where the sign problem occurs. Remember in Chapter 4, if the number of walkers exeeds a critical value, the sign problem vanishes. (For larger systems this maximum walker limit is given by the size of the main memory of the computer.) If the maximum number of walkers is reached, the current Nodal Release simulation is finished and all walkers are deleted. For the next one, again a walker configuration from the FNA is used to start with.

A positive result of this Nodal Release method is depicted in Figure (5.1) for the system $L_X \times L_Y = 3 \times 3$ with $N_\uparrow = N_\downarrow = 5$ electrons and $U/t = 4$. One can realise, after the nodal release, the energy decreases and before it starts to fluctuate it has converged to the groundstate energy.
Another example is shown in Figure (5.2) for the system $L_X \times L_Y = 2 \times 4$ with $N_\uparrow = N_\downarrow = 4$ electrons and $U/t = 4$. As discussed above, if the trial function is not in good agreement with the groundstate wavefunction, the Nodal Release method does not converge.
The errorbars in Figure (5.1) and (5.2) are plotted for a confidence interval of $\pm\sigma$ are computed using Equation (A.4).

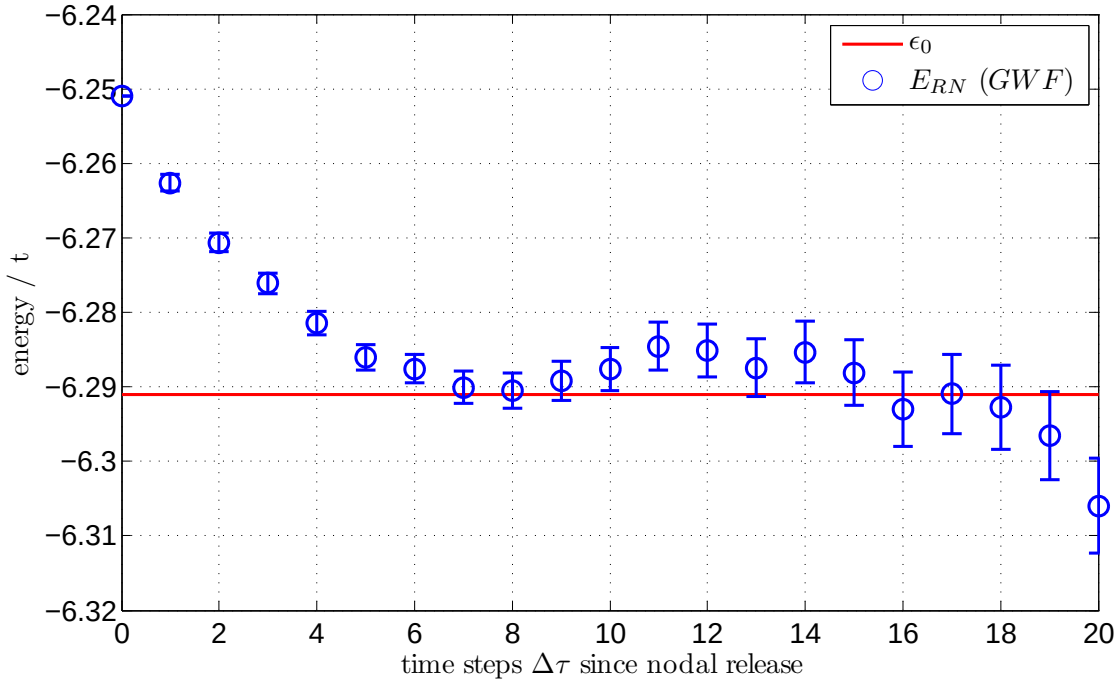

Figure 5.1.: Comparison of the exact groundstate energy ϵ_0 to the results of the Nodal Relaxation E_{RN} method as a function of the time steps since nodal release for the system $L_X \times L_Y = 3 \times 3$ with $N_\uparrow = N_\downarrow = 5$ electrons and $U/t = 4$.
The GWF was used as atrial function for the FNA. The energies are given in units of t.

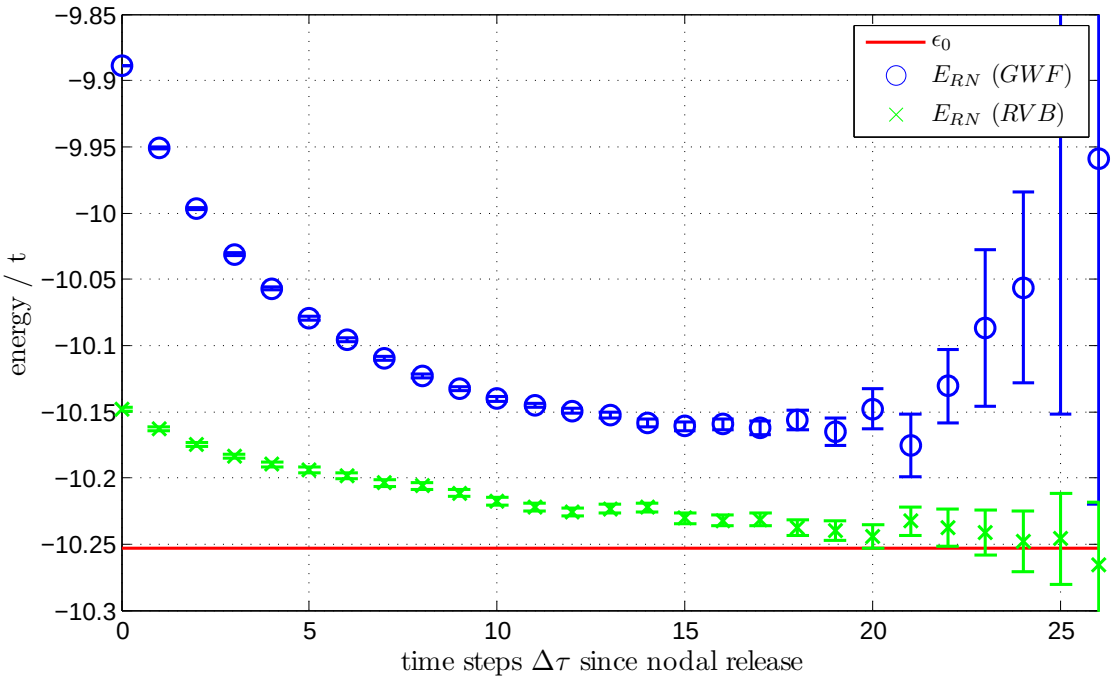

Figure 5.2.: Comparison of the exact groundstate energy ϵ_0 to the results of the Nodal Relaxation E_{RN} method as a function of the time steps since nodal release for the system $L_X \times L_Y = 2 \times 4$ with $N_\uparrow = N_\downarrow = 4$ electrons and $U/t = 4$.
Both the GWF and the RVB wavefunction were used as a trial function for the FNA. The energies are given in units of t.

6. Conclusion and Outlook

In this last Chapter, we try to give a short explanation, why neither the Nodal Release method, in combination with a trial wavefunction and the Fixed Node Approximation, nor the straight forward Diffusion Monte Carlo is a suitable procedure to calculate groundstate properties for the Hubbard model.

The latter fails because of the sign problem, described in Chapter 4. However, Alavi and his co-workers described in Ref. [22] that there are systems for which the critical number of walkers N_C is in the range of 10^{-5} and not around 1.
This is why we did an exact diagonalisation for a system in real space ($L_X \times L_Y = 4 \times 4$ with $N_\uparrow = N_\downarrow = 2$ and $U/t = 4$) to obtain the groundstate vector

$$|\,\phi_0\,\rangle = \sum_i c_i\,|\,\chi_i\,\rangle \quad ,$$

sorted the coefficients c_i by its absolute value and plotted them versus a consecutive number, depicted in red in Figure (6.1).
As you can see, nearly all c_i's have a non negligible absolute value, so the line is almost horizontal. (Also in momentum space this plot looks like that.) That means, the walkers of the DMC simulation have to sample the whole Hilbert space and it explains why the RVB wavefunction with nearest neighbour bonds is for larger systems no longer in a good agreement with the groundstate wavefunction.

The authors of Ref. [30] also work on the two-dimensional Hubbard model, but they use a different method, namely *Unrestricted Hartree Fock* (UHF).
Unrestricted Hartree Fock means to perform the standard linearization of the Hubbard Hamiltonian which leads to the mean field Hamiltonian

$$\hat{H}_{HF} \;=\; \hat{H}^{\uparrow}_{HF} + \hat{H}^{\downarrow}_{HF}$$

with

$$\hat{H}^{\sigma}_{HF} \;=\; -t \sum_{\langle i,j \rangle} c^{\dagger}_{i,\sigma}\, c_{j,\sigma} + U \sum_i n_{i,\sigma}\, \langle n_{i,\bar{\sigma}} \rangle - \frac{1}{2}\, U \sum_i \langle n_{i,\uparrow} \rangle\, \langle n_{i,\downarrow} \rangle \quad ,$$

whereby the $\langle n_{i,\sigma} \rangle$ are variational parameters. For further information see also Ref. [31].

Thereby, the idea arises not to compute in real or momentum space, but in UHF space. This is why we performed a basis transformation of the groundstate vector of the abovementioned system to UHF space. The result is plotted in blue in Figure (6.1).
As one can see, this is promising, because many basis states have coefficients c_i with not noteworthy absolute values.
If one looks more closely, one realises that the absolute value of the first few c_i's is much bigger than all the others. That means, the UHF basis is also interesting for the Initiator DMC method, described in Section 4.1.

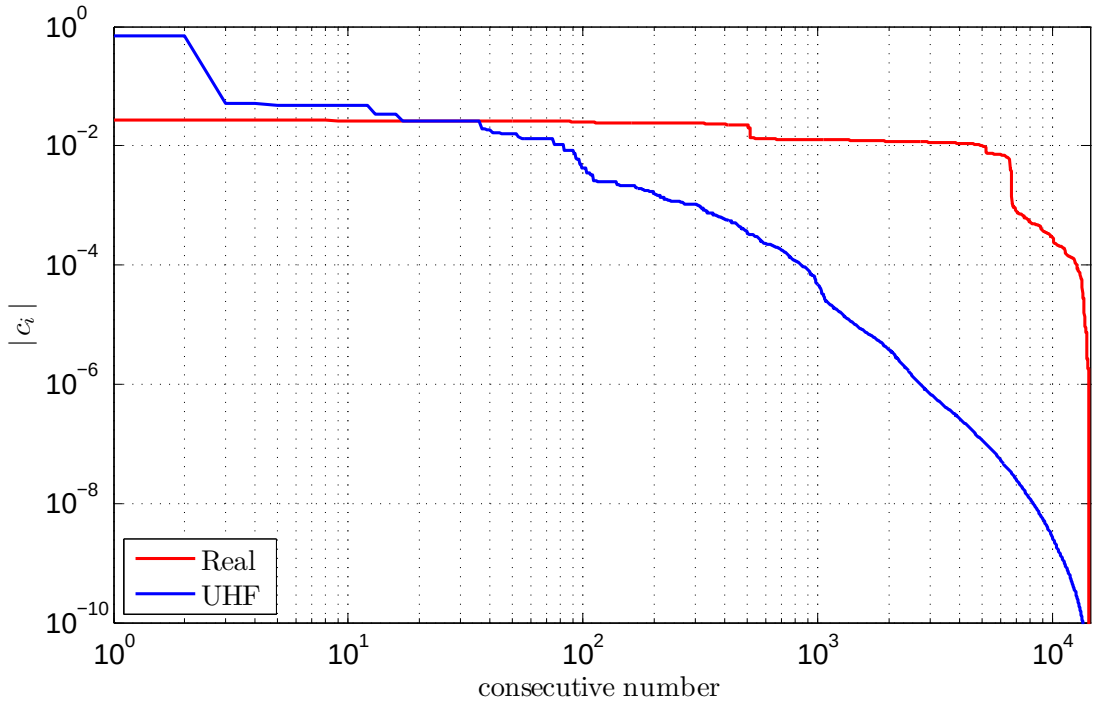

Figure 6.1.: The coefficients c_i of the groundstate vector $|\phi_0\rangle = \sum_i c_i |\chi_i\rangle$ for the system $L_X \times L_Y = 4 \times 4$ with $N_\uparrow = N_\downarrow = 2$ and $U/t = 4$ were sorted by their absolute value and plotted them versus a consecutive number for real and UHF space. Note the log-log scale.

A. Ratio Estimation

In this Appendix, we first discuss how to compute the error propagation of a ratio of two parameters according to Ref. [32]. Subsequently we show that the estimator in Equation (2.10) is biased of order $1/N$ and that it is possible to construct an unbiased estimator therefore. In Section A.3, the Jackknife Algorithm is presented, which is able to remove such a bias numerically. Finally, we use a small example to illustrate these topics.

In the following, we will again need the Taylor series expansion. This is why we illustrate the formular for a function $f(x,y)$ around the point (a,b) to second order at this point .

$$\begin{aligned} f(x,y) &= f(a,b) + (x-a)\, f_x(a,b) + (y-b)\, f_y(a,b) \\ &\quad + \frac{1}{2!}\left((x-a)^2\, f_{xx}(a,b) + 2\,(x-a)\,(y-b) f_{xy}(a,b) + (y-b)^2\, f_{yy}(a,b)\right) + \mathcal{O}(f^{(3)}) \end{aligned}$$

In this context, for example, f_x denotes $\frac{\partial}{\partial x} f(x,y)$.

A.1. Error Propagation

Let us suppose a function

$$z(x,y) = \frac{x}{y} \quad .$$

In this Section, we want to estimate how uncertainties in the parameters x and y affect the corresponding value of z.
Without loss of generality, one can assume that the independent variables x and y are random numbers normally distributed around their means x_0 respectively y_0 with standard deviations σ_x respectively σ_y. We develop this function around (x_0,y_0) and neglect quadratic and higher order terms.

$$\begin{aligned} z(x,y)\Big|_{(x_0,y_0)} &= z(x_0,y_0) + (x-x_0)\,\frac{1}{y_0} - (y-y_0)\,\frac{x_0}{y_0^2} \\ z(x,y) - z(x_0,y_0) &= \Delta x\,\frac{1}{y_0} - \Delta y\,\frac{x_0}{y_0^2} \quad \Big| \cdot \frac{y_0}{x_0} \\ \frac{\Delta z}{z_0} &= \frac{\Delta x}{x_0} - \frac{\Delta y}{y_0} \end{aligned}$$

The next step is to square both sides and to take the expectation value. In consideration of

$$\left\langle (\Delta x)^2 \right\rangle = \sigma_x^2 \quad , \quad \left\langle (\Delta y)^2 \right\rangle = \sigma_y^2 \quad \text{and} \quad \langle \Delta x\, \Delta y \rangle = 0$$

we gain the following result.

$$\begin{aligned} \frac{\langle (\Delta z)^2 \rangle}{z_0^2} &= \frac{\langle (\Delta x)^2 \rangle}{x_0^2} + \frac{\langle (\Delta y)^2 \rangle}{y_0^2} - 2\,\frac{\langle \Delta x\, \Delta y \rangle}{x_0\, y_0} \\ \frac{\sigma_z}{z_0} &= \sqrt{\left(\frac{\sigma_x}{x_0}\right)^2 + \left(\frac{\sigma_y}{y_0}\right)^2} \end{aligned} \tag{A.1}$$

Thus, we set $\langle \Delta x\, \Delta y \rangle = 0$, it is assumed that x and y are uncorrelated.

A.2. Ratio Estimation

We are interested in the estimator

$$E^* = \frac{\bar{f}}{\bar{g}} \quad . \tag{A.2}$$

Suppose there are N random numbers r_i, then $\bar{f}$ is defined to be the arithmetic mean of the function values $f(r_i)$.

$$\bar{f} = \frac{1}{N}\sum_{i=1}^{N} f(r_i) = \frac{1}{N}\sum_{i=1}^{N} f_i = \bar{\vec{f}}$$

Because of that definition $\bar{f}$, is also a stochastic variable with expectation value $\langle \bar{f} \rangle = f$. The same definitions are essential for $\bar{g}$.

To give a statement concerning E^*, one has to calculate its expectation value $\langle E^* \rangle$. Therefore, we start with a Taylor series expansion of $\bar{f}/\bar{g}$ around the point (f, g).

$$\begin{aligned} E^* = \left.\frac{\bar{f}}{\bar{g}}\right|_{(f,g)} &= \frac{f}{g} + (f-\bar{f})\frac{1}{g} - (g-\bar{g})\frac{f}{g^2} \\ &\quad + 0 - (f-\bar{f})(g-\bar{g})\frac{1}{g^2} + (g-\bar{g})^2\,\frac{f}{g^3} + \mathcal{O}\left(\frac{\bar{f}}{\bar{g}}\right)^{(3)} \end{aligned}$$

We disregard terms of higher order as quadratic and take the expectation value of E^*. The linear terms cancels out and we obtain

$$\begin{aligned} \langle E^* \rangle = \left\langle \frac{\bar{f}}{\bar{g}} \right\rangle &= \frac{f}{g} + \mathrm{var}(\bar{g})\,\frac{f}{g^3} - \mathrm{cov}(\bar{f},\bar{g})\,\frac{1}{g^2} \\ &\approx \frac{f}{g} + \frac{1}{N}\left(\mathrm{var}(\vec{g})\,\frac{f}{g^3} - \mathrm{cov}(\vec{f},\vec{g})\,\frac{1}{g^2}\right) \end{aligned} \tag{A.3}$$

In the last line we used the approach that $\mathrm{var}(\bar{g}) \approx 1/N\ \mathrm{var}(\vec{g})$. As one can realise, $\langle E^* \rangle$ is only an asymptotically unbiased estimator.

$$\langle E^* \rangle \overset{N\to\infty}{=} \frac{f}{g}$$

In addition, we also want to compute an approach for the variance of $\langle E^* \rangle$. In the following we use the abbreviations

$$\Delta f = (f - \bar{f}) \qquad \text{respectively} \qquad \Delta g = (g - \bar{g}) \quad ,$$

and again start with a Taylor series expansion.

$$
\begin{aligned}
(E^*)^2 \;=\; \left(\frac{\bar{f}}{\bar{g}}\right)^2 &= \left(\frac{f}{g} + \Delta f\,\frac{1}{g} - \Delta g\,\frac{f}{g^2} + \Delta f\,\Delta g\,\frac{1}{g^2} + \Delta g^2\,\frac{f}{g^3} + \mathcal{O}\left(\frac{\bar{f}}{\bar{g}}\right)^{(3)}\right)^2 \\
&= \frac{f^2}{g^2} + 2\,\Delta f\,\frac{f}{g^2} - 2\,\Delta g\,\frac{f^2}{g^3} - 4\,\Delta f\,\Delta g\,\frac{f}{g^3} + \Delta f^2\,\frac{1}{g^2} + 3\,\Delta g^2\,\frac{f^2}{g^4} + \mathcal{O}(\Delta f + \Delta g)^3 \\
\left\langle (E^*)^2 \right\rangle \;=\; \left\langle \left(\frac{\bar{f}}{\bar{g}}\right)^2 \right\rangle &= \frac{f^2}{g^2} - 4\,\mathrm{cov}(\bar{f},\bar{g})\,\frac{f}{g^3} + \mathrm{var}(\bar{f})\,\frac{1}{g^2} + 3\,\mathrm{var}(\bar{g})\,\frac{f^2}{g^4} + \mathcal{O}\left\langle(\Delta f + \Delta g)^3\right\rangle
\end{aligned}
$$

$$
\begin{aligned}
\langle E^* \rangle^2 \;=\; \left\langle \frac{\bar{f}}{\bar{g}} \right\rangle^2 &= \left(\frac{f}{g} + \mathrm{var}(\bar{g})\,\frac{f}{g^3} - \mathrm{cov}(\bar{f},\bar{g})\,\frac{1}{g^2}\right)^2 \\
&= \frac{f^2}{g^2} + 2\,\mathrm{var}(\bar{g})\,\frac{f^2}{g^4} - 2\,\mathrm{cov}(\bar{f},\bar{g})\,\frac{f}{g^3} + \mathcal{O}\left\langle(\Delta f + \Delta g)^3\right\rangle
\end{aligned}
$$

$$
\begin{aligned}
\mathrm{var}\,\langle E^* \rangle &= \left\langle (E^*)^2 \right\rangle - \langle E^* \rangle^2 \\
&= \mathrm{var}(\bar{f})\,\frac{1}{g^2} + \mathrm{var}(\bar{g})\,\frac{f^2}{g^4} - 2\,\mathrm{cov}(\bar{f},\bar{g})\,\frac{f}{g^3} \\
&\approx \frac{1}{N}\left(\mathrm{var}(\vec{f})\,\frac{1}{g^2} + \mathrm{var}(\vec{g})\,\frac{f^2}{g^4} - 2\,\mathrm{cov}(\vec{f},\vec{g})\,\frac{f}{g^3}\right)
\end{aligned}
\tag{A.4}
$$

In the previous derivation, we showed that the estimator E^* is only asymptotically unbiased. Due to the fact that we obtained an analytical expression for $\langle E^* \rangle$ in Equation (A.3), we are able to construct an unbiased estimator E.

$$
E \;=\; \frac{\bar{f}}{\bar{g}} - \frac{1}{N}\left(\mathrm{var}(\vec{g})\,\frac{f}{g^3} - \mathrm{cov}(\vec{f},\vec{g})\,\frac{1}{g^2}\right) \tag{A.5}
$$

The expectation value of this estimator is of course

$$
\langle E \rangle \;=\; \left\langle \frac{\bar{f}}{\bar{g}} - \frac{1}{N}\left(\mathrm{var}(\vec{g})\,\frac{f}{g^3} - \mathrm{cov}(\vec{f},\vec{g})\,\frac{1}{g^2}\right)\right\rangle \approx \frac{f}{g} \quad .
$$

The variance of $\langle E \rangle$ is consistent with the variance of $\langle E^* \rangle$.

A.3. The Jackknife Approach

As already mentioned, the Jackknife method provides a possibility to remove a bias of an estimator, like in Equation (A.3), numerically, but it costs extra computational effort.
Suppose there are N data points

$$
\vec{r} \;=\; \{r_1,\, r_2,\, \ldots,\, r_N\}
$$

and one wants to compute some estimator of interest q^* using the available information $\vec{r}$. In this context, q is an arbitrary function depending on r_i and $\hat{q}$ should be the true unbiased value of this quantity.
Using the Jackknife algorithm one has to perform the data analysis $N + 1$ times. Once using the whole data

$$
\bar{q} \;=\; \frac{1}{N}\sum_{i=1}^{N} q(r_i)
$$

and N times leaving out one of the data points

$$\bar{q_j} = \frac{1}{N-1}\sum_{i\neq j}^{N} q(r_i) \quad .$$

The Jackknife estimator of the mean q_J and variance σ_J^2 of the mean are defined by

$$\begin{aligned} q_J &= \frac{1}{N}\sum_{i=1}^{N} \left(N\,\bar{q} - (N-1)\,\bar{q_j}\right) \\ &= N\,\bar{q} - (N-1)\,\dot{q} \end{aligned} \tag{A.6}$$

respectively

$$\sigma_J^2 = \frac{N-1}{N}\sum_{i=1}^{N}\left(\bar{q_j} - \dot{q}\right)^2, \tag{A.7}$$

whereby $\dot{q}$ is the arithmetic mean of the $\bar{q_j}$.

The bias of an estimator q^* is typically given by

$$\text{bias}(q^*) = \hat{q} - \langle q^* \rangle = \frac{a_1}{N} + \frac{a_2}{N^2} + \mathcal{O}\left(\frac{1}{N^3}\right) \quad ,$$

whereby a_1 and a_2 are constants, which do not depend on N. It can be shown [33], that the Jackknife estimator for the mean cancels the $1/N$ term. That means, q_J is biased $\mathcal{O}\left(1/N^2\right)$ compared to $\mathcal{O}\left(1/N\right)$ for the original estimator.

A.4. Example for Ratio Estimation

In this Section, we show an example for ratio estimation to illustrate, that Equation (A.5) respectively the Jackknife method produces a better result than the straightforward estimator E^* in Equation (A.2).

We decided for the following example.

$$E^* = \frac{\sum_{i=1}^{N} a\,r_i + b}{\sum_{i=1}^{N} r_i} = \frac{\overline{a\,r_i + b}}{\overline{r_i}} \quad , \quad r_i \in U(0,1) \tag{A.8}$$

In this context, a and b are constants and the r_i are uniformly distributed random numbers. The true value of this ratio $\hat{E}$ is given by $a + 2b$.

Figure (A.1) shows the results for E^* (Equation (A.2)), E (Equation (A.5)) and E_J (Equation (A.6)) averaged over 10000 values for $a = 1$ and $b = 1$ as a function of N in comparison to $\hat{E}$. It is no surprise that the naive estimator E^* yields the worst result.

If one considers the example in (A.8) for the case of $b = 0$, the estimator E^* is simple a and its variance is zero. Figure (A.2) shows the results for E^* with errorbars according to Equation (A.1) in comparison to Equation (A.4) and the Jackknife method. As one can realise, if one uses the simple error propagation, described in Section A.1, the result is completely wrong.

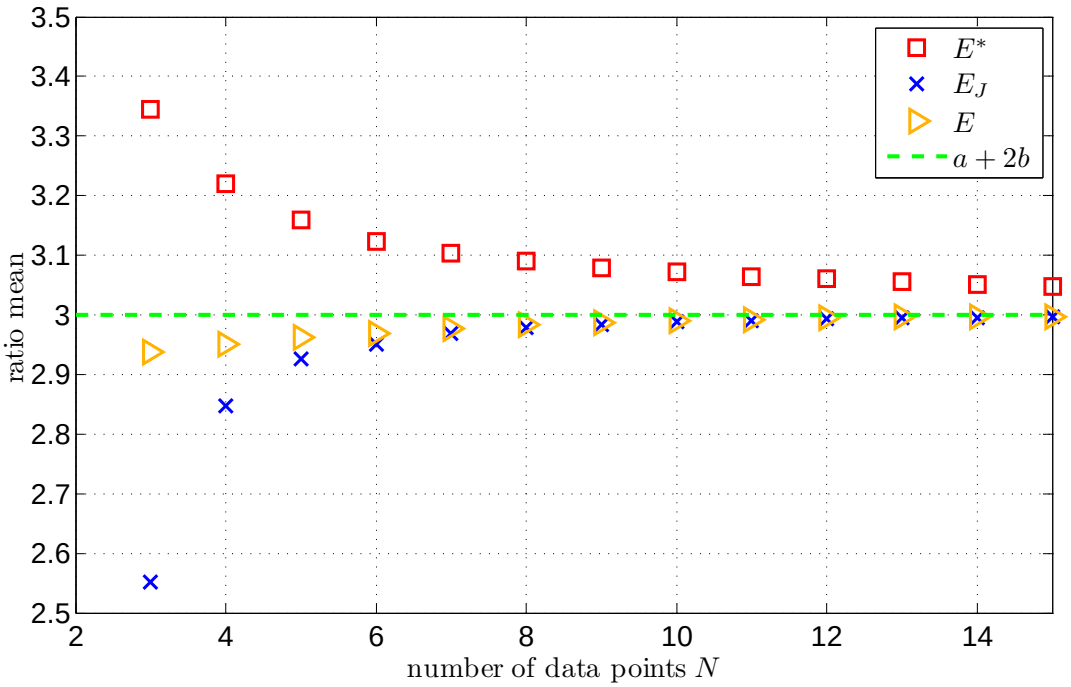

Figure A.1.: Results, using the example (A.8), for E^* (Equation (A.2)), E (Equation (A.5)) and E_J (Equation (A.6)) averaged over 10000 values for $a = 1$ and $b = 1$ as a function of N in comparison with the true value $\hat{E} = a + 2b$.

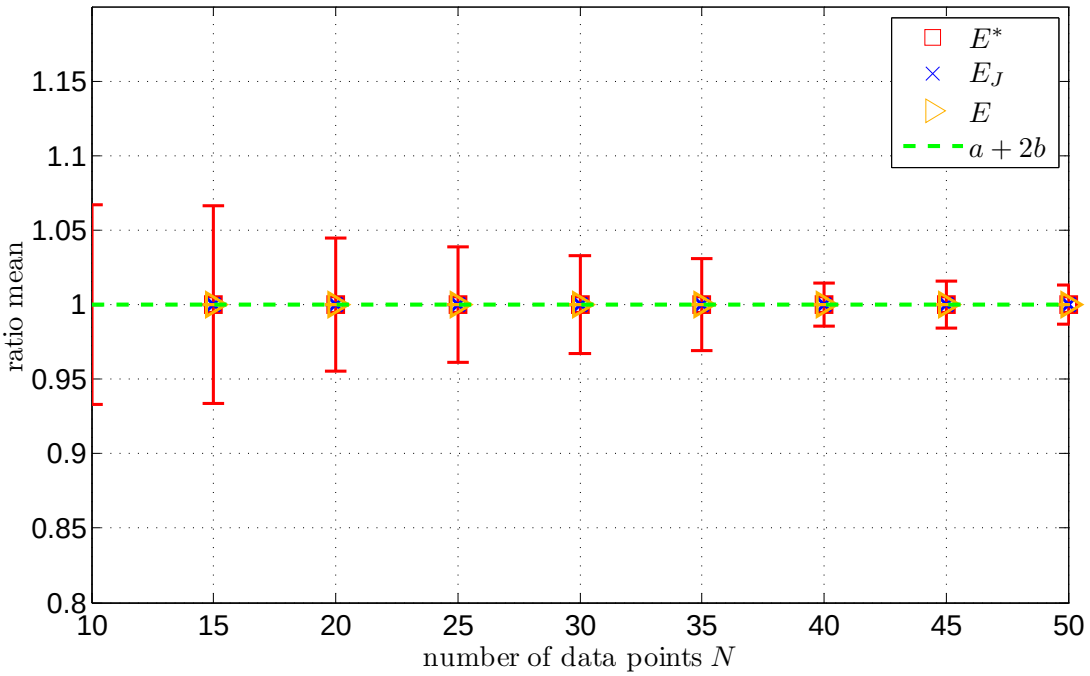

Figure A.2.: Results, using the example (A.8), for E^* with errorbars according to Equation (A.1) in comparison to Equation (A.4) and the Jackknife method for $a = 1$ and $b = 0$. As one can realise, the simple error propagation, described in Section A.1, yields a completely wrong result.

B. Additional Information

B.1. Program to generate the basis states

In this Appendix a C++ program is displayed to generate the basis states for the Hubbard Hamiltonian for one spin direction.

The program stores the states in a bool vector of length $N\_SITES = L_X \times L_Y$, whereby the element of the vector is true if the corresponding site is occupied by an electron and false if not.
The output of this program is depicted below. As one can see, the states are sorted in ascending order if one would transform them to decimal.
Furthermore, one realises that this sequence of basis states implicates that the matrices to calculate the determinants used in a basis transformation (for example from real to k-space in the Gutzwiller Wavefunction, see Section 3.1) differ mostly only by one column from one basis state to the next. That means, one can use the determinant of the current basis state to calculate the determinant of the next one. This is expedient numerically in view of computing time.
In the following, we want to sketch that procedure starting with the matrix identity

$$\text{tr } \ln(M) = \ln \det(M) \quad ,$$

whereby in this case on the left hand side, ln is the matrix logarithm. Suppose the matrix of the current basis state is A and the next one is B. As already mentioned, they differ only by one column v.

$$\begin{aligned} A &= B + v = B\left(\mathbb{1} + B^{-1} v\right) \\ \text{tr } \ln(A) &= \text{tr } \ln(B) + \text{tr } \ln\left(\mathbb{1} + B^{-1} v\right) = \ln \det(A) \\ \det(A) &= \mathrm{e}^{\text{tr } \ln(B)} \cdot \mathrm{e}^{\text{tr } \ln\left(\mathbb{1} + B^{-1} v\right)} \\ &= \det(A) \cdot \underbrace{\det\left(\mathbb{1} + B^{-1} v\right)}_{\otimes} \end{aligned}$$

The term on the right hand side, marked with $\otimes$, can be calculated using the so-called *Woodbury matrix identity*.

```
#include <iostream>
#include <vector>

void printBoolVec(const std::vector<bool> &vec);

// ----- ----- ----- ----- -----
// ----- main programm
int main()
{
  unsigned N_SPIN = 2;    // number of electrons for this spin diretion
  unsigned N_SITES = 4;   // number of lattice sites

  // generate and store the basis states
  std::vector< bool > one_state(N_SITES,false);  // allocate memory and set to false
  for(unsigned i=0; i<N_SPIN; i++) {
    one_state[i].flip();                         // Flip N_SPIN bits
  }
  std::sort(one_state.begin(), one_state.end());

  std::vector< std::vector< bool > > all_states;

  do
{
      all_states.push_back(one_state);              // store the current state
} while(std::next_permutation(one_state.begin(), one_state.end()));

  // output of all states
  for(unsigned i=0; i<all_states.size(); i++) {
    printBoolVec(all_states[i]);
  }

  return 0;
}
// ----- ----- ----- ----- -----

// ----- ----- ----- ----- -----
// ----- programm to write a bool vector to stream
void printBoolVec(const std::vector<bool> &vec)
{
  for(unsigned i=0; i<vec.size(); i++) {
    if(vec[i]) {
      std::cout << "1";
    } else {
      std::cout << "0";
    }
  }
  std::cout << std::endl;
}
// ----- ----- ----- ----- -----
```

Output:

```
0011
0101
0110
1001
1010
1100
```

B.2. Exact interval bounds

Suppose there is a wavefunction ψ, which already gives quite a good approach for a normalized eigenvector of the Hamiltonian $\hat{H}$. The corresponding energy is given by

$$\epsilon = \langle \psi | \hat{H} | \psi \rangle \quad .$$

In this appendix, we derive exact interval bounds $I = [\epsilon - \sigma, \epsilon + \sigma]$, in which there is at least one exact eigenvalue of $\hat{H}$.
First, we expand ψ in the basis ϕ_i of eigenvectors of the Hamiltonian

$$| \psi \rangle = \sum_i c_i | \phi_i \rangle$$

and subsequently give an expression for the variance σ^2.

$$\begin{aligned}
\sigma^2 &= \langle \psi | \hat{H}^2 | \psi \rangle - \langle \psi | \hat{H} | \psi \rangle^2 \\
&= \langle \psi | \left(\hat{H} - \underbrace{\langle \hat{H} \rangle}_{\epsilon} \right)^2 | \psi \rangle \\
&= \sum_i |c_i|^2 \, (\epsilon_i - \epsilon)^2 \\
&\geq \underbrace{\sum_i |c_i|^2}_{=1} \min (\epsilon_i - \epsilon)^2 \; = \; (\epsilon_m - \epsilon)^2
\end{aligned}$$

In this context ϵ_m denotes that eigenvalue of $\hat{H}$ which is closest to ϵ.

B.3. Generate the Hamiltonian on the fly

In Section 1.4, we discussed the size of the Hilbert space of the Hubbard model with the result that it is a hard task to store three Lanczos vectors for larger systems than $L_X \times L_Y = 4 \times 4$. The same is true for the Hamiltonian itself, that means, whenever one needs entries of $\hat{H}$ (e.g. for calculating the expectation value) one has to generate them on the fly (schematically depicted in Equation (B.1) for the real space).

$$\hat{H}\,|\,\chi_i\,\rangle \;=\; \begin{pmatrix} U\,|\,\chi_i\,\rangle \\ -t\,s_j|\,\chi_j\,\rangle \\ -t\,s_k|\,\chi_k\,\rangle \\ \vdots \\ -t\,s_l|\,\chi_l\,\rangle \\ -t\,s_m|\,\chi_m\,\rangle \end{pmatrix} \tag{B.1}$$

In this context the $|\,\chi_j\,\rangle, \ldots, |\,\chi_m\,\rangle$ describe the basis states, which can be reached by hopping processes from state $|\,\chi_j\,\rangle$ and s describes the sign that can occur.
In the following, a part of a C++ program is displayed to realise this procedure.

```
// ----- ----- ----- ----- -----
std::vector< State > State::scatterState() const
{
  std::vector< State > tmp;  // vector with scattered basis states
  State dummy_state;
  unsigned ones_between;

  // ----- loop all sites
  for(unsigned i=0; i<basis.N_SITES; i++)
  {
    // loop all neighbours
    for(unsigned j=0; j<basis.neighbour[0].size(); j++)
    {
      // ----- spin direction up
      if( (basis.basis_up[i] == true) &&
        (basis.basis_up[basis.neighbour[i][j]] == false) )
      {
        // hopping is possible
        dummy_state = *this;

        dummy_state.basis.basis_up[i].flip();
        dummy_state.basis.basis_up[basis.neighbour[i][j]].flip();

        // required for calculate the fermion sign
        ones_between = countOnes(dummy_state.basis.basis_up, i,
          dummy_state.basis.neighbour[i][j]);

        dummy_state.value = -pow(-1,ones_between) * value * basis.T; // H = -T ...

        // add the state to the vector
        tmp.push_back(dummy_state);
      }
      // ----- -----

      // ----- once again for spin diretion down
      if(  (basis.basis_down[i] == true) &&
```

```
        (basis.basis_down[basis.neighbour[i][j]] == false) )
      {
        // hopping is possible
        dummy_state = *this;

        dummy_state.basis.basis_down[i].flip();
        dummy_state.basis.basis_down[basis.neighbour[i][j]].flip();

        // required for calculate the fermion sign
        ones_between = countOnes(dummy_state.basis.basis_down, i,
         dummy_state.basis.neighbour[i][j]);

        dummy_state.value = -pow(-1,ones_between) * value * basis.T; // H = -T ...

        // add the state to the vector
        tmp.push_back(dummy_state);
        // ----- -----
      }
    }
  }
  return tmp;
}
// ----- ----- ----- ----- -----
```

References

[1] J. Hubbard. Electron correlations in narrow energy bands. *Proceedings of the Royal Society of London. Series A. Mathematical and Physical Sciences*, 276(1365):238–257, 1963.

[2] B. Sriram Shastry and Bill Sutherland. Twisted boundary conditions and effective mass in heisenberg-ising and hubbard rings. *Physical Review Letter*, 65:243–246, Jul 1990.

[3] Jean Louis Richard Alain Messager. An rvb approach to the hubbard model. *Physics Letters A*, 143(6-7):345–348, January 1990.

[4] Cornelius Lanczos. An iteration method for the solution of the eigenvalue problem of linear differential and integral operators. *Journal Of Research Of The National Bureau Of Standards*, 45(4):255–282, 1950.

[5] Nandini Trivedi and D. M. Ceperley. Ground-state correlations of quantum antiferromagnets: A green-function monte carlo study. *Physical Review B*, 41(7), 1990.

[6] Byron Faber Ioan Kosztin and Klaus Schulten. Introduction to the diffusion monte carlo method. *American Journal of Physics*, 64(5), May 1996.

[7] L.J. van Vliet G.M.P. van Kempen. Mean and variance of ratio estimators used in fluorescence ratio imaging. *Cytometry*, 39(4):300–305, April 2000.

[8] N Hatano and M Suzuki. Finding exponential product formulas of higher orders. Technical Report math-ph/0506007, Jun 2005.

[9] Alex J. W. Thom George H. Booth and Ali Alavi. Fermion monte carlo without fixed nodes: A game of life, death, and annihilation in slater determinant space. *The Journal of Chemical Physics*, 131(054106), 2009.

[10] Wolfgang von der Linden and Hans Gerd Evertz. Continuous time. Private Communication, 2011.

[11] Wolfgang von der Linden. Master equation. Private Communication, 2011.

[12] K. E. Schmidt, Parhat Niyaz, A. Vaught, and Michael A. Lee. Green's function monte carlo method with exact imaginary-time propagation. *Physical Review E*, 71:016707, Jan 2005.

[13] Ceperley D. and Alder B. Quantum monte carlo. *Science*, 231(555), 1986.

[14] D. M. Ceperley. The statistical error of green's function monte carlo. *Journal of Statistical Physics*, 43(5-6):815–826, 1986.

[15] Martin C. Gutzwiller. Correlation of electrons in a narrow s band. *Physcal Review*, 137, Mar 1965.

[16] S. Baroni R. Car M. Parrinello E. Tosatti A. Parola, S. Sorella. Recent numerical results on the two dimensional hubbard model. *Physica C*, 162-164:771–772, 1989.

[17] P. W. Anderson. The resonating valence bond state in la_2cuo_4 and superconductivity. *Science*, 235(4796):1196–1198, March 1987.

[18] P.L. Iske and W.J. Caspers. A mechanism for symmetry breaking in antiferromagnetic heisenberg systems. *Physica A*, 142(1-3):360–373, 1987.

[19] William H. Press, Saul A. Teukolsky, William T. Vetterling, and Brian P. Flannery. *Numerical Recipes 3rd Edition: The Art of Scientific Computing*. Cambridge University Press, New York, NY, USA, 3 edition, 2007.

[20] N. Canosa, A. Plastino, and R. Rossignoli. Ground-state wave functions and maximum entropy. *Phys. Rev. A*, 40:519–525, Jul 1989.

[21] A. Plastinoa R. Rossignoli L. Arracheaa, N. Canosab. Ground state of the hubbard model: a variational approach based on the maximum entropy principle. *Physics Letters A*, 176:353–359, 1993.

[22] Deidre Cleland, George H Booth, and Ali Alavi. Communications: Survival of the fittest: accelerating convergence in full configuration-interaction quantum monte carlo. *The Journal of Chemical Physics*, 132(4):041103, 2010.

[23] Michael H Kolodrubetz and Bryan K Clark. Fci-qmc approach to the fermi polaron. Technical Report arXiv:1204.1490, April 2012. Comments: 10 pages, 5 figures + 2 page appendix.

[24] J S Spencer, N S Blunt, and W M C Foulkes. The sign problem and population dynamics in the full configuration interaction quantum monte carlo method. Technical Report arXiv:1110.5479, Oct 2011. Comments: 11 pages. 6 figures.

[25] George H. Booth James J. Shepherd and Ali Alavi. Investigation of the full configuration interaction quantum monte carlo method using homogeneous electron gas models. *The Journal of Chemical Physics*, 136, 2012.

[26] D. M. Ceperley and B. J. Alder. Ground state of the electron gas by a stochastic method. *Phys. Rev. Lett.*, 45:566–569, Aug 1980.

[27] Guozhong An and J. M. J. van Leeuwen. Fixed-node monte carlo study of the two-dimensional hubbard model. *Phys. Rev. B*, 44:9410–9417, Nov 1991.

[28] D. F. B. ten Haaf, H. J. M. van Bemmel, J. M. J. van Leeuwen, W. van Saarloos, and D. M. Ceperley. Proof for an upper bound in fixed-node monte carlo for lattice fermions. *Phys. Rev. B*, 51:13039–13045, May 1995.

[29] D. M. Ceperley and B. J. Alder. Quantum monte carlo for molecules: Green´s function and nodal release. *The Journal of Chemical Physics*, 81(5833), 1984.

[30] Jie Xu, Chia-Chen Chang, Eric J Walter, and Shiwei Zhang. Spin- and charge-density waves in the hartree-fock ground state of the two-dimensional hubbard model. *Journal of Physics: Condensed Matter*, 23(50):505601, 2011.

[31] Edwin Langmann and Mats Wallin. Mean field magnetic phase diagrams for the two dimensional t t u hubbard model. *Journal of Statistical Physics*, 127(4):825–840, May.

[32] D.S. Sivia and J. Skilling. *Data Analysis: A Bayesian Tutorial*. Oxford Science Publications. Oxford University Press, 2006.

[33] Bradley Efron. *The Jackknife, the bootstrap and other resampling plans*. Number 38 in Regional Conference Series in applied mathematics. Society for Industrial and applied mathematics, Philadelphia, Pa., 1982.